A Task for Molecular Motors: Maintaining the Cortical Division Zone in *Arabidopsis thaliana*

Dissertation

der Mathematisch-Naturwissenschaftlichen Fakultät

der Eberhard Karls Universität Tübingen

zur Erlangung des Grades eines

Doktors der Naturwissenschaften

(Dr. rer. nat.)

vorgelegt von

Elisabeth Lipka

aus Räckelwitz

Tübingen

2015

Tag der mündlichen Qualifikation:	25.09.2015
Dekan:	Prof. Dr. Wolfgang Rosenstiel
1. Berichterstatter:	Dr. Sabine Müller
2. Berichterstatter:	Prof. Dr. Gerd Jürgens

DANKSAGUNG

Mein besonderer Dank gilt Dr. Sabine Müller. Sie hat mir die Möglichkeit eröffnet meine Doktorarbeit in ihrer Arbeitsgruppe anfertigen und an diesem spannenden Projekt arbeiten zu können. Ich durfte so viel lernen. Vielen Dank dafür und auch für die stets besondere Unterstützung, Geduld und wissenschaftliche Begeisterung.

Bei Prof. Dr. Gerd Jürgens möchte ich mich für die Bereitschaft bedanken, diese Arbeit zu begutachten.

Herzlich danke ich der FG Müller, Steffi Zimmermann, Dorothee Stöckle, Mayank Chugh, Arvid Herrmann und Richard Gavidia für die tatkräftige und fachliche Hilfe. Es macht Spaß, mit euch zu arbeiten.

Des Weiteren möchte ich Kerstin Huhn, Sabine Brumm, Dr. Sandra Richter, Ulrike Hiller, Marika Kientz, Simone Frühholz und der gesamten EntGen des ZMBPs meinen Dank aussprechen. Ihr habt mich in den Jahren meiner Doktorarbeit begleitet und habt mir immer mit Rat und Tat zur Seite gestanden. Vielen Dank für die kritischen Diskussionen, die aufmunternden Worte und eure unermüdliche Hilfsbereitschaft.

An dieser Stelle möchte ich mich auch bei Uschi Kluge und Brigitte Schneck bedanken. Sie halten uns mit ihrer Arbeit täglich den Rücken frei. Dankeschön!

Nicht zuletzt bin ich meinen Freunden und meiner Familie, besonders meinem Philip dankbar, für die Unterstützung in allen Höhen und Tiefen, die diese Doktorarbeit mit sich brachten, sowie die fortwährende Motivation. Danke, dass ihr an mich glaubt.

TABLE OF CONTENTS

1. SUMMARY

Plant cells are confined and immobilized by rigid cell walls, which determine their shape and location within tissues. Therefore plant cells demand specific spatial control over cell division and have evolved unique cytoskeletal structures, which aid in coping with these spatial demands. Prior to mitosis a prominent but transient band of microtubules and actin filaments, called the preprophase band (PPB) marks the site where the future cell plate will fuse with the parental plasma membrane. Thus, the PPB is a faithful predictor of the division plane. PPBs spatial information is preserved after its disassembly by the cortical division zone (CDZ), which provides guidance for localized cell plate fusion. Cell plate formation by vesicle fusion initiates in the center of the cell and is aided by the plant specific cytokinetic apparatus, the phragmoplast. Yet only little is known about the molecular identity of the CDZ and how it attracts the phragmoplast and cell plate.

A pair of kinesin-12 class motor proteins, PHRAGMOPLAST ORIENTING KINESIN 1 (POK1) and POK2, is essential for the spatial control of cytokinesis. Here we report that a functional full length POK1 fusion protein (YFP-POK1) is dynamically recruited to the PPB and permanently resides at the CDZ until cell plate fusion takes place. *In vivo* analysis of phragmoplast expansion in *pok1 pok2* double mutants revealed a PPB – phragmoplast misalignment caused by phragmoplast tilting, which results in cell wall mis-positioning. Moreover, maintenance of the CDZ identity marker TANGLED is dependent on POK function, suggesting that POK motor proteins might act as a scaffold to retain CDZ identity markers at the plasma membrane, thus maintaining the molecular memory of the division plane.

The second project intends to elucidate the effects of a specific posttranslational tubulin modification (PTM) on microtubule organization and CDZ establishment in *Arabidopsis thaliana*. We demonstrate, that low concentrations of NO_2Tyr, which is incorporated into the C-terminus of α-tubulin, are not detrimental for plant health. However the NO_2Tyr treatment affects the organization of the cortical microtubule array, resulting in non-polar cell expansion and induces oblique cell wall integration. The results indicate that PTM of α-tubulin might be important for microtubule organization and for division plane establishment during plant development.

2. ZUSAMMENFASSUNG

Pflanzenzellen sind von einer starren Zellwand umgeben, welche die Form und die Lage der Zelle im Gewebe festlegt. Deshalb stellen Pflanzenzellen besondere räumliche Ansprüche an die Zellteilung und haben einzigartige Zytoskelettstrukturen entwickelt, welche helfen diese räumlichen Ansprüche zu meistern. Ein bedeutendes aber transientes Band aus Mikrotubuli und Aktinfilamenten, das Präprophaseband (PPB) kennzeichnet vor der Mitose die Stelle, wo die zukünftige Zellplatte mit der Plasmamembran fusionieren wird. Somit ist das PPB eine zuverlässige Vorhersage der Zellteilungsebene. Nach dem Abbau des PPBs wird seine positionelle Information durch die kortikale Teilungszone (CDZ) erhalten, welche die Ausrichtung des ortsgebundenen Einbaus der Zellplatte bestimmt. Die Synthese der Zellplatte mittels Vesikelfusion wird vom pflanzenspezifischen zytokinetischen Apparat, dem Phragmoplasten unterstützt. Die genaue molekulare Zusammensetzung der CDZ und wie die CDZ mit dem Phragmoplasten und der Zellplatte kommuniziert ist wenig untersucht.

Ein Paar von Motorproteinen der Kinesinklasse-12, das PHRAGMOPLAST ORIENTIERENDE KINESIN 1 (POK1) und das POK2 ist für die räumliche Kontrolle der Zytokinese essentiell ist. Hier zeigen wir, dass ein funktionales Volllänge-POK1-Fusionsprotein (YFP-POK1) dynamisch an das PPB rekrutiert wird und bis zur Insertion der Zellplatte an der CDZ präsent ist. Die Expansion des Phragmoplasten wurde *in vivo* in der *pok1 pok2*-Doppelmutante analysiert. Durch ein Kippen des Phragmoplasten weicht seine Ausrichtung von der des PPBs ab und verursacht den Fehleinbau der Zellwand. Des Weiteren ist die Erhaltung des CDZ-Identitätsmarkers TANGLED von POK abhängig. Diese Beobachtung weist darauf hin, dass POK-Motorproteine als Gerüst fungieren, um CDZ-Identitätsmarker an der Plasmamembran zu erhalten und folglich das molekulare Gedächtnis an die Zellteilungsebene zu bewahren.

Ein zweites Projekt untersucht den Einfluss von einer spezifischen posttranslationalen Tubulinmodifikation (PTM) auf die Organisation von Mikrotubuli und Festlegung der CDZ in *Arabidopsis thaliana*. Wir zeigen, dass eine geringe Konzentration von NO_2-Tyr, welches post-translational an den C-Terminus von α-

Tubulin bindet, für die Gesundheit der Pflanzen nicht schädlich ist. Allerdings wird durch die Behandlung mit NO_2-Tyr die Organisation der kortikalen Mikrotubuli verändert, was zu einer ungerichteten Zellexpansion führt. Des Weiteren verursacht die Behandlung mit NO_2-Tyr einen schiefen Einbau der Zellwand. Die Ergebnisse weisen darauf hin, dass PTMs von α-tubulin die Organisation der Mikrotubuli in Zellteilung und Zellstreckung regulieren und daher in der pflanzlichen Entwicklung wichtig sind.

3. INTRODUCTION

In contrast to animal cells, plant cells are embedded in a rigid cell wall, prohibiting cell movement and migration. Therefore plant development calls for an accurately performed growth, coordinated by two vital processes, cell division and cell expansion.

During plant cell division the position of the division plane is absolutely critical, because it specifies the placement of the new wall, the cell plate, thus contributing to plant cell shape and tissue patterning. In symmetric, proliferative cell division, the division plane is established following simple, geometric rules fulfilling the “shortest wall” rule (Rasmussen et al., 2013; Yoshida et al., 2014). In the *Arabidopsis* root meristem most division planes are therefore arranged at right angle to the root axis, thereby contributing to longitudinal organ growth (Figure 1; Kost et al., 1999). Specific cytoskeletal arrays fulfill the spatial demands of plant cell division (Goddard et al., 1994). Before entering mitosis, the cortical microtubule array rearranges in a cortical band, called the preprophase band (PPB). This band of microtubules and actin filaments marks the future cell plate insertion site, thus establishing the division plane (Figure 1; Pickett-Heaps and Northcote, 1966; Palevitz, 1987). During cytokinesis this spatial information is precisely implemented by the phragmoplast. Between the two reforming daughter nuclei, two opposing sets of microtubules form the phragmoplast from the spindle microtubule remnants. The phragmoplast aids in cell plate formation and expands from the center of the cell towards the site formerly occupied by the PPB (Figure 1; Goddard et al., 1994; Jürgens, 2005). Thus,

the PPB and the phragmoplast share the same orientation and are essential for accurate positioning of the cell plate and therefore determine the shape and the position of the daughter cells.

The ultimate shape of plant cells is dependent on the establishment of cell expansion axis, aided by the cytoskeleton. As hypothesized in the "alignment theory", cortical microtubules guide the movement of cellulose synthase complexes (CESAs), thereby determining the orientation of newly synthesized cellulose microfibrils (Ledbetter and Porter, 1963; Giddings and Staehelin, 1988; Bringmann et al., 2012). In elongating cells, the cortical microtubule array and subsequently cellulose microfibrils are oriented transversely to the elongation axis, leading to a polar anisotropic cell expansion in longitudinal direction (Figure 1; Green, 1965; Wick et al., 1981; Granger and Cyr, 2001; Paredez et al., 2006).

The microtubule cytoskeleton is therefore essential for the establishment of the plane of cell division and the axis of cell expansion and consequently is a major determinant for plant morphogenesis.

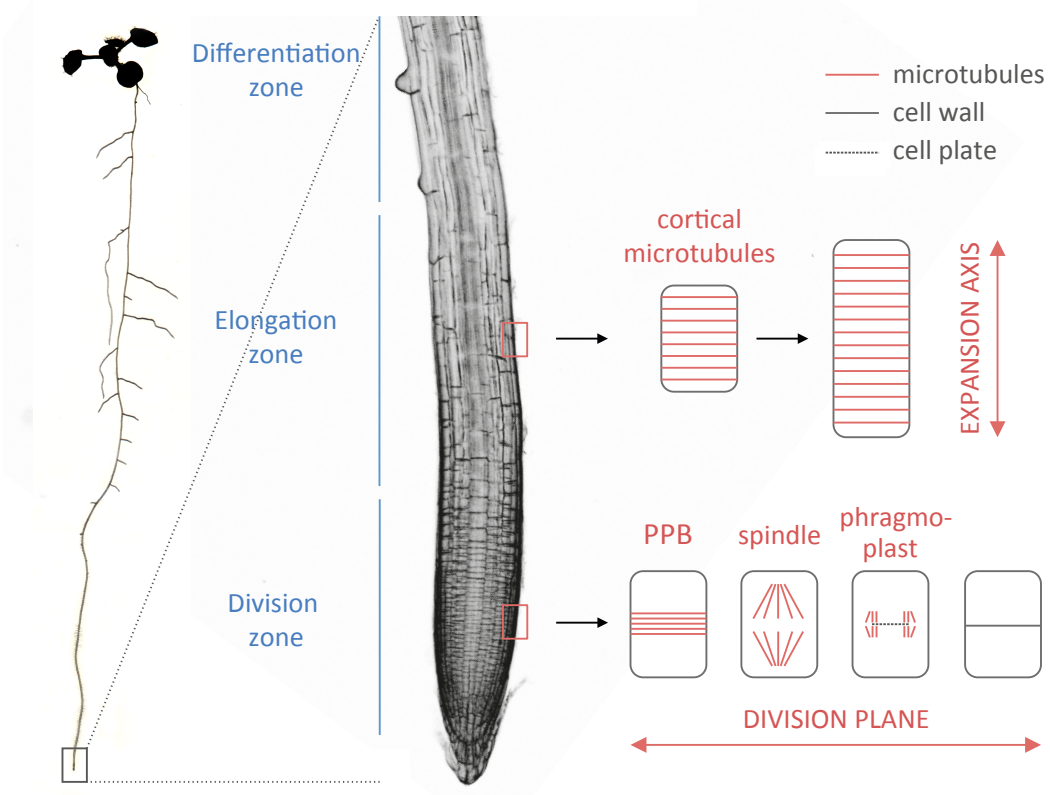

Figure 1: Orientation of division plane and expansion axis in the root meristem of *Arabidopsis thaliana*.

3.1 Microtubule structure and dynamics

Heterodimers of α-tubulin and β-tubulin subunits assemble in head-to-tail orientation resulting in a polar protofilament. The β-tubulin end is the designated plus end and the α-tubulin end is termed minus end. Generally, microtubules consist of 13 laterally bound linear protofilaments forming a hollow "tube" (Figure 2; Ledbetter and Porter, 1964; Goddard et al., 1994). *In vivo*, the minus end usually exhibits little dynamics, whereas the plus end contributes to most of the observed microtubule growth and shrinkage. This dynamic behavior depends on the guanosine nucleotide status of the β-tubulin. Both, α- and β-tubulin bind to guanosine triphosphate (GTP). The GTP bound to α-tubulin is not exchangeable. In contrast, the GTP bound to β-tubulin at the plus end is hydrolyzed to GDP once an additional tubulin heterodimer binds during polymerization (Mitchison and Kirschner, 1984). The GTP-bound β-tubulin is termed the GTP cap, stabilizes the plus end and is required for microtubule polymerization (Weisenberg, 1972; MacNeal and Purich, 1978). When the GTP cap is lost, the GDP end subunits are rapidly disassociated due to conformational changes resulting in outward curvation and, subsequently, microtubule depolymerization (Wang and Nogales, 2005; Nogales and Wang, 2006). The transition from microtubule growth to shrinkage is termed catastrophe. When either hitting upon a GTP-bound β-tubulin within the microtubule lattice during depolymerization (Dimitrov et al., 2008) or a GTP-bound β-tubulin gets incorporated (Bayley et al., 1990), the microtubule plus end is subjected to polymerization, termed rescue. Microtubules co-exist in polymerization/growth and depolymerization/shrinkage phases and stochastically change between the two phases, a property called dynamic instability (Figure 2; Mitchison and Kirschner, 1984). Under certain circumstances, treadmilling may be observed. Polymerization at the plus end accompanied by the simultaneous, depolymerization at the minus end, results in the impression of microtubule migration (Margolis and Wilson, 1978; Waterman-Storer and Salmon, 1997) Dynamic instability and treadmilling are also characterized in plants and provide the basis for microtubule organization

(Dhonukshe and Gadella, 2003; Shaw et al., 2003; Dixit and Cyr, 2004; Horio and Murata, 2014).

In vivo, dynamic instability must be regulated, since the microtubule cytoskeleton is extensively reorganized during the cell cycle (Wasteneys, 2002; Vos et al., 2004; Horio and Murata, 2014). Plant cells lack centrosomes, the canonical microtubule organizing centers (MTOCs), but instead nucleation of microtubules occurs at dispersed MTOCs, containing the conserved γ-tubulin ring complex (γ-TuRC). The γ-tubulin small complex (γ-TuSC) consists of γ-tubulin and γ-tubulin complex protein 2 (GCP2) and GCP3. Together with GCP4, GCP5 and GCP6, γ-TuSC constitutes the γ-TuRC and provides the template for the 13 protofilaments that align to form the microtubule (Evans et al., 1985; Kollman et al., 2011). Microtubule-associated proteins (MAPs) modulate microtubule dynamics and promote microtubule stability by different mechanisms. A large number of MAPs bundle microtubules by crosslinking parallel and antiparallel microtubules (Ho et al., 2012; Stoppin-Mellet et al., 2013) and promote microtubule polymerization (Fache et al., 2010; Stoppin-Mellet et al., 2013) or prevent depolymerization at the plus end, for instance +TIP proteins (Ambrose et al., 2011). Kinesins, microtubule dependent motor proteins, bind to microtubules and function in microtubule organization. They may also contribute to cellular transport by moving along microtubules (Lee and Liu, 2004). In addition, posttranslational tubulin modifications (PTM) modulate microtubule dynamics, e.g. the detyrosination / tyrosination of α -tubulin is well characterized in mammalian cells (Gundersen and Bulinski, 1986; Gundersen et al., 1987). PTMs might serve as a road map for MAPs and are therefore contributing to the specific subcellular organization of the microtubule cytoskeleton and its related functions (Verhey and Gaertig, 2007; Verhey and Hammond, 2009).

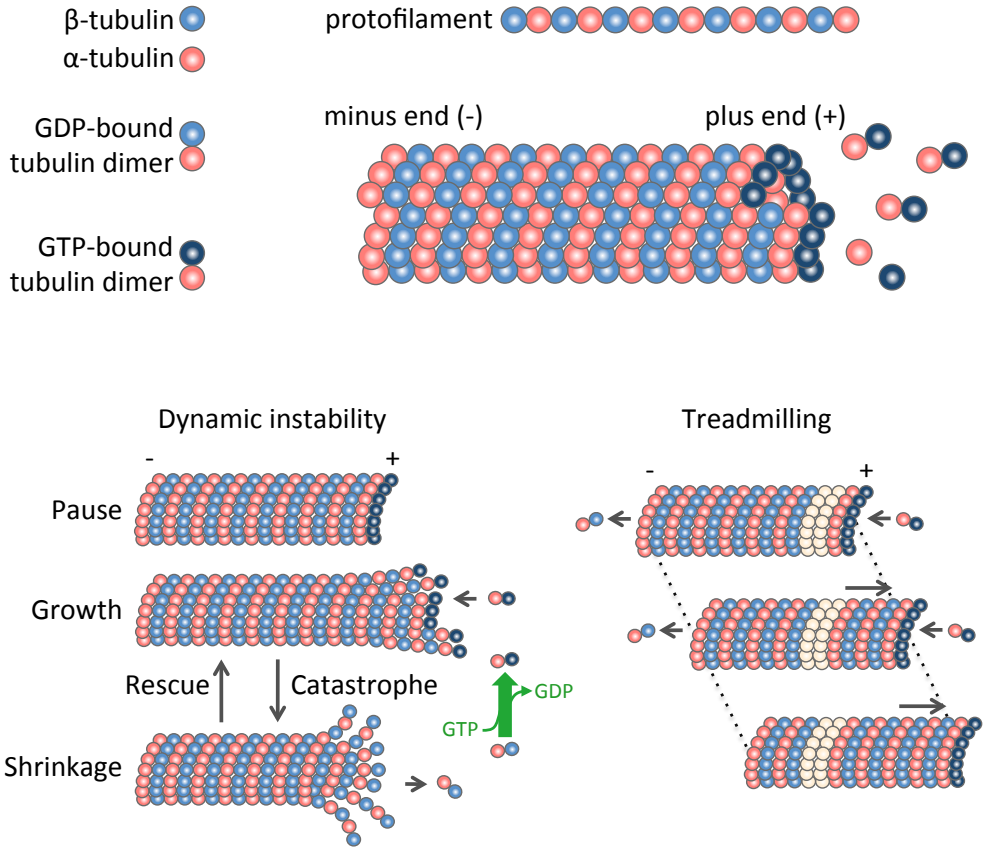

Figure 2: Microtubule structure and dynamics. Modified from (Dixit and Cyr, 2004 and Horio and Murata, 2014).

3.2 Kinesin-12 class proteins of Arabidopsis thaliana

Kinesins are microtubule-based motor proteins executing a variety of force generating functions in unidirectional transport of vesicles and organelles, microtubule organization, signal transduction and cell division (Reddy and Day, 2001; Lee and Liu, 2004; Hirokawa et al., 2009). They generally consist of a motor domain and a stalk region and the majority forms homodimers (Figure 3A). The motor domain contains both a microtubule- and an adenosine triphosphate (ATP) binding site. ATP hydrolysis leads to conformational changes that generate forces to perform steps along microtubules (Vale and Fletterick, 1997; Zhu and Dixit, 2012). In general, carboxy-terminal (C-terminal) motor domains mediate minus end-directed motility and amino-terminal (N-terminal) motor domains mediate plus end-directed motility. In addition, the directionality of the kinesin is influenced by the neck linker

consensus motif adjacent the motor domain (Endow, 1999). The stalk region encodes for coiled-coil domains for dimerization and the tail region is required for cargo binding. The highly conserved motor domains in combination with various non-motor regions mediate the variety of specific cellular functions fulfilled by kinesins. The kinesin superfamily has been classified into 14 subfamilies based on the location and conservation of the motor domain and sequence similarities (Lawrence et al., 2004). The *Arabidopsis thaliana* genome encodes for an exceeding number of 61 kinesins in comparison to animals (e.g. human 45). In plants, kinesin-7 and kinesin-14 class are expanded suggesting a plant specific function (Reddy and Day, 2001; Lee and Liu, 2004), whereas classes 2, 3, 9 and 11 are absent from plants (Zhu and Dixit, 2012). During cell division, about three quarter of the kinesins in *Physcomitrella patens* localize at the spindle and/or the phragmoplast (Miki et al., 2014), but only one third of kinesins are upregulated during cell division in *Arabidopsis thaliana* (Vanstraelen et al., 2006).

Kinesin-12 members in both plants and animals possess a N-terminal motor domain and a signature neck linker sequence predicting plus end-directed motility (Figure 3A; Lee and Liu, 2000; Miki et al., 2005). Indeed, in animals, the *Xenopus* kinesin-12 XlKLP2 and its human orthologous Kif15 exhibits plus end-directed motility *in vitro* (Boleti et al., 1996; Sturgill et al., 2014). However, in plants there is no evidence for microtubule motility yet. The kinesin-12 class comprises six members in *Arabidopsis thaliana* (Figure 3B and 3C; Zhu and Dixit, 2012). The phragmoplast-associated kinesin-related protein 1 (PAKRP1/kinesin-12A) and PAKRP1-like protein (PAKRP1L, kinesin-12B) group into one cluster (Figure 3B). PAKRP1 and PAKRP1L localize to the plus ends of interdigitating microtubules in the phragmoplast midzone (Lee and Liu, 2000; Pan et al., 2004) and are required for cell plate formation in the male gametophyte (Lee et al., 2007). The kinesin-12 PHRAGMOPLAST ORIENTING KINESIN 1 (POK1) and POK2 function in the spatial control of cytokinesis (Müller et al., 2006) and cluster together with POK-like (Figure 3B). Interestingly, POK1 and POK2 are unusually large compared to other kinesins and feature an extended N-terminal region upstream of the motor domain (Figure 3C). Neither At3g44050 (POK-like), nor

At3g20150, the other members of the plant kinesin-12 class are characterized yet (Zhu and Dixit, 2012).

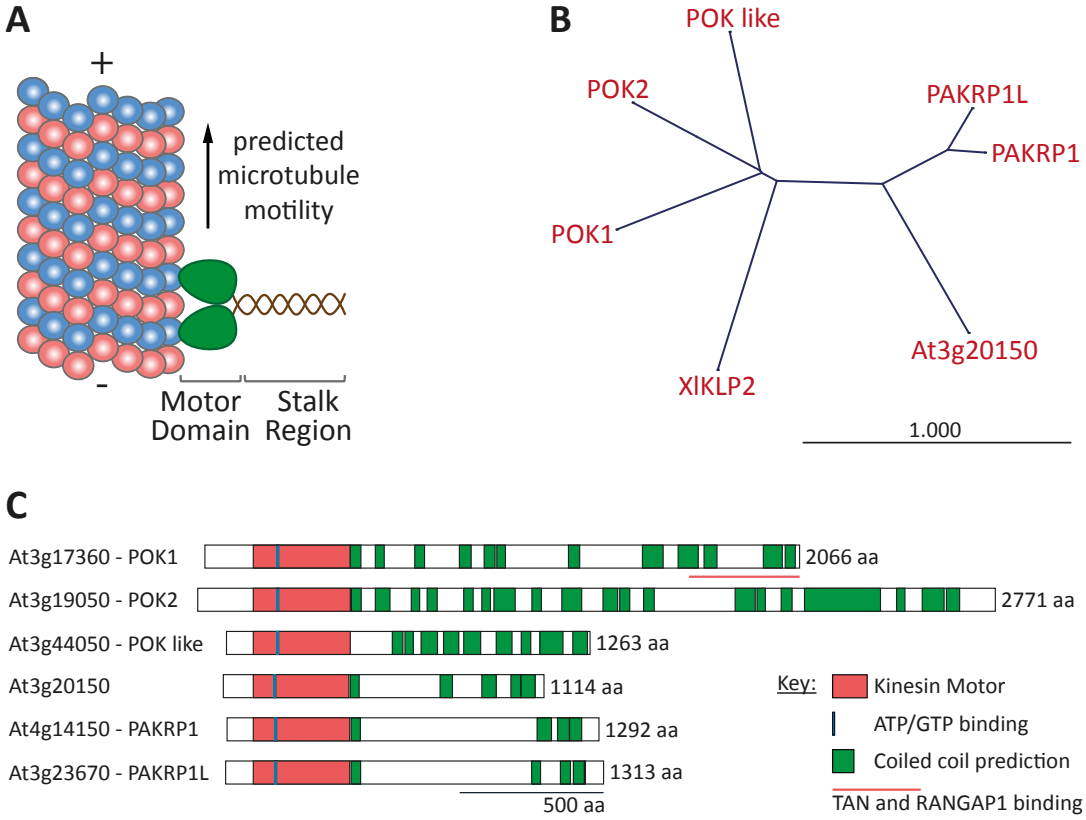

Figure 3: Kinesin-12 class motor proteins of *Arabidopsis thaliana*. Domain structure (motor domains are predicted by prosite (Sigrist et al., 2013) and coiled coil predictions by paircoil2 (cutoff: 0.025, 28 window) (McDonnell et al., 2006)) and phylogenetic tree (prepared with CLC main workbench, based on amino acid (aa) sequence).

3.3 Posttranslational tubulin modifications: cyclic detyrosination / tyrosination of α-tubulin

Posttranslational tubulin modifications (PTMs) confer a distinguishing label to microtubules, which is specifically recognized by MAPs to regulate microtubule dynamics and organization accordingly, in mammalian cells (Wloga and Gaertig, 2010). α-Tubulin and β-tubulin are target for the following posttranslational modifications, acetylation, polyglycylation, polyglutamylation, cyclic

detyrosination/tyrosination, phosphorylation and palmitoylation (Westermann and Weber, 2003). These PTMs occur at the tubulin C-terminus, which is exposed to the outside of the microtubule to interact with MAPs and kinesins (Figure 4; Westermann and Weber, 2003; Verhey and Gaertig, 2007). For instance, detyrosinated and tyrosinated microtubules are preferentially bound by kinesin-1 and +TIP protein, CLIP170, respectively (Hammond et al., 2008).

The reversible addition and removal of tyrosine at the C-terminus of α-tubulin is one of the best-characterized PTM. In the 1970s the reversible posttranslational addition of a C-terminal tyrosine in free tubulin dimers by the tubulin-tyrosine-ligase (TTL) and the removal by the tubulin carboxypeptidase (TCP) was described in mammalian cells (Figure 4A; Raybin and Flavin, 1975; Argarana et al., 1978; Barra et al., 1988). Antibodies against tyrosinated (Tyr-tub) and detyrosinated (Glu-tub) α-tubulin C-termini recognize different microtubule populations (Gundersen et al., 1984), but also microtubules that carry both, tyrosinated and detyrosinated α-tubulin isotypes (Geuens et al., 1986). Though a putative TTL homolog was identified in *Arabidopsis* (Gardiner and Marc, 2003), there is no report about a TCP specifically cleaving the C-terminal tyrosine in plants so far.

Nitric oxide signaling produces nitrotyrosine (N-Tyr), the nitrated form of the amino acid tyrosine (Abello et al., 2009), which is incorporated into the C-terminus of α-tubulin by the TTL (Eiserich et al., 1999). Structural modelling of the α-tubulin C-terminus of goosegrass (*Eleusine indica* (L.) Gaerth.) discloses that the nitrotyrosination of α-tubulin mediates conformational changes in its C-terminus. In particular, it is proposed, that N-Tyr substitution leads to an intermediate lifetime of microtubules between short time living, dynamic tyrosinated microtubules and long-lived, more stable detyrosinated microtubules (Blume, 2005). 3-Nitro-L-tyrosine (NO_2Tyr), an exogenous source for N-Tyr, co-localizes with PPBs, mitotic spindles and phragmoplasts of tobacco Bright Yellow (BY)-2 cells (Blume et al., 2013). Furthermore, upon NO_2Tyr treatment, supplied in the growth medium, the occurrence of detyrosinated α-tubulin forms is diminished in BY-2 cells (Jovanovic et al., 2010). As a result cell division is inhibited and oblique cross wall positioning is induced (Jovanovic et al., 2010). These findings suggest a role for PTMs, especially

the detyrosination/tyrosination state of α-tubulin in cell division, regulating the binding of specific effector proteins, which are required for proper spatial control of cytokinesis.

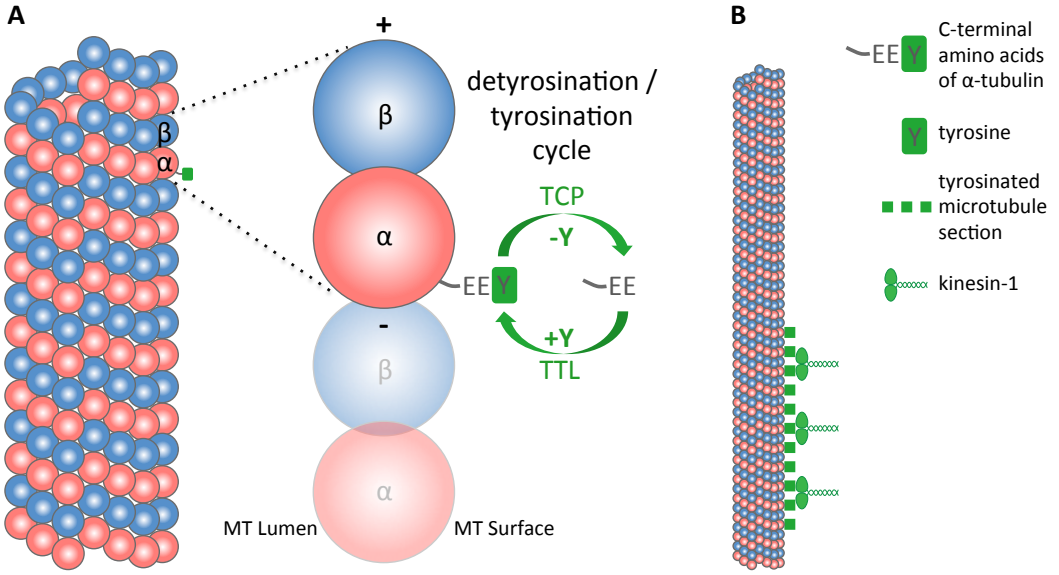

Figure 4: Posttranslational detyrosination/tyrosination of α-tubulin.

3.4 Establishment and Maintenance of the Division Plane in *Arabidopsis thaliana*

In preparation for cell division the nucleus enters a central position in the cell and microtubule organization changes (Müller, 2012). At the transition from G2 to M phase microtubules outside the forming preprophase band (PPB) display increased dynamic instability (Vos et al., 2004). As mentioned before, the PPB predicts the future cell plate insertion site and therefore is critical for division plane establishment. Mutants that fail to form PPBs show oblique cell plate insertion resulting in misshaped, dwarfed phenotypes as it is the case for *tonneau (ton) 2/fass* mutants and *ton1A ton1B* mutants (Torres-Ruiz and Jürgens, 1994; Traas et al., 1995; Camilleri et al., 2002; Azimzadeh et al., 2008). *TON2/FASS* encodes for the regulatory subunit of protein phosphatase 2A (PP2A) and is required for cortical microtubule organization and PPB formation (Camilleri et al., 2002). Together with TON1, TON2/FASS are components of the recently identified TTP (TON1/TRM/PP2A) multi-

protein complex, in which TONNEAU RECRUITING MOTIF (TRM) proteins direct PP2A activity to the cortical microtubule array enabling PPB formation (Figure 5; Spinner et al., 2013). However, the PPB disassembles upon nuclear envelope breakdown during prometaphase. Yet, the spatial information of the PPB is preserved throughout cell division by the cortical division zone (CDZ). Little is known about the molecular identity that is left behind by the PPB a t this plasma membrane region.

The first indication that a CDZ exists was conveyed by the localization pattern of F-actin, which is mostly absent from the CDZ region. This particular actin distribution was described as the actin depleted zone (ADZ) (Cleary, 1992). To date it is not clear whether the ADZ and the CDZ are a perfect match. However, the ADZ is flanked by actin twin peaks, readily visible in BY-2 cells (Sano et al., 2005). In the meantime in addition to the ADZ, several proteins have been identified as positive markers of the CDZ because of their specific localization. TANGLED (TAN), a highly basic protein, which binds to microtubules, was first characterized in maize (Smith et al., 2001). Mutation of *TAN* leads to oblique cell plate insertions in leave epidermis cells, pointing to TANs function in phragmoplast guidance (Smith et al., 1996). Interestingly, the *Arabidopsis* TAN homologue is recruited to the PPB in prophase and maintained at the CDZ throughout mitosis and cytokinesis (Figure 5; Walker et al., 2007; Rasmussen et al., 2011). In addition, Ran GTPase-activating protein 1 (RANGAP1) is reportedly a continuous marker of the CDZ (Figure 5; Xu et al., 2008). Loss of RANGAP1 function by knockout/knockdown mutant combinations of *RANGAP1* and *RANGAP2* also leads to oblique and incomplete cell walls (Xu et al., 2008). The localization and phenotypic mutant analysis of TAN and RANGAP1 point to their function in the maintenance of the division plane / CDZ. However, the retention of both proteins at the CDZ is dependent on the function of PHRAGMOPLAST ORIENTING KINESIN 1 (POK1) and POK2, since both TAN and RANGAP1 are lost in *pok1 pok2* double mutants (Müller et al., 2006; Walker et al., 2007; Xu et al., 2008). *POK1* and *POK2* encode for a pair of closely related kinesin-12 class proteins, which were identified as interaction partners of TAN (Müller et al., 2006) and are mainly expressed in meristematic tissues. The dwarfed phenotype of the *pok1 pok2* double mutant is due to mispositioned cell walls. In wild type, PPBs

are mainly oriented perpendicular to the cell axis, just like the orientation of the phragmoplast. Whereas *pok1 pok2* double mutants only rarely exhibit misplaced PPBs, the phragmoplast is frequently misoriented and tilted. These findings suggest a role for POK proteins in the spatial control of cytokinesis via maintenance of the CDZ and phragmoplast guidance (Müller et al., 2006) and indicate that POK localizes at the CDZ (Figure 5).

During cytokinesis, the CDZ is recognized by the phragmoplast. Coordinated microtubule depolymerization at the inner edge and polymerization at the leading edge allows centrifugal phragmoplast expansion towards the CDZ (Sasabe et al., 2006; Smertenko et al., 2011; Murata et al., 2013). During the progression of cytokinesis the CDZ narrows to precisely determine the cell plate insertion site, the cortical division site (CDS) (Lipka et al., 2015). The establishment, maintenance and recognition of the CDZ as a "hallmark" of the division plane is required for accurate cell plate integration and contribute to plant cells shape.

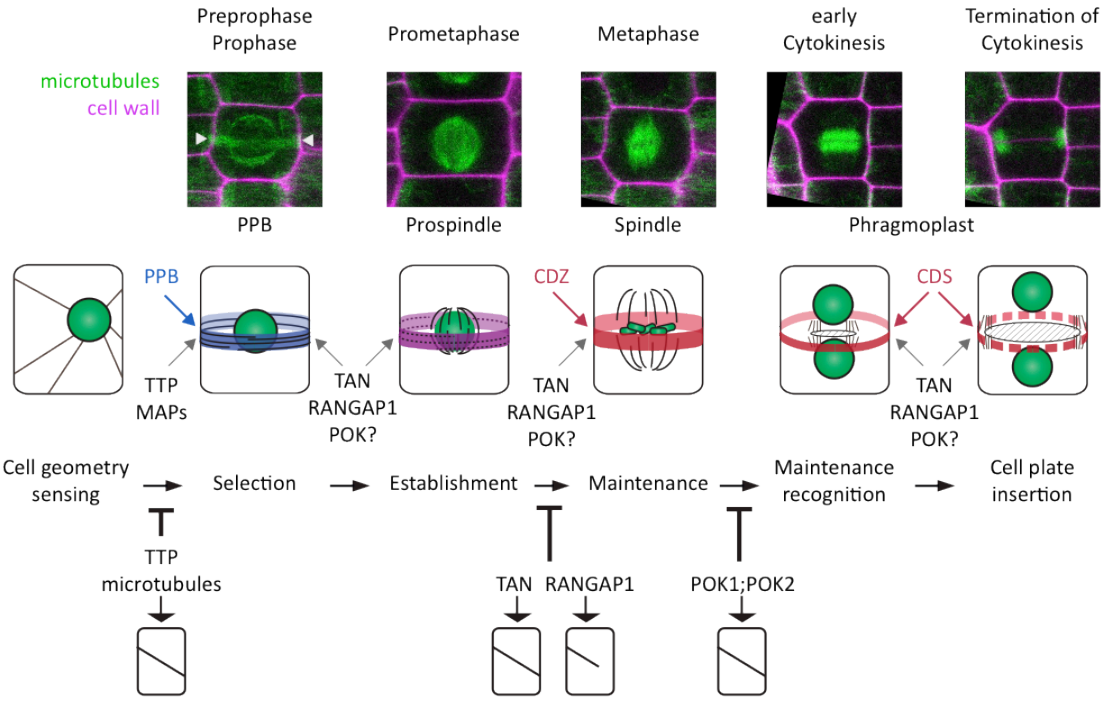

Figure 5: Plant cell division in *Arabidopsis thaliana.* Mitotic cell cycle stages are depicted in chronological order. A schematic overview of the establishment and maintenance of the cortical division zone (CDZ) is illustrated. Modified from (Lipka et al., 2015).

4. AIM OF THIS WORK

The aim of this project is to decipher the molecular contribution of POK motor proteins to the establishment, maintenance and recognition of the CDZ. As the morphology and the location of plant cells depends on the cell wall, the positioning of the new cell wall after division is quite critical and requires proper preservation of the division plane by the CDZ. POK motor proteins are suggested to maintain the CDZ, however, this molecular mechanism and their localization are unknown. This work attempts to functionally characterize POK proteins and therefore it is contributing to the further understanding of the molecular identity and function of the CDZ.

5. RESULTS AND DISCUSSION

5.1 Research articles

5.1.1 Establishment and maintenance of the cortical division zone requires the phragmoplast-orienting kinesin-12 class proteins

In the study "The Phragmoplast-Orienting Kinesin-12 Class Proteins Translate the Positional Information of the Preprophase Band to Establish the Cortical Division Zone in *Arabidopsis thaliana*", POK1 is identified as a novel continuous marker of the CDZ, adding a novel component to the molecular identity of the CDZ. Together with TAN and RANGAP1, POK proteins faithfully preserve the spatial information of the division plane throughout cell division.

A new mutant allele of *POK2* (*pok2-3*) containing a premature STOP codon was identified in screen for *pok1-1* enhancers. The resultant double mutant *pok1-1 pok2-3* displayed dramatic dwarfism. *Live cell* imaging revealed, that *pok1-1 pok2-3* mutant phragmoplasts lose their initial orientation during expansion and tilt. Phragmoplast organization does not seem to be altered, but phragmoplast expansion rate is mildly reduced. Although cytokinesis is prolonged in these mutants, the cell plate eventually fuses with the parental plasma membrane, indicating that

cell plate formation per se is not affected. Furthermore, we can learn that the entire parental cell wall is receptive for cell plate fusion all over. However, PPBs show normal orientation relative to the root axis, indicating that the selection of the division plane is not impaired in the *pok1-1 pok2-3* double mutant. Tilting of the phragmoplast leads to oblique cell wall positioning. In contrast, very similar phenotypes such as mis-positioned cell walls and severe dwarfism are also observed in TTP subunit mutants, that are impaired in PPB formation (Kirik et al., 2012; Spinner et al., 2013). The similarity of the mutant phenotypes of TTP subunit and *pok1 pok2* mutants further underpins the spatial relationship between the PPB and the phragmoplast..

The CDZ marker TAN-YFP co-localizes with the PPB in *pok1-1 pok2-3*, but in metaphase the signal disappears from the CDZ. Similarly, RANGAP1 localization to the PPB was intact in *pok1 pok2* mutants but also disappeared upon metaphase (Xu et al., 2008). Therefore TAN (Walker et al., 2007) as well as RANGAP1 (Xu et al., 2008) recruitment to the PPB is independent of POK while their maintenance is strictly dependent on POK, indicating that POKs are necessary for the maintenance of CDZ identity during cytokinesis.

A genomic YFP-POK1 fusion protein fully complements the double mutant phenotype. YFP-POK1 co-localizes with the PPB and is maintained at the CDZ throughout mitosis and cytokinesis just like TAN and RANGAP1. Fluorescence recovery after photobleaching (FRAP) experiments in combination with oryzalin induced microtubule depolymerization showed that YFP-POK1 is dynamically recruited from the cytosol to the PPB in prophase. In contrast, the maintenance of YFP-POK1 at the CDZ after PPB disassembly is stable and occurs independently of microtubules. How POK1 is anchored at the plasma membrane upon PPB disassembly is still unclear. Most likely CDZ anchoring requires the C-terminal tail domain of POK1, which is sufficient for CDZ localization.

The question remains how exactly the POKs are guiding the phragmoplast, whether they have an active role in attracting the phragmoplast or whether they serve merely as a positional cue. Microtubules nucleating from the phragmoplast, are transiently contacting the CDZ, most likely with their plus end. POK might bind those

microtubules mediated by its motor domain to guide phragmoplast expansion. Thereby, the conspicuous long stalk region of POKs might help to expose the motor domain far in the cytosol for microtubule binding. The POK motor domains share homology with kinesin-12 class proteins with predicted plus end motility (Lee and Liu, 2004; Müller et al., 2006; Lipka and Müller, 2012). But, so far there are no *in vitro* studies that have characterized the POK motors. Such characterization should yield valuable information about microtubule motility and the forces exerted by POK motor proteins. This information might help to device a model for the putative active phragmoplast guidance mechanism. However, the probable microtubule orientation rather calls for a minus end-directed kinesin at the CDZ to pull on those transient microtubules for phragmoplast guidance. This task might be fulfilled by the recently identified CDZ resident kinesin-like calmodulin-binding protein (KCBP), which shows minus end motility (Buschmann et al., 2015). Nevertheless, a force-balancing mechanism including plus- and minus-end directed motor proteins could also be required for phragmoplast guidance. The presence of predicted plus-end directed POK1 and minus-end directed KCBP certainly support this idea.

Alternatively, if POKs have only scaffolding functions, phragmoplast guidance might be accomplished by TAN, whose function is lost in the *pok1 pok2* double mutant. Bimolecular fluorescence complementation studies further confirmed the interaction of TAN with the C-terminal fragment $POK1_{1683\text{-}2066}$ *in planta* (Müller et al., 2006; Xu et al., 2008). The stabilization of TAN - $POK1_{1683\text{-}2066}$ interaction showed localization along filamentous structures, suggesting that the interaction initially occurs on microtubules. Therefore, POK1 together with TAN might stabilize the transient microtubules and thus the connection between the phragmoplast and the CDZ.

Another open question is the cell cycle dependent regulation of POK localization and dynamics. POK1 is only present during cell division, implicating rigid post-translational regulation of protein abundance. POK proteins contain several cyclin dependent kinase (CDK) consensus motifs (Lipka and Müller, 2012), suggesting that POKs might be phospho-regulated. Phospho-regulation of POK, potentially via CDKs and/or TON2-dependent protein phosphatase (PP) 2A, might be necessary to

promote changes from the dynamic state during its recruitment to the PPB, to the stable state at the CDZ.

Taken together, our data contribute to the elucidation of the molecular identity of the CDZ and extend our current understanding of how the positional information of the PPB is translated. Furthermore, the results provide a model for POK function, thus creating a basis for future studies.

5.1.2 Effects of NO_2-Tyr on division plane establishment of *Arabidopsis thaliana*

The intention of the study "Nitrosative stress triggers microtubule reorganization in *Arabidopsis thaliana*" was to investigate the effects of NO_2-Tyr on the position of the division plane. NO_2-Tyr treatment was found to induce oblique cross walls in BY-2 cells and it was suggested, that they occur, as a result of phragmoplast expansion defects (Jovanovic et al., 2010). Furthermore, the authors hypothesized that kinesins, required for proper phragmoplast guidance and cell plate formation, were preferentially interacting with detyrosinated microtubules, which in turn might be pronounced target of nitrotyrosination (Jovanovic et al., 2010). POK kinesins are involved in phragmoplast guidance and division plane positioning (Lipka et al., 2014). Therefore, POK proteins are suspected targets for nitrotyrosination of α-tubulin. Here we found, that long-term treatment with low concentration of NO_2-Tyr leads to mild cell wall positioning defects in *Arabidopsis thaliana* wild type seedlings. However, *pok1* and *pok2* single mutants as well as *pok1 pok2* double mutants showed growth reduction to the same extent as control seedlings, when treated with NO_2-Tyr. Apparently, POKs show no preference in microtubule binding with respect to detyrosination/tyrosination state of microtubules. Furthermore, no induction of cell wall mis-positioning could be observed in *pok* single and double mutants, stronger than the mild cell wall mis-positioning in wild type. In conclusion, phragmoplast expansion might not be impaired by NO_2-Tyr treatment and might not cause the oblique division planes. Oblique cell walls rather seem a plausible result of

microtubule disorganization affecting division plane selection, early before phragmoplast guidance and cell plate formation.

Upon NO_2Tyr treatment, disorganization of the cortical microtubule array is evident by the reduction of microtubule bundles and the random microtubule orientation angles. Nevertheless, in this *in vivo* study we could not observe dynamic differences caused by nitrotyrosinated microtubules (Blume, 2005). The dynamic changes might be too mild to be visualized with GFP-MBD fusion protein. Nevertheless, NO_2Tyr-induced microtubule disorganization evidently leads to the isotropic cell expansion in the elongation zone, comparable to expansion defects through oryzalin-induced microtubule depolymerization. In consequence of the disorganization of the cortical microtubule array in elongating cells, cellulose microfibrils are randomly organized, leading to non-polar cell expansion.

There is experimental evidence for NO_2-Tyr incorporation into plant microtubules (Blume, 2005; Jovanovic et al., 2010; Lozano-Juste et al., 2011; Blume et al., 2013). Furthermore, we showed that NO_2-Tyr treatment antagonized the effects of taxol and oryzalin on cortical microtubule array organization and cell morphogenesis, supporting the idea, that NO_2-Tyr is incorporated into microtubules. The C-terminus of α-tubulin might undergo conformational changes through the substitution of the C-terminal Tyr by NO_2-Tyr, which likely reduces the binding efficiency for taxol and oryzalin. The C-terminus of α-tubulin is target for different PTMs (Westermann and Weber, 2003). However, mutation of the C-terminal tyrosine to alanine does not interfere with the incorporation of α-tubulin into microtubules. In contrast, tyrosine224 within helix H7 of α-tubulin and close to the oryzalin binding pocket (Morrissette et al., 2004) appears to be crucial for microtubule incorporation.

Nitrotyrosinated microtubules, which are constituents of dynamic microtubules in all the mitotic arrays (Blume et al., 2013). Hence, NO_2-Tyr treatment inhibits cell division accompanied with a reduction of root growth rate. These effects occur in a concentration-dependent manner and were reversible in case of low NO_2-Tyr concentrations. The reversibility of the growth defects suggests the presence of a carboxypeptidase for the removal of the C-terminal bound NO_2-Tyr. This result conflicts with the proposed irreversible binding and blockage of a TCP (Eiserich et al.,

1999; Jovanovic et al., 2010). In contrast, high concentrations caused cell cycle arrest and reduction of the meristematic and the elongation zone. This dramatic disturbance of cellular functions could not be reversed. Our findings were recently confirmed (Blume et al., 2013).

In summary, we demonstrate that treatment with NO_2-Tyr affects organization of the microtubule cortical array and cell wall positioning in the *Arabidopsis thaliana* root meristem, likely caused by the interference with the detyrosination/tyrosination cycle. NO_2-Tyr is a natural intermediate of nitrosative stress in mammals as well as plants and is incorporated into a number of proteins including alpha tubulin (Eiserich et al., 1999; Lozano-Juste et al., 2011). NO_2-Tyr treatment could serve as a tool for the investigation of division plane establishment in respect to requirements of PTM state, microtubule organization and MAP interaction.

5.2 Review articles

The review articles “Potential roles for kinesins at the cortical division site” and “Mechanisms of plant cell division” focus on the recent findings of plant specific mechanisms underlying cell division, which were partly referred to in the introduction. “Potential roles for kinesins at the cortical division site” lists all the kinesins, with reported localization at the cortical division site or related mutant phenotypes and discusses their function and interaction with other mitosis-specific proteins. In “Mechanisms of plant cell division” we focused on the latest research literature regarding plant cell division. Along with positional cues for the determination of the division plane, early and late mechanisms for maintaining the plane of division are highlighted.

6. REFERENCES

Abello N, Kerstjens HA, Postma DS, Bischoff R (2009) Protein tyrosine nitration: selectivity, physicochemical and biological consequences, denitration, and proteomics methods for the identification of tyrosine-nitrated proteins. *Journal of proteome research* **8:** 3222-3238

Ambrose C, Allard JF, Cytrynbaum EN, Wasteneys GO (2011) A CLASP-modulated cell edge barrier mechanism drives cell-wide cortical microtubule organization in Arabidopsis. *Nature communications* **2:** 430

Argarana CE, Barra HS, Caputto R (1978) Release of [14C]tyrosine from tubulinyl-[14C]tyrosine by brain extract. Separation of a carboxypeptidase from tubulin-tyrosine ligase. *Molecular and cellular biochemistry* **19:** 17-21

Azimzadeh J, Nacry P, Christodoulidou A, Drevensek S, Camilleri C, Amiour N, Parcy F, Pastuglia M, Bouchez D (2008) Arabidopsis TONNEAU1 proteins are essential for preprophase band formation and interact with centrin. *The Plant cell* **20:** 2146-2159

Barra HS, Arce CA, Argarana CE (1988) Posttranslational tyrosination/detyrosination of tubulin. *Molecular neurobiology* **2:** 133-153

Bayley PM, Schilstra MJ, Martin SR (1990) Microtubule dynamic instability: numerical simulation of microtubule transition properties using a Lateral Cap model. *Journal of cell science* **95 (Pt 1):** 33-48

Blume YB, Krasylenko YA, Demchuk OM, Yemets AI (2013) Tubulin tyrosine nitration regulates microtubule organization in plant cells. *Frontiers in plant science* **4:** 530

Blume YBN, A. and Demchuk, O. (2005) Nitrotyrosination of plant α -tubulin: potential mechanisms of influence on cellular processes. *BMC Plant Biology*

Boleti H, Karsenti E, Vernos I (1996) Xklp2, a novel Xenopus centrosomal kinesin-like protein required for centrosome separation during mitosis. *Cell* **84:** 49-59

Bringmann M, Landrein B, Schudoma C, Hamant O, Hauser MT, Persson S (2012) Cracking the elusive alignment hypothesis: the microtubule-cellulose synthase nexus unraveled. *Trends in plant science* **17:** 666-674

Buschmann H, Dols J, Kopischke S, Pena EJ, Andrade-Navarro MA, Heinlein M, Szymanski DB, Zachgo S, Doonan JH, Lloyd CW (2015) Arabidopsis KCBP interacts with AIR9 but stays in the cortical division zone throughout mitosis via its MyTH4-FERM domain. *Journal of cell science* **128:** 2033-2046

Camilleri C, Azimzadeh J, Pastuglia M, Bellini C, Grandjean O, Bouchez D (2002) The Arabidopsis TONNEAU2 gene encodes a putative novel protein phosphatase 2A

regulatory subunit essential for the control of the cortical cytoskeleton. *The Plant cell* **14:** 833-845

Cleary ALG, B. E. S.; Wasteneys, G. O.; Hepler, P. K. (1992) Microtubule and F-actin dynamics at the division site in living Tradescantia stamen hair cells. *Journal of cell science* **103:** 977-988

Dhonukshe P, Gadella TW, Jr. (2003) Alteration of microtubule dynamic instability during preprophase band formation revealed by yellow fluorescent protein-CLIP170 microtubule plus-end labeling. *The Plant cell* **15:** 597-611

Dimitrov A, Quesnoit M, Moutel S, Cantaloube I, Pous C, Perez F (2008) Detection of GTP-tubulin conformation in vivo reveals a role for GTP remnants in microtubule rescues. *Science (New York, NY)* **322:** 1353-1356

Dixit R, Cyr R (2004) The cortical microtubule array: from dynamics to organization. *The Plant cell* **16:** 2546-2552

Eiserich JP, Estevez AG, Bamberg TV, Ye YZ, Chumley PH, Beckman JS, Freeman BA (1999) Microtubule dysfunction by posttranslational nitrotyrosination of alpha-tubulin: a nitric oxide-dependent mechanism of cellular injury. *Proceedings of the National Academy of Sciences of the United States of America* **96:** 6365-6370

Endow SA (1999) Determinants of molecular motor directionality. *Nature cell biology* **1:** E163-E167

Evans L, Mitchison T, Kirschner M (1985) Influence of the centrosome on the structure of nucleated microtubules. *The Journal of cell biology* **100:** 1185-1191

Fache V, Gaillard J, Van Damme D, Geelen D, Neumann E, Stoppin-Mellet V, Vantard M (2010) Arabidopsis kinetochore fiber-associated MAP65-4 cross-links microtubules and promotes microtubule bundle elongation. *The Plant cell* **22:** 3804-3815

Gardiner J, Marc J (2003) Putative microtubule-associated proteins from the Arabidopsis genome. *Protoplasma* **222:** 61-74

Geuens G, Gundersen GG, Nuydens R, Cornelissen F, Bulinski JC, DeBrabander M (1986) Ultrastructural colocalization of tyrosinated and detyrosinated alpha-tubulin in interphase and mitotic cells. *The Journal of cell biology* **103:** 1883-1893

Giddings TH, Jr., Staehelin LA (1988) Spatial relationship between microtubules and plasma-membrane rosettes during the deposition of primary wall microfibrils in Closterium sp. *Planta* **173:** 22-30

Goddard RH, Wick SM, Silflow CD, Snustad DP (1994) Microtubule Components of the Plant Cell Cytoskeleton. *Plant physiology* **104:** 1-6

Granger CL, Cyr RJ (2001) Spatiotemporal relationships between growth and microtubule orientation as revealed in living root cells of Arabidopsis thaliana transformed with green-fluorescent-protein gene construct GFP-MBD. *Protoplasma* **216:** 201-214

Green PB (1965) Pathways of cellular morphogenesis. A diversity in Nitella. *The Journal of cell biology* **27:** 343-363

Gundersen GG, Bulinski JC (1986) Microtubule arrays in differentiated cells contain elevated levels of a post-translationally modified form of tubulin. *European journal of cell biology* **42:** 288-294

Gundersen GG, Kalnoski MH, Bulinski JC (1984) Distinct populations of microtubules: tyrosinated and nontyrosinated alpha tubulin are distributed differently in vivo. *Cell* **38:** 779-789

Gundersen GG, Khawaja S, Bulinski JC (1987) Postpolymerization detyrosination of alpha-tubulin: a mechanism for subcellular differentiation of microtubules. *The Journal of cell biology* **105:** 251-264

Hammond JW, Cai DW, Verhey KJ (2008) Tubulin modifications and their cellular functions. *Current opinion in cell biology* **20:** 71-76

Hirokawa N, Noda Y, Tanaka Y, Niwa S (2009) Kinesin superfamily motor proteins and intracellular transport. *Nat Rev Mol Cell Bio* **10:** 682-696

Ho CM, Lee YR, Kiyama LD, Dinesh-Kumar SP, Liu B (2012) Arabidopsis microtubule-associated protein MAP65-3 cross-links antiparallel microtubules toward their plus ends in the phragmoplast via its distinct C-terminal microtubule binding domain. *The Plant cell* **24:** 2071-2085

Horio T, Murata T (2014) The role of dynamic instability in microtubule organization. *Frontiers in plant science* **5:** 511

Jovanovic AM, Durst S, Nick P (2010) Plant cell division is specifically affected by nitrotyrosine. *Journal of experimental botany* **61:** 901-909

Jürgens G (2005) Cytokinesis in higher plants. *Annual review of plant biology* **56:** 281-299

Kirik A, Ehrhardt DW, Kirik V (2012) TONNEAU2/FASS regulates the geometry of microtubule nucleation and cortical array organization in interphase Arabidopsis cells. *The Plant cell* **24:** 1158-1170

Kollman JM, Merdes A, Mourey L, Agard DA (2011) Microtubule nucleation by gamma-tubulin complexes. *Nature reviews Molecular cell biology* **12:** 709-721

Kost B, Mathur J, N.-H. C (1999) Cytoskeleton in plant development. *Current opinion in plant biology* **2:** 462–470

Lawrence CJ, Dawe RK, Christie KR, Cleveland DW, Dawson SC, Endow SA, Goldstein LSB, Goodson HV, Hirokawa N, Howard J, Malmberg RL, McIntosh JR, Miki H, Mitchison TJ, Okada Y, Reddy ASN, Saxton WM, Schliwa M, Scholey JM, Vale RD, Walczak CE, Wordeman L (2004) A standardized kinesin nomenclature. *Journal of Cell Biology* **167:** 19-22

Ledbetter MC, Porter KR (1963) A "MICROTUBULE" IN PLANT CELL FINE STRUCTURE. *The Journal of cell biology* **19:** 239-250

Ledbetter MC, Porter KR (1964) Morphology of Microtubules of Plant Cell. *Science (New York, NY)* **144:** 872-874

Lee YR, Li Y, Liu B (2007) Two Arabidopsis phragmoplast-associated kinesins play a critical role in cytokinesis during male gametogenesis. *The Plant cell* **19:** 2595-2605

Lee YR, Liu B (2000) Identification of a phragmoplast-associated kinesin-related protein in higher plants. *Current biology : CB* **10:** 797-800

Lee YR, Liu B (2004) Cytoskeletal motors in Arabidopsis. Sixty-one kinesins and seventeen myosins. *Plant physiology* **136:** 3877-3883

Lipka E, Gadeyne A, Stöckle D, Zimmermann S, De Jaeger G, Ehrhardt DW, Kirik V, Van Damme D, Müller S (2014) The Phragmoplast-Orienting Kinesin-12 Class Proteins Translate the Positional Information of the Preprophase Band to Establish the Cortical Division Zone in Arabidopsis thaliana. *The Plant cell* **26:** 2617-2632

Lipka E, Herrmann A, Mueller S (2015) Mechanisms of plant cell division. *Wiley interdisciplinary reviews Developmental biology*

Lipka E, Müller S (2012) Potential roles for Kinesins at the cortical division site. *Frontiers in plant science* **3:** 158

Lozano-Juste J, Colom-Moreno R, Leon J (2011) In vivo protein tyrosine nitration in Arabidopsis thaliana. *Journal of experimental botany* **62:** 3501-3517

MacNeal RK, Purich DL (1978) Stoichiometry and role of GTP hydrolysis in bovine neurotubule assembly. *The Journal of biological chemistry* **253:** 4683-4687

Margolis RL, Wilson L (1978) Opposite end assembly and disassembly of microtubules at steady state in vitro. *Cell* **13:** 1-8

McDonnell AV, Jiang T, Keating AE, Berger B (2006) Paircoil2: improved prediction of coiled coils from sequence. *Bioinformatics* **22:** 356-358

Miki H, Okada Y, Hirokawa N (2005) Analysis of the kinesin superfamily: insights into structure and function. *Trends Cell Biol* **15:** 467-476

Miki T, Naito H, Nishina M, Goshima G (2014) Endogenous localizome identifies 43 mitotic kinesins in a plant cell. *Proceedings of the National Academy of Sciences of the United States of America* **111:** E1053-1061

Mitchison T, Kirschner M (1984) Dynamic instability of microtubule growth. *Nature* **312:** 237-242

Morrissette NS, Mitra A, Sept D, Sibley LD (2004) Dinitroanilines bind alpha-tubulin to disrupt microtubules. *Mol Biol Cell* **15:** 1960-1968

Müller S (2012) Universal rules for division plane selection in plants. *Protoplasma* **249:** 239-253

Müller S, Han S, Smith LG (2006) Two kinesins are involved in the spatial control of cytokinesis in Arabidopsis thaliana. *Current biology : CB* **16:** 888-894

Murata T, Sano T, Sasabe M, Nonaka S, Higashiyama T, Hasezawa S, Machida Y, Hasebe M (2013) Mechanism of microtubule array expansion in the cytokinetic phragmoplast. *Nature communications* **4:** 1967

Nogales E, Wang HW (2006) Structural mechanisms underlying nucleotide-dependent self-assembly of tubulin and its relatives. *Current opinion in structural biology* **16:** 221-229

Palevitz BA (1987) Actin in the preprophase band of Allium cepa. *The Journal of cell biology* **104:** 1515-1519

Pan R, Lee YR, Liu B (2004) Localization of two homologous Arabidopsis kinesin-related proteins in the phragmoplast. *Planta* **220:** 156-164

Paredez AR, Somerville CR, Ehrhardt DW (2006) Visualization of cellulose synthase demonstrates functional association with microtubules. *Science (New York, NY)* **312:** 1491-1495

Pickett-Heaps JD, Northcote DH (1966) Organization of microtubules and endoplasmic reticulum during mitosis and cytokinesis in wheat meristems. *Journal of cell science* **1:** 109-120

Rasmussen CG, Sun B, Smith LG (2011) Tangled localization at the cortical division site of plant cells occurs by several mechanisms. *Journal of cell science* **124:** 270-279

Rasmussen CG, Wright AJ, Müller S (2013) The role of the cytoskeleton and associated proteins in determination of the plant cell division plane. *The Plant journal : for cell and molecular biology* **75:** 258-269

Raybin D, Flavin M (1975) An enzyme tyrosylating alpha-tubulin and its role in microtubule assembly. *Biochemical and biophysical research communications* **65:** 1088-1095

Reddy AS, Day IS (2001) Kinesins in the Arabidopsis genome: a comparative analysis among eukaryotes. *BMC genomics* **2:** 2

Sano T, Higaki T, Oda Y, Hayashi T, Hasezawa S (2005) Appearance of actin microfilament 'twin peaks' in mitosis and their function in cell plate formation, as visualized in tobacco BY-2 cells expressing GFP-fimbrin. *The Plant journal : for cell and molecular biology* **44:** 595-605

Sasabe M, Soyano T, Takahashi Y, Sonobe S, Igarashi H, Itoh TJ, Hidaka M, Machida Y (2006) Phosphorylation of NtMAP65-1 by a MAP kinase down-regulates its activity of microtubule bundling and stimulates progression of cytokinesis of tobacco cells. *Genes Dev* **20:** 1004-1014

Shaw SL, Kamyar R, Ehrhardt DW (2003) Sustained microtubule treadmilling in Arabidopsis cortical arrays. *Science (New York, NY)* **300:** 1715-1718

Sigrist CJ, de Castro E, Cerutti L, Cuche BA, Hulo N, Bridge A, Bougueleret L, Xenarios I (2013) New and continuing developments at PROSITE. *Nucleic acids research* **41:** D344-347

Smertenko AP, Piette B, Hussey PJ (2011) The Origin of Phragmoplast Asymmetry. *Current Biology* **21:** 1924-1930

Smith LG, Gerttula SM, Han S, Levy J (2001) Tangled1: a microtubule binding protein required for the spatial control of cytokinesis in maize. *The Journal of cell biology* **152:** 231-236

Smith LG, Hake S, Sylvester AW (1996) The tangled-1 mutation alters cell division orientations throughout maize leaf development without altering leaf shape. *Development (Cambridge, England)* **122:** 481-489

Spinner L, Gadeyne A, Belcram K, Goussot M, Moison M, Duroc Y, Eeckhout D, De Winne N, Schaefer E, Van De Slijke E, Persiau G, Witters E, Gevaert K, De Jaeger G, Bouchez D, Van Damme D, Pastuglia M (2013) A protein phosphatase 2A complex spatially controls plant cell division. *Nature communications* **4:** 1863

Stoppin-Mellet V, Fache V, Portran D, Martiel JL, Vantard M (2013) MAP65 coordinate microtubule growth during bundle formation. *PloS one* **8:** e56808

Sturgill EG, Das DK, Takizawa Y, Shin Y, Collier SE, Ohi MD, Hwang W, Lang MJ, Ohi R (2014) Kinesin-12 Kif15 Targets Kinetochore Fibers through an Intrinsic Two-Step Mechanism. *Current Biology* **24:** 2307-2313

Torres-Ruiz RA, Jürgens G (1994) Mutations in the FASS gene uncouple pattern formation and morphogenesis in Arabidopsis development. *Development (Cambridge, England)* **120:** 2967-2978

Traas J, Bellini C, Nacry P, Kronenberger J, Bouchez D, Caboche M (1995) Normal differentiation patterns in plants lacking microtubular preprophase bands. *Nature* **375:** 676-677

Vale RD, Fletterick RJ (1997) The design plan of kinesin motors. *Annual review of cell and developmental biology* **13:** 745-777

Vanstraelen M, Inze D, Geelen D (2006) Mitosis-specific kinesins in Arabidopsis. *Trends in plant science* **11:** 167-175

Verhey KJ, Gaertig J (2007) The tubulin code. *Cell cycle* **6:** 2152-2160

Verhey KJ, Hammond JW (2009) Traffic control: regulation of kinesin motors. *Nature reviews Molecular cell biology* **10:** 765-777

Vos JW, Dogterom M, Emons AMC (2004) Microtubules become more dynamic but not shorter during preprophase band formation: A possible "search-and-capture" mechanism for microtubule translocation. *Cell Motil Cytoskel* **57:** 246-258

Walker KL, Müller S, Moss D, Ehrhardt DW, Smith LG (2007) Arabidopsis TANGLED identifies the division plane throughout mitosis and cytokinesis. *Current biology : CB* **17:** 1827-1836

Wang HW, Nogales E (2005) Nucleotide-dependent bending flexibility of tubulin regulates microtubule assembly. *Nature* **435:** 911-915

Wasteneys GO (2002) Microtubule organization in the green kingdom: chaos or self-order? *Journal of cell science* **115:** 1345-1354

Waterman-Storer CM, Salmon ED (1997) Microtubule dynamics: treadmilling comes around again. *Current biology : CB* **7:** R369-372

Weisenberg RC (1972) Microtubule formation in vitro in solutions containing low calcium concentrations. *Science (New York, NY)* **177:** 1104-1105

Westermann S, Weber K (2003) Post-translational modifications regulate microtubule function. *Nature reviews Molecular cell biology* **4:** 938-947

Wick SM, Seagull RW, Osborn M, Weber K, Gunning BE (1981) Immunofluorescence microscopy of organized microtubule arrays in structurally stabilized meristematic plant cells. *The Journal of cell biology* **89:** 685-690

Wloga D, Gaertig J (2010) Post-translational modifications of microtubules. *Journal of cell science* **123:** 3447-3455

Xu XM, Zhao Q, Rodrigo-Peiris T, Brkljacic J, He CS, Müller S, Meier I (2008) RanGAP1 is a continuous marker of the Arabidopsis cell division plane. *Proceedings of the National Academy of Sciences of the United States of America* **105:** 18637-18642

Yoshida S, Barbier de Reuille P, Lane B, Bassel GW, Prusinkiewicz P, Smith RS, Weijers D (2014) Genetic control of plant development by overriding a geometric division rule. *Developmental cell* **29:** 75-87

Zhu C, Dixit R (2012) Functions of the Arabidopsis kinesin superfamily of microtubule-based motor proteins. *Protoplasma* **249:** 887-899

7. PUBLICATIONS

7.1 Research articles

7.1.1 The Phragmoplast-Orienting Kinesin-12 Class Proteins Translate the Positional Information of the Preprophase Band to Establish the Cortical Division Zone in *Arabidopsis thaliana*

Lipka, E., Gadeyne, A., Stockle, D., Zimmermann, S., De Jaeger, G., Ehrhardt, D.W., Kirik, V., Van Damme, D., and Müller, S. The Phragmoplast-Orienting Kinesin-12 Class Proteins Translate the Positional Information of the Preprophase Band to Establish the Cortical Division Zone in Arabidopsis thaliana. *The Plant Cell* **26**, 2617-2632 (2014).

Link: *http://www.plantcell.org/content/26/6/2617*

Title: The phragmoplast-orienting kinesin-12 class proteins translate the positional information of the preprophase band to establish the cortical division zone in Arabidopsis

Elisabeth Lipka[1], Astrid Gadeyne[2,3], Dorothee Stöckle[1], Steffi Zimmermann[1], Geert De Jaeger[2,3], David W. Ehrhardt[4], Viktor Kirik[5], Daniel Van Damme[2,3], Sabine Müller[1]*

[1] Center for Plant Molecular Biology, ZMBP, Developmental Genetics, University of Tübingen, 72076 Tübingen, Germany

[2] Department of Plant Systems Biology, VIB, Technologiepark 927, B-9052 Gent, Belgium

[3] Department of Plant Biotechnology and Bioinformatics, Ghent University, B-9052 Gent, Belgium

[4] Department of Plant Biology, Carnegie Institution for Science, Stanford, California 94305, USA

[5] School of Biological Sciences, Illinois State University, Normal, Illinois 61790, USA

Running title: Kinesin dependent phragmoplast guidance

* Corresponding author: Sabine Müller
Center for Plant Molecular Biology, ZMBP
Developmental Genetics
University of Tübingen
Auf der Morgenstelle 32
72076 Tübingen, Germany

13 pages

The author responsible for distribution of materials integral to the findings presented in this article in accordance with the policy described in the Instructions for Authors (www.plantcell.org) is: Sabine Müller (sabine.mueller@zmbp.uni-tuebingen.de)

Synopsis: Kinesin-12 class motor proteins at the cortical division site maintain cortical division site identity proteins for efficient guidance of the phragmoplast in late cytokinesis.

Abstract
The preprophase band (PPB) is a faithful but transient predictor of the division plane in somatic cell divisions. Throughout mitosis the PPBs positional information is preserved by factors that continuously mark the division plane at the cell cortex, the cortical division zone (CDZ), by their distinct spatio-temporal localization patterns. However, the mechanism maintaining these identity factors at the plasma membrane after PPB disassembly remain obscure.
The pair of kinesin-12 class proteins PHRAGMOPLAST ORIENTING KINESIN (POK) 1 and POK2 are key players in division plane maintenance. Here we show that POK1 is continuously present at the cell cortex, providing a spatial reference for the site formerly occupied by the PPB. FRAP analysis combined with microtubule-destabilization revealed dynamic microtubule-dependent recruitment of POK1 to the PPB during prophase, while POK1 retention at the cortical division zone in the absence of cortical microtubules appeared static.

POK function is strictly required to maintain the division plane identity factor TANGLED (TAN) post PPB disassembly, although POK1 and TAN recruitment to the PPB occur independently during prophase. Together our data suggest that POKs represent fundamental early anchoring components of the cortical division zone, translating and preserving the positional information of the PPB by maintaining downstream identity markers.

Introduction

The plant microtubule (MT) cytoskeleton demonstrates remarkable plasticity in its ability to form complex arrays characteristic of distinct cell cycle phases and required for specific cellular functions. In expanding interphase cells, parallel aligned cortical MTs guide cellulose synthase complexes along transverse trajectories and permit cell expansion in a perpendicular direction (Paredez et al., 2006). Furthermore, vascular plants developed a specialized cytoskeletal array aiding the correct positional execution of cytokinesis. Entry into mitosis is characterized by the preprophase band (PPB) (Pickett-Heaps and Northcote, 1966), an equatorial assembly of actin filaments and cortical MTs shaped by differential modulation of MT dynamic instability and selective MT stabilization in distinct regions of the cell cortex (Dhonukshe and Gadella, 2003; Vos et al., 2004). PPB formation requires the enzymatic action of a PP2A phosphatase holo-enzyme complex containing FASS as a regulatory B subunit, complexed with the helper/assembly proteins TON1a and b, which is targeted to the MTs via the Tonneau Recruitment Motif (TRM) proteins (Spinner & Gadyne et al., 2013). However, the PPB persists only transiently until pro-metaphase when its disassembly fuels the polymerization of spindle MT. After chromosome segregation and the subsequent condensation of daughter nuclei, the cytokinetic phragmoplast, a dual array of parallel-oriented MTs connecting at the cell division plane, evolves from the anaphase spindle remnants and assists in the synthesis of the cell plate, a *de novo* established membrane compartment generated by transport and fusion of endomembrane derived vesicles to the division plane, to bisect the daughter cells. The cell plate grows centrifugally and physically separates the daughter nuclei upon fusion with the plasma membrane at the end of plant cytokinesis. Intriguingly, the PPB anticipates the site of fusion between the cell plate and the parental cell wall despite the considerable time lag between the PPB's disassembly at pro-metaphase and the end of cytokinesis when the position of the PPB is converted into the actual cell plate position (Gunning and Wick, 1985).

The correlation between PPB position and the site of cell plate fusion led to the hypothesis that the PPB determines the plane of cell division and recruits molecules that serve as positional information to establish and maintain the cortical division zone (CDZ) identity throughout mitosis (reviewed in Rasmussen et al., 2013). However, the first proteins described to serve as a reference beyond PPB disassembly were negative markers such as F-actin (Mineyuki and Palevitz, 1990; Cleary et al., 1992) and later the *Arabidopsis* kinesin-14 KCA1, both characterized by their low protein abundance or deficiency at the CDZ (Sano et al., 2005, Vanstraelen et al., 2006). In *Arabidopsis* the microtubule binding protein TANGLED (TAN) and the Ran GTPase regulatory protein RanGAP1 both co-localized with the PPB and remained at the CDZ throughout mitosis (Walker et al., 2007; Xu et al., 2008). During the course of mitosis the CDZ seems to alter from an initially wide zone (the cortical division zone, CDZ) to a narrow site (cortical division site, CDS) at the end of cytokinesis (Van Damme, 2009). The initial recruitment of both TAN and RanGAP1 to the cell cortex requires PPB formation (Walker et al., 2007; Xu et al., 2008), whereas TAN residency at the CDZ/CDS post PPB disassembly does not require MTs (Walker

et al., 2007). In *Arabidopsis*, both TAN and RanGAP1 maintenance at the CDZ is abolished in a mutant background lacking a pair of kinesin-12 proteins, PHRAGMOPLAST ORIENTING KINESIN (POK) 1 and 2 (Walker et al., 2007; Xu et al., 2008). *Arabidopsis pok1 pok2* double mutants display severe cell wall positioning defects, reminiscent of the *Zea mays* (maize) *tan1* phenotype (Smith et al., 1996). The majority of phragmoplasts in the *pok1 pok2* double mutant do not correspond to a transverse orientation relative to the cell longitudinal axis, while PPBs were predominantly transverse with respect to the long axis of the cell supporting a role of POKs in the spatial control of cytokinesis (Muller et al., 2006). TAN and RanGAP1 have been shown to interact with the C-terminal domain of POK1 (Muller et al., 2006, Xu et al., 2008), suggesting that POK1, TAN and RanGAP1 are part of a functional module required for CDZ identity maintenance. The exact nature of this module remains however unclear due to the lack of positional information on the POK kinesins.

Here we provide novel insight into POK function by characterizing a novel *pok2* allele from a mutant screen for *pok1-1* enhancers. *In vivo* observations of the novel allele combination *pok1-1 pok2-3* revealed lengthy cytokinesis due to a reduced rate of phragmoplast expansion and frequent tilting of late phragmoplasts from their initial orientation. Nevertheless, fusion of the cell plate with the parental wall occurred at seemingly indiscriminate sites resulting in a highly dis-organized framework of cell walls, underpinning POKs role in an efficient phragmoplast guidance mechanism and the timely progression through cytokinesis.

Localization studies using a functional YFP-POK1 fusion protein showed that POK1 is recruited to the PPB and remains at the cortex throughout mitosis. Similar to TAN, POK1 initially marks the CDZ and its localization domain narrows down to the CDS prior to cell plate fusion with the parental plasma membrane. POK1 is progressively and dynamically loaded onto the PPB from the cytosol in prophase while its association with the plasma membrane at the CDZ following PPB degradation appears static. Throughout telophase, the ring-shaped localization narrows from an initial broad band to a sharp string like pattern that disappears shortly after cell plate fusion. In *pok1 pok2* mutants, the cortical division zone marker TAN disappeared from the CDZ upon entry into metaphase, emphasizing that the POK kinesins function as molecular anchors for other CDZ/CDS identity markers.

Results

POK1 and POK2 are required for guidance of the phragmoplast toward the cortical division site

Previously, we described two independent *pok1 pok2* double mutant allele combinations, with similar phenotypic defects differing predominantly in their growth rate (Müller et al., 2006). In a sensitized EMS-induced mutant screen to identify second site mutations in phenotypically wild-type looking *pok1-1* single mutants, we discovered a severe mutant reminiscent of previously characterized *pok1 pok2* double mutants. The novel mutant co-segregated with the *pok1-1* genotype (Supplemental Figure 1A, B online) and did not complement the *pok1 pok2* double mutant phenotype in test-crosses, suggesting that the mutation was located in *POK2*. Sequencing of *POK2* revealed a C to T substitution in exon 16, 2197 bp of the coding sequence downstream of the ATG (Figure 1A). The mutation resulted in a premature STOP codon predicted to obliterate about three quarters of the POK2 protein. The allele was designated *pok2-3*. Due to the close linkage of *POK1* and *POK2* on chromosome III, *pok2-3* single mutants were not accessible for analysis.

Overall, the *pok1-1 pok2-3* double mutant displayed an aggravated phenotype compared to the previously described allele combinations *pok1-1 pok2-1* and *pok1-2 pok2-2* (Supplemental Figure 1 A online, Müller et al., 2006). We reasoned that POK activity was further diminished in these plants and thus the novel mutant was used to expand on the *in vivo* characterization of POK function. The *pok1-1 pok2-3* seedlings displayed shorter and wider roots and hypocotyls and succulent leaves (Figure 1B and D). Mature plants were dwarfed similar to weak *ton2* alleles (Kirik et al., 2012; Spinner & Gadeyne et al., 2013), but in contrast to *ton2*, *pok1-1 pok2-3* mutants were fertile (Supplemental Figure 1A online). Double *pok1-1 pok2-3* mutants grew significantly shorter roots (Figure 1C) and displayed smaller leaves than *pok1-1 pok2-1* or *pok1-1* (Figure 1D). Although organ formation apparently was not affected, at the cellular level, cell division patterns were dramatically disturbed in *pok1-1 pok2-3* double mutants (Figure 1E right panel), compared to wild type and single mutant *pok1-1* root meristems (Figure 1E, left panel).

Previously, immuno-localization of tubulin in root squashes established that phragmoplasts in *pok1 pok2* did not expand in the direction of the former PPB (Muller et al., 2006). To investigate phragmoplast guidance *in vivo*, the MT reporter line GFP-MBD was introgressed into the *pok1-1 pok2-3* double mutants. As in *pok1-1 pok2-1* and *pok1-2 pok2-2* (Muller et al., 2006), PPB, spindles and phragmoplasts formed normally in the *pok1-1 pok2-3* double mutant root meristem cells (Supplemental Fig. 2 online). Time lapse recordings of phragmoplast expansion, encompassing the stage of spindle-to-phragmoplast transition until completion of phragmoplast disassembly, revealed that phragmoplasts frequently tilted (Figure 2A, 2B, 2D, Supplementary movies 1 and 2, Sup. Fig. 3A, B), and that the duration of cytokinesis was prolonged in *pok1-1 pok2-3* double mutants (Figure 2C). While in the wild type cytokinesis lasted 37 min ± 11 min (n= 24) on average, in the double mutant cytokinesis lasted on average 57 min ± 24 min (n = 17, *$P<0.05$*) (Figure 2C). In wild type meristems, optical sections through phragmoplasts typically display the transverse double layer of anti-parallel MTs connecting in the midzone (Figure 2A), which expands laterally throughout cytokinesis. In the wild type, periclinal root divisions, allowing a view of the phragmoplast torus/ring while it expands, occur with a very low frequency close to the root apical meristem as the *Arabidopsis* root contains a single layer of epidermal, cortical and endodermal tissue. Remarkably, 23% of cytokinetic cells in *pok1-1 pok2-3* double mutants displayed the phragmoplast ring-view (Figure 2D), while only 2.4% of cytokinetic cells in the wild type exhibited the phragmoplast ring, in agreement with altered division plane orientations in *pok1-1 pok2-3*.

To determine whether the rate of phragmoplast expansion contributed to the prolonged cytokinesis in the *pok1-1 pok2-3* double mutant, we compared the rate of phragmoplast expansion using kymograph analysis (Figure 2E and 2F). Regardless of the genotype, most phragmoplasts displayed an expansion asymmetry as reflected by varying inclines of the kymograph (Figure 2F, left panel). This demonstrated that lateral expansion of the phragmoplast did not occur at a steady velocity, also indicated by the high standard deviation (Figure 2G). Nevertheless, in *pok1-1 pok2-3* double mutants, the average expansion rate was moderately, but significantly reduced (0.18 ± 0.09 µm/min; *$P<0.02$, n = 22) compared to the wild type (0.21 ± 0.09 µm/min; n = 43) (Figure 2G), suggesting that slowing of the expansion rate in the double mutant contributes to the observed prolonged cytokinesis together with the frequent tilting of the phragmoplast.

POK1 interacts with TAN through its C-terminal domain and is required for TAN maintenance at the CDZ, but not for its recruitment

As previously reported, TAN maintenance at the CDZ requires POK function, while recruitment to the PPB occurred, although inefficient, in *pok1 pok2* mutants (Walker et al., 2007), in agreement with two distinct TAN protein domains mediating TAN recruitment to the CDZ before and after PPB disassembly (Rasmussen et al., 2011). To clarify the role of POKs in TAN recruitment, we analyzed TAN localization in the severe po*k1-1 pok2-3* allele combination (Figure 3). In the wild type, the majority of cells displaying either the PPB (95%, n = 19 cells), pro-spindle (100%, n = 6 cells), spindle (92%, n = 12 cells) or phragmoplast (98%, n = 43 cells) also contained associated cortical TAN-rings (Figure 3A to 3D). In contrast, the TAN recruitment in cells with PPBs (55%, n = 11 cells seemed less efficient or delayed, but not abolished in *pok1-1 pok2-3* double mutants, consistent with results from previous studies. Interestingly, the cortical association of TAN in cells containing pro-spindles was high (89%, n = 9 cells, Figure 3E), suggesting that POK function was not critically required for TAN localization at prophase. However, the percentage of TAN rings in cells displaying spindles in metaphase dropped to 19% (n = 16 cells, Figure 3F, G and I), indicating that binding of POK1 and TAN becomes essential during this cell cycle stage. Moreover, TAN rings were entirely absent from cells with phragmoplasts (0%, n =18 cells, Figure 3H) in *pok1 pok2* double mutants. This result further supports the partial POK-dependence of TAN at the PPB and the essential POK1-dependent maintenance of TAN following prophase. In addition, we showed *in planta* interaction of nYFP-POK1$_{1683\text{-}2066}$ and cYFP-TAN in *Arabidopsis* protoplasts using BiFC (Figure 3J and K), supporting that interaction between TAN and POK1 mediates TAN maintenance at the CDZ. In contrast to control experiments (Figure 3L to 3N), strong expressing protoplasts displayed a filamentous YFP pattern reminiscent of cortical MTs (Figure 3O), suggesting that stabilization of POK1 and TAN interaction increases their capacity for MT binding

POK1 localizes to the cortical division zone

We analyzed the localization pattern of a functional YFP-POK1 fusion (Supplemental Figure 1C, and D) in four- to six-day-old wild type seedlings (Figure 4, Sup. Fig. 3). Only a subset of meristematic cells displayed a fluorescent YFP-POK1 signal, suggesting cell cycle-controlled expression or degradation of POK1. POK1-expressing cells displayed distinct fluorescent patterns of broad bands, sharp bands or pairs of focused spots (Figure 4A) in single optical sections. Three-D reconstruction of confocal image stacks revealed that YFP-POK1 formed continuous rings at the cell cortex.

To correlate the distinct YFP-POK1 rings with the corresponding cell cycle stages, we co-expressed YFP-POK1 and the MT reporter RFP-MBD. In root and leaf meristems, YFP-POK1 rings were associated with mitotic cells exhibiting PPBs, spindles and phragmoplasts (Figure 4B, Supplemental Figure 4A and B online). The observed YFP-POK1 patterns were reminiscent of the ring-shaped localization observed for the two POK1 inter-actors TAN and RanGAP1, which both co-localize with the PPB and continuously mark the CDZ throughout mitosis (Walker et al., 2007; Xu et al., 2008).

The short C-terminal fragment POK1$_{1683\text{-}2066}$ shown to be sufficient to bind TAN (Müller et al., 2006 and this study) and RanGAP1 (Xu et al., 2008) fused to YFP (*Pro35S*:YFP-POK1$_{1683\text{-}2066}$, Figure 4C) accumulated mainly in aggregates in *Arabidopsis* root meristem cells (Supplemental Figure 4C online), constraining detection of a potential cortex localization.

Since POK1$_{1683-2066}$ showed substantial aggregation, we tested whether aggregation could be prevented by expressing longer fluorophore-tagged constructs of the POK1 C-term (*Pro35S:GFP-POK1$_{1213-2066}$*) and (*ProTP1:dTom-POK1$_{1265-2066,}$* Supplemental Figure 4D online). Both fusion proteins displayed a cell cycle-dependent subcellular localization pattern similar to the full-length YFP-POK1 and vastly diminished aggregation (Supplemental Figure 4E and 4F).

POK1 cortical recruitment shows cell phase-dependent dynamicity

To further characterize POK1 cortical recruitment, FRAP analysis was performed (Figures 5 and 6). In the *Arabidopsis* root meristem, epidermis cells in pro- and metaphase were selected based on the presence or absence of condensed nuclei in bright field. In transverse sections, YFP-POK1 localized to both lateral cell sides (Figure 5A to D). YFP-POK1 was specifically bleached at one side of the confocal section and migration of fluorescent signal into the bleached region was subsequently monitored. In prophase cells, fluorescence clearly recovered during the observation period (Figure 5A, 5C, 5E,). By contrast, metaphase YFP-POK1 fluorescence hardly recovered (Figure 5B, 5D, 5E), indicating a more dynamic YFP-POK1 recruitment or dispersal mechanism during prophase and a fairly static maintenance mechanism during subsequent cell cycle phases. The POK1 C-terminal fragment GFP-POK1$_{1213-2066}$ in BY-2 cells displayed differential dynamicity in FRAP experiments similar to YFP-POK1 in *Arabidopsis* (Figure. 6A to D). Also in prophase BY-2 cells, fluorescent signal recovered, although at a longer half time (Figure 6D) than YFP-POK1 (Figure 5E), while BY-2 metaphase cells displayed sluggish GFP-POK1$_{1213-2066}$ signal recovery similar to YFP-POK1. Due to the superior imaging accessibility, we clarified whether the initial recruitment of POK1 to the CDZ requires MTs, using BY-2 cells. Prophase cells expressing *ProS35:POK1$_{1213-2066}$-GFP* were treated with oryzalin and subjected to FRAP analysis. The oryzalin treatment completely abolished fluorescence recovery to the CDZ at prophase following photobleaching (n=6) (Figure 6E to L), suggesting the MT-dependent recruitment of POK1$_{1213-2066}$-GFP.

In *Arabidopsis*, a proportion of mitotic cells accumulated full-length YFP-POK1 signal in the cytoplasm, both in the absence and presence of YFP-POK1 cortical rings (Figure 4A, asterisk). We determined the proportion of cells containing cytoplasmic YFP-POK1 and/or YFP-POK1 at the CDZ for each cell cycle stage (Sup. Figure 4A). In the presence of PPBs, YFP-POK1 accumulates in the cytoplasm and progressively associates with the PPB and the CDZ in pro-metaphase, suggesting that YFP-POK1 is dynamically recruited to the CDZ. From metaphase until the termination of cytokinesis, the majority of YFP-POK1 was found to be associated with the CDZ. Taken together, our data suggest a cell cycle-dependent re-localization from cytoplasmic to cortical, CDZ/CDS resident YFP-POK1.

Similar to TAN (Walker et al., 2007, Rasmussen et al., 2011 and Sup. Fig. 4B, C) and RanGAP1 (Xu et al., 2008), the ring-shaped localization of POK1 narrowed during cytokinesis in BY-2 cells (Figure 6B, C, Supplemental Figure 5D, E) and *Arabidopsis* (Figure 5A and B) in a cell cycle progression-dependent manner. While the sharp punctate signal corresponds to the site of cell plate fusion, the CDS, the broad POK1 signal corresponded to the wider CDZ.

YFP-POK1 CDZ/CDS localization is independent of microtubules

To analyze the microtubule dependency of the subcellular YFP-POK1 localization, seedlings co-expressing YFP-POK1 and RFP-MBD were treated with the MT polymerization inhibitor oryzalin. The effect of oryzalin was visualized by the

depolymerization of RFP-MBD-labeled MTs. While mitotic MT arrays disappeared upon oryzalin treatment (Figure 5F and 5H), YFP rings associated with cells containing PPBs (Figure 5G), spindles or phragmoplasts prior to oryzalin treatment were still present after MT de-polymerization (Figure 5G and 5I and Table 1). In two instances, the PPB was not associated with a YFP-POK1 ring (Table 1, n = 10 PPBs), which is consistent with the progressive recruitment of POK1 to the CDZ during prophase. In addition to the YFP-POK1 rings present in cells with phragmoplasts (n=15), five more (sharp) YFP-POK1 rings associated with recently synthesized cell walls (Table 1), which we also frequently observed in untreated cells. Maintenance of cortical POK1 upon oryzalin treatment demonstrates the MT-independent maintenance of CDZ-resident YFP-POK1.
Taken together, these results suggest that dynamic POK1 is continuously recruited to the CDZ in a microtubule-dependent manner during prophase, most likely from a cytoplasmic pool that is depleted prior to metaphase. Upon PPB disassembly, POK1 becomes immobilized and its localization subsequently narrows as mitosis progresses likely involving a self-associating mechanism. Independently of POK function, TAN and RanGAP1 arrive at the PPB where they become tethered by a POK-dependent mechanism. Together these proteins constitute a modular hub to maintain the positional information of the division plane and to guide the phragmoplast during cytokinesis.

Discussion

The correlation between the orientation of the PPB and the direction of phragmoplast expansion is a long-standing dogma in plant cell biology (Gunning and Wick, 1985). Cell biological studies on cell cultures and the use of a variety of chemicals interfering with cytoskeletal organization/dynamics as well as mutant analysis demonstrated the causal relation of PPB position and guidance of the phragmoplast towards the site specified by the PPB (Torres-Ruiz and Jurgens, 1994; Traas et al., 1995; Smith et al., 1996; Camilleri et al., 2002; Sano et al., 2005). Yet the molecular mechanisms involved remain poorly characterized. In contrast, upstream processes such as auxin-dependent transcriptional control of local cell divisions, essential for embryonic patterning, are intensively studied (reviewed in Lau et al., 2012). For instance, the ectopic expression of the bHLH transcription factor TMO5 is sufficient to induce periclinal divisions (De Rybel et al., 2013).
The proteins TAN and the POK kinesin-12 proteins were implicated in phragmoplast guidance due to the mis-positioning of cell walls in the corresponding mutants with respect to the former PPB position (Smith et al., 1996; Muller et al., 2006), but how these proteins functionally interacted was unclear due to the lack of subcellular data regarding the POK kinesins. Our *in vivo* analysis confirmed the frequent mis-match of PPB and phragmoplast orientation in dividing *pok1 pok2* cells, showing that the POK kinesins function downstream of PPB formation and division plane determination. In contrast, in mutant alleles of microtubule associated proteins such as CLASP (Ambrose et al., 2007; Kirik et al., 2007), PP2A subunit mutants (Spinner & Gadeyne et al., 2013) and the putative membrane protein SABRE (Pietra et al., 2013), oblique cell walls and mis-guidance of the phragmoplast are a consequence of mis-positioning of the PPB or lack thereof and thus these proteins act upstream of the POKs.
Consistent with phragmoplast expansion in BY-2 cells (Buschmann et al., 2010), we determined distinct expansion velocities for the left and right edge of wild type and *pok1-1 pok2-3* phragmoplasts. The rate of phragmoplast expansion was diminished in *pok1-1 pok2-3* cytokinesis, but could not solely account for the difference with

respect to wild type cytokinesis duration. Tilting of the *pok1-1 pok2-3* phragmoplast contributes to the extended duration of *pok1-1 pok2-3* cytokinesis as well, since the tilted cell plate apparently does not follow the shortest distance rule (Rasmussen et al., 2013) in the absence of POK-dependent phragmoplast guidance. The postulated direct correlation of cytokinesis duration and cell size (Gorst et al., 1986) is consistent with this assumption.

The cell cycle-dependent association of POK1 with the CDZ/CDS closely resembles the localization of CDZ/CDS identity markers TAN and RanGAP1 (Walker et al., 2007; Xu et al., 2008). Interaction of POK1-Cterm with TAN as determined by BiFC (Figure 3) and the phenotype similarity of the maize mutant *tan* (Smith et al., 1996; Cleary and Smith, 1998) and the *pok1 pok2* double mutant in *Arabidopsis* further support a joint function of POK1 and TAN in the phragmoplast guidance mechanism.

POK1, TAN (Walker et al., 2007) and RanGAP1 (Xu et al., 2008) share the feature of narrowing from a broad towards a sharp ring during cytokinesis, suggesting that the proteins are co-regulated and/or act in a complex. POK1 seems to be particularly important for CDZ identity maintenance throughout mitosis, since both TAN (this study and Walker et al., 2007) as well as RanGAP1 (Xu et al., 2008) fail to remain present in *pok1 pok2* double mutants upon the metaphase/anaphase transition. Thus, the narrowing of TAN (Walker et al., 2007) and RanGAP1 (Xu et al., 2008) might reflect the narrowing of POK1 at the CDZ. With respect to TAN and RanGAP1 maintenance, POK1 provides a scaffolding function to retain CDZ resident proteins, thereby sustaining CDZ identity. Although the C-terminal $POK1_{1683-2066}$ is sufficient for TAN interaction, GFP-$POK1_{1683-2066}$ localization at the CDZ could not be unambiguously confirmed, in contrast to GFP-$POK1_{1213-2066}$, indicating that the necessary additional domain for efficient POK1 targeting to the PPB and CDZ lies directly upstream of $POK1_{1683-2066}$. With few exceptions, most kinesin class proteins act as homo- or heterodimers (Endow et al., 2010), mediated by multiple coiled coil domains, which are also predicted for POK1 and POK2 C-termini (Figure. 4C). Thus, the POK1C-terminal fusion proteins might associate with the PPB/CDZ through self-dimerization or with endogenous full-length POKs. Alternatively, the POK1C-terminal might be necessary and sufficient to recruit POK1 to the PPB and CDZ via interactions with yet unknown membrane-anchored binding partners.

Although the localization of POK2 was not directly investigated here, the rescue ability of the full-length YFP-POK1 fusion protein and the absence of aberrant single mutant phenotypes indicate functional redundancy of POK1 and POK2 and therefore also similarity in localization. In light of functional redundancy of POK1 and POK2, the aggravated phenotype of the novel *pok1-1 pok2-3* allele combination can be explained by the fact that some POK2 activity might still be present in previously described double mutants.

Genetic evidence suggests that TAN arrives at the PPB independently of POK1, and yet, both POK1 and TAN1 (Walker et al., 2007) recruitment to the PPB require an intact microtubule cytoskeleton. To clarify the sequence of independent recruitment events at the PPB, time-resolved *in vivo* co-localization studies of POK1, TAN and RanGAP1 proteins would proove useful, since genetic analysis in *Arabidopsis* is hampered by the lack of clear *tan* loss of function alleles as well as the pleiotropic phenotypes of *ran gap* double knock down mutants (Xu et al., 2008) and gametophytic lethality of *ran gap* double knock out mutants (Rodrigo-Peiris et al., 2011), respectively.

Based on homology of the motor domains, POK1 clusters with kinesin-12 class proteins, predicted to display MT plus end directed motility (Lee and Liu, 2004; Muller et al., 2006; Lipka and Muller, 2012). Although POK1 motor activity has not been

investigated, given its localization at the plasma membrane, it potentially contributes to the phragmoplast guidance mechanism by directly binding to peripheral phragmoplast MTs and exerting a motor-activity-related force. Alternatively, POK, together with TAN might simply function to stabilize outreaching MTs. Indeed, TAN is a highly basic protein that co-sedimented with MTs *in vitro* (Smith et al., 2001), showing that it has MT-binding capacities. In this hypothesis, the motor-activity required for orienting the phragmoplast might be delivered by phragmoplast-associated kinesins. Stabilization of the $POK1_{1683-2066}$ and TAN protein complex by reconstitution of YFP in the BiFC experiment drew the complex to filamentous cellular structures, closely resembling MTs, thus likely unmasking a normally transient interaction of the POK1-TAN protein complex with MTs (Figure 3). This observation raises the exciting possibility that the CDZ resident POK1-TAN complex might indeed stabilize transient interactions with phragmoplast emanating MTs that approach the CDS, to direct the phragmoplast/cell plate to its final destination.

Intriguingly, the localization pattern of POK1 is complementary to that of the cell cycle-regulated kinesin-14, KCA1 (Vanstraelen et al., 2006). KCA1 interacts with PPB-localized CDKA;1 (Vanstraelen et al., 2006), the MT severing protein katanin (Boutte et al., 2010) and the actin cytoskeleton (Suetsugu et al., 2010). *kca1 kca2* double mutants are primarily affected in chloroplast movement (Suetsugu et al., 2010). The predicted MT minus end directed motor activity of KCA1 seems well suited to accomplish a cortical pulling force to orient a mitotic MT array, similar to dynein, which is required for spindle/division plane orientation in animals (Kiyomitsu and Cheeseman, 2013). The complementary localization at the plasma membrane of two sets of kinesins leads to the intriguing hypothesis that the KCA and POK kinesin proteins might act antagonistically to position/guide mitotic MT arrays. However, the role of KCA1 in division plane orientation awaits further scrutiny.

The overall phenotype of *pok1-1 pok2-3* seedlings is strikingly similar to weak alleles of *ton2* (Kirik et al., 2012; Spinner & Gadeyne et al., 2013). Intriguingly, the POK-independent TAN and RanGAP1 recruitment to the CDZ correlates with the presence of TON2 at the CDZ, which disappears from the CDZ upon anaphase, as was shown for the TON2 homolog DCD1 in maize (Wright et al., 2009) and for *A. thaliana* TON1 and FASS (Spinner & Gadeyne et al., 2013). Interestingly, the MAPK cascade controlling MT turnover in the expanding phragmoplast is initiated by interaction of the HINKEL/At-NACK1 kinesin with the respective MAPKKK NPK1. Phosphorylation of both proteins by CDKs prevents their binding, while their dephosphorylation at the metaphase/anaphase transition is critically required for successful cytokinesis (Sasabe et al., 2011). Similarly, phospho-regulation might direct the anchoring of POK1 at the cell cortex upon PPB disassembly and/or control the binding of TAN and POK1 involving TON2-dependent dephosphorylation. Indeed, TAN is a potential target of phospho-regulation, as pharmacological inhibition of phosphatases as well as genetic interference with TON2 function prevented its cortical localization (Rasmussen et al., 2011, Walker et al., 2007).

In summary, we provide evidence for POK's critical function for the maintenance of CDZ/CDS identity. In a MT-dependent manner, dynamic POK1 is continuously recruited to the CDZ during prophase, most likely from a cytoplasmic pool that is depleted prior to metaphase. Upon its arrival at the CDZ, POK1 becomes immobilized and subsequently its localization narrows by a yet unknown mechanism as mitosis progresses (Figure 7). Independent from POK function, TAN and RanGAP1 arrive at the CDZ, where they become tethered by a POK-dependent mechanism possibly involving TON2-mediated dephosphorylation of TAN (Figure 7).

Together these proteins provide positional information of the division plane and might even actively participate in the phragmoplast guidance mechanism. However, at this point it still remains to be elucidated whether POKs are actively engaged in the phragmoplast guidance mechanism or whether their function is primarily a scaffolding activity to provide a spatial reference for CDZ components following PPB disassembly. Future studies are geared towards resolving these open questions.

Methods

Plant Material

Arabidopsis thaliana plants, accession Columbia, were used throughout the study unless otherwise indicated. SALK T-DNA insertion lines for *pok1-1, pok1-2, pok2-1* and *pok2-2*, as well as the double mutants *pok1-1pok2-1* and *pok1-2pok2-2* have been described previously (Muller et al., 2006). *Agrobacterium*-mediated transformation to create diverse transgene lines was performed according to (Clough and Bent, 1998).

Growth Conditions

For examination of mutant phenotypes and localization studies at the seedling stage, seedlings were grown on plates containing Murashige and Skoog basal medium (Sigma-Aldrich) and 1% agarose or agar. For reproduction and crossing, plants were grown in soil. Plates and pots were incubated at 20ºC–22ºC on a 16-h-light/8-h-dark cycle.

EMS mutagenesis and identification of *pok2-3*

Plants homozygous for the *pok1-1* mutation where imbibed in dH_2O, mutagenized with 0.3% ethylmethansulfonate overnight and thoroughly washed subsequently. Five-hundred M1 progeny were scored for short roots on standard MS medium plates and seeds were collected individually for each M1 plant. Among eight preselected M2 families, one segregated the *pok1-1 pok2-3* phenotype. We performed test crosses with *pok1-1 pok2-1* and since the progeny (n = 120) showed the *pok1 pok2* phenotype we concluded that *POK2* was mutated. Sequencing of the *POK2* locus identified a C to T substitution in exon 16 leading to a premature stop codon.

Microtubule marker line

The MT binding domain MBD contained in a Gateway® (Invitrogen) compatible destination vector pEG104-*Pro35S*:mCherry-MBD (Gutierrez et al., 2009) was recombined into pDONR207 (Invitrogen) by the BP clonase reaction. Subsequently, the LR reaction was performed with the destination vector *pUBN*:RFP containing the *Arabidopsis* Ubiquitin10 promoter (Grefen et al., 2010). Transgenic plant lines expressing XFP-MBD fusion protein have been used as a faithful MT marker (Marc et al., 1998; Gutierrez et al., 2009).

Generation of YFP-POK1 fusion protein

A recombineering-based approach was used to genetically insert the YFP tag at the 5' of *POK1.* All recombineering steps were essentially performed as described in (Tursun et al., 2009). In brief, recombineering primers (Supplemental Table 1 online) encoding 50 nt of POK1 homology arms immediately upstream and downstream of the ATG and about 50 nt of a plasmid pBALU6 (Tursun et al., 2009), containing a YFP and GalK cassette, were used to amplify the fluorophore and the GalK selection marker. The binary BAC 79I20 carrying the genomic region of *POK1* was transformed into *E. coli* strain SW105, which allowed homologous recombination

upon heat induction. Electro-competent SW105 containing BAC 79I20 were incubated at 42°C for 15 min to induce *λ red* recombinase and subsequently transformed with the PCR product amplified from the YFP-GalK cassette. Then cells were propagated for 3 h at 32°C and plated on galactose minimal medium. Colonies were streaked on McConkey indicator plates to screen for Galactokinase activity, which lead to changes in pH of the medium turning colonies pink. Positive clones were further analyzed by PCR for the integration of the cassette into the BAC. Selected clones were cultured in liquid medium and split after propagation. One aliquot was supplied with 1/100 volume of 10% Arabinose solution for induction of FLP recombinase to remove the GalK selection marker. Both aliquots were propagated for two additional hours before DNA was extracted. Induced and non-induced samples were analyzed by PCR with primers (Supplemental Table 1 online) flanking the recombination site. Clones where GalK was efficiently excised were sequence verified and used for transformation into Agrobacterium strain GV3101. After *Arabidopsis* transformation, five independent T1 lines were recovered on nutrient agar plates containing 0.05% phosphinotrycin, PPT) and T2 plants were inspected for YFP-POK1 localization. Two independent T2 lines showed YFP fluorescence and were selected for further analysis. Both lines rescued the *pok1 pok2* double mutant phenotype and showed an identical localization pattern of the YFP-POK1 fusion protein in Col and *pok1 pok2* rescue plants.

TAN with and without stop codon was amplified from full-length cDNA clones obtained from the RIKEN institute (pda14314) (primers are listed in Supplemental Table 2 online). Because these primers were flanked with the minimal attB sites, all PCR products were amplified with the full-length attB1F and attB2R primers (Supplemental Table 2 online) and cloned into pDONR221 via a Gateway BP reaction (Invitrogen). $POK1_{1213-2066}$ coding sequences with and without stop codon were amplified from entry clone pENTR-POK1 described in (Xu et al., 2008).

The dTom-$POK1_{1265-2066}$ fusion construct was created in the pK7m34GW vector (Karimi et al., 2007) using the dTomato coding sequence and the POK cDNA fragment corresponding to amino acids 1265-2066 (Supplemental Table 3 online) under control of the constitutive promoter from the At3g16640 gene (Berkowitz et al., 2008).

The short -terminal fragment $POK1_{1683-2066}$ was cloned into pENTR3C via EcoRI/XhoI from pAD-POK1C (Müller et al., 2006) and recombined with pEG104 (Earley et al., 2006) to create *Pro35S:YFP-POK1*$_{1683-2066.}$

Pro35S:RFP-MBD expressed in BY-2 cells was described elsewhere (Marc et al., 1998; Van Damme et al., 2004). Entry clones of $POK1C_{1213-2066}$, and TAN with stop codon (Supplemental Table 2 online were used in a single Gateway LR reaction with pK7WGF2 to generate N-terminal GFP fusion proteins. Entry clones of POK1C without stop codon were combined with pK7FWG2 to create C-terminal GFP fusion proteins.

Subcellular distribution fo YFP-POK1 signal (Supplemental Figure 5 online) was analyzed in indirect immuno-localization experiments using anti-GFP (Invitrogen) and anti-tubulin (YL1/2, Abcam) and secondary antibodies anti-rabbit-Alexa488 (Invitrogen) and anti-rat-Cy3 (Jackson Immuno Research).

Confocal imaging and image processing

Imaging was performed on a Leica SP2 equipped with a point scanner and a Leica SP8 confocal microscope equipped with a Resonant Scanner. A 63 x, N.A. = 1.20, water-immersion objective lens was used for image acquisition. YFP fluorescence was excited by the 514 nm laser line from an Argon/Krypton laser and detected with

a standard PTM on the SP2 or a HyD detector on the SP8 set to a detection window between 520 nm and 550 nm. RFP was excited with a 561 nm He/Ne laser and fluorescence was detected with a standard PMT or a HyD detector set at 570 nm to 650 nm. GFP was excited with a 488 nm laser line from an Argon/Krypton laser and detected with a PMT or a HyD detector at 500 nm to 550 nm.
BY-2 cells were imaged on an Olympus FV1000 inverted confocal microscope equipped with a water-corrected 60x objective (N.A.= 1.2) using a 488 nm laser excitation and a spectral detection bandwidth of 500-530 nm for EGFP and a 559 nm laser excitation together with a spectral detection bandwidth of 570-670 nm for RFP detection and with a Zeiss 710 inverted confocal microscope with the ZEN 2009 software package and equipped with a 63x water corrected objective (N.A. = 1.2). GFP was visualized using 488 nm laser excitation and 500-530 nm spectral detection; RFP was visualized using 458 nm laser excitation and 592-754 nm spectral detection.
Two-dimensional projections and three-dimensional reconstructions of Z stacks were generated with either ImageJ v.1.48a (http://rsb.info.nih.gov/ij/) or Leica LF Image processing. Color merges were carried out with NIH ImageJ v.1.48s or Adobe Photoshop CS5 v12.0.4 (Adobe Systems). Only linear adjustments to pixel values were applied.
To determine the duration of cytokinesis and the orientation of phragmoplasts (transverse versus torus view), a *pok1-1 pok2-3* segregating population derived from a cross with the GFP-MBD marker line described in Marc et al. (1998) was used. Time lapse imaging of cells displaying spindle stages was performed and continued throughout mitosis at 3 to 5 min intervals. Time intervals were shorter at the beginning of the time lapse to determine the transition from spindle to phragmoplast and at the end of cytokinesis, while longer interval times were chosen during phragmoplast expansion. The duration was timed from the spindle/phragmoplast transition until phragmoplast disassembly.
The rate of phragmoplast expansion was determined using kymograph analysis (Buschmann et al., 2010). We recorded time lapse images of cells displaying spindles or earlier cell cycle stages at 2.5 min intervals until the phragmoplast made contact with the cell wall. In ImageJ, the segmented line tool was used to select the distance for the measurement, spanning the diameter of the phragmoplast. To determine relative velocities and to visualize the narrowing of the POK1C or TAN localization at the CDZ, the ImageJ kymograph plugin (http://www.embl.de/eamnet/html/body_kymograph.html) was used. Based on these measurements, the velocities of phragmoplast expansion were calculating in Excel.

rBiFC

The ratiometric bimolecular fluorescence complementation Gateway compatible 2in1 System (Grefen and Blatt, 2012) was used to examine interaction between $POK1_{1683-2066}$ and TAN. ROP2 was used as a negative control since, like POK1, it localized to the plasma membrane. The potential binding partners were expressed under the control of the Pro35S promoter on the same plasmid, which also carries RFP as an internal expression control. The ratio between YFP and RFP is used to estimate interaction strength. The primers used to amplify the cDNA of binding partners are listed in Supplemental Table 2 online. Amplicons were cloned via the BP reaction into pDONR221-P1P4 or pDONr221-P2P3, respectively. The resulting entry clones were used in subsequent LR reactions with destination vector pBiFCt-2in1-NN. All steps were performed according to Grefen and Blatt, 2012. Protoplasts from *Arabidopsis thaliana* suspension culture were transformed with the pBiFCt-2in1-NN plasmids

according to (Schütze et al., 2009). YFP and RFP fluorescence were excited with 514 nm and 561 nm excitation wavelength by sequential scan using the Leica TCS SP8 resonant scanner and hybrid detector HyD2 set to 518 nm to 552 nm for YFP fluorescence and PMT4 set to 645 to 731 nm for RFP fluorescence. All images were taken at identical settings. Quantification of fluorescence intensity was performed in ImageJ. The segmented line tool, set to a 7.5 pixel width, was used to trace the protoplasts and mean fluorescence intensity was measured along this line. Calculation of mean YFP/RFP ratio and the graph were performed in Excel. The mCherry-ROP2 control was generated using CreLox according to Geldner et al., via recombination of *pUNI-ROP2* with pNIGL17 (Geldner et al., 2009). As localization control for TAN, the plasmid *pEZRK:TAN-YFP* described in Walker et al., 2007, was used.

BY-2 transformation

Stable BY-2 transformation was carried out as described before (Geelen and Inzé, 2001). BY-2 cell lines expressing two fluorescent constructs were created by consecutive super-transformation of single transformed lines. Stably transformed calli were screened for fluorescence and localization patterns of tagged proteins were confirmed by analyzing several independent transformants.

FRAP analysis

FRAP experiments for the POK1 C-terminal fragment GFP-POK1$_{1213\text{-}2066}$ were conducted on an Olympus FluoView1000 inverted confocal microscope. One pre bleach images was taken. A certain region of interest (ROI) was bleached for 10 s with 100% laser power. Subsequent images were taken every 60 s. BY-2 cells were mounted in a chambered cover glass system (Lab-Tek) in 1% low melting point agarose containing BY-2 medium.

The average fluorescence intensity of the bleached region (ROI1) was measured using ImageJ (I(t)). The position of ROI1 was adjusted manually during the time lapse to correct for cell drifting. The average intensity of a second ROI (ROI2) outside the cell was measured to compensate for background fluorescent signal (Ibase). Because Ibase approaches a constant value, we subtracted the average Ibase from I(t) to obtain the actual fluorescence intensity Ifrap(t) (I(t)-average(Ibase)=Ifrap(t)). To estimate the amount of photobleaching due to image acquisition, we measured the average intensity of the whole cell (ROI3). From these values we also subtracted the background signal (average Ibase). These values were set out in a scatter plot and fitted to a linear trendline, which allowed us to determine the theoretical reduction in fluorescence intensity due to image acquisition for each time point (Ibleach(t)).

To obtain a normalized value for fluorescence recovery (Inorm(t)), we first determined the ratio of fluorescence loss due to Image acquisition:

Ibleach(t=0)/Ibleach(t) (1)

Next, the remaining fluorescence intensity after photobleaching (Ifrap(post)) was set to zero and all intensity values were adjusted accordingly:

Ifrap(t)-Ifrap(post) (2)

Ifrap(t=0)-Ifrap(post) (3)

Finally, to obtain the normalized values for fluorescence recovery after photobleaching (Inorm(t)), the previous equations were combined as follows:

Inorm(t)=(1)*((2)/(3))

The average Inorm(t) (FRAP Figure 6D: prophase cells, n=4; metaphase cells, n=7; FRAP Figure 6L, n=6) was set out in a scatter plot using Sigmaplot 12. A single exponential regression with rise to a maximum (y=a*(1-exp(-b*t))) was fitted to the

data points. The half time ($t_{1/2}$) for fluorescence recovery was calculated using the above formula with the fluorescence intensity value corresponding to half of the fitted maximum recovery at the latest timepoint as y.
FRAP experiments of full-length YFP-POK1 were performed using 4- to 7-day-old seedlings expressing *ProPOK1*:YFPgPOK1 in the *pok1-1 pok2-3* background. Seedlings were mounted in water on solid half strength nutrient (0.5 x MS salt, 1.5% agar). Using the LEICa SP8, four pre-bleach images were taken, and then the selected region of interest (ROI1) was bleached with identical laser settings for each experiment. Fluorescent signal recovery was imaged at 60 s time intervals for 30 min. FRAP data analysis was performed as described for GFP-POK1C. The background was determined outside of the root (ROI2) and the average intensity of the whole cell (ROI3) was used to correct for photobleaching during image acquisition without trendline fitting.

Oryzalin treatment
Four- to five-day-old seedlings co-expressing YFP-POK1 and RFP-MBD were imaged and subsequently treated by exchanging mounting medium with 10 µM oryzalin solution. Fluorescence of cells that had PPBs, spindles or phragmoplasts and YFP-POK1 prior to oryzalin treatment were re-analyzed at 5 min intervals for 10 to 30 min. BY-2 cells were mounted in a chambered cover glass system (Lab-Tek). Cells were immobilized in a thin layer (1 mL) of BY-2 medium containing vitamins (Geelen and Inze 2001), 0.8-1% low-melting-point agarose (Invitrogen) and 10 µM oryzalin. BY-2 cells were imaged to the point where MT depolymerization was evident followed by FRAP analysis.

Accession Numbers
Sequence data from this article can be found in the Arabidopsis Genome Initiative or GenBank/EMBL databases under the following accession numbers: At3g17360, At3g19050, At3g05330.

Supplemental Data
The following materials are available in the online version of this article.
Supplemental Figure 1. Adult phenotype of *pok1 pok2* and rescue with YFP-POK1.
Supplemental Figure 2. Mitotic microtubule arrays in *pok1-1 pok2-3* mutants.
Supplemental Figure 3. Cell cycle progression.
Supplemental Figure 4. Subcellular localization of different fluorescent POK1-fusions.
Supplemental Figure 5. Subcellular distribution of YFP-POK1 signal in *Arabidopsis* mitotic cells.
Supplemental Figure 6. Examples of transient microtubules reaching from the phragmoplast towards the putative cortical division site.
Supplemental Table 1. Primers used for cloning full length YFP-POK1 and genotyping of *pok1-1*.
Supplemental Table 2. List of primers used for cloning 2in1 plasmids.
Supplemental Table 3. List of primers used for cloning.
Supplemental Movie 1. Time lapse of wild type cell division.
Supplemental Movie 2. Time lapse of *pok1-1 pok2-3* cell division.

Acknowledgements
We acknowledge the ABRC and NASC for distribution of seed used in this study. The instructive advice and provision of *E.coli* SW105 and the recombineering plasmid collection by Baris Tursun is gratefully acknowledged. We thank Dr. Christopher Grefen for advice and the rBiFC plasmids. We thank Daniela Daumüller, Phillip Reichert, Hs Lee, Richard Gavidia, Angela Kirik and Samantha Atkinson for help with data collection. We thank Katharina Brancato from the ZMBP Transformation service. We appreciate the support from the Department of Developmental Genetics lead by Prof. Gerd Jürgens. Funding for this work was provided by Deutsche Forschungsgemeinschaft grant to S.M. (DFG MU 3133/1-1) and by the National Institute of Health grant (1R15GM102839)-01A1 (VK)**.** AG was indebted to the Agency for Innovation by Science and Technology for a predoctoral fellowship.

Authors contributions: E.L, A.G., D.V.D, G.D.J, D.E., V.K. and S.M. designed the research; E.L., A.G., D.S., S.Z., D.V.D, V.K. and S.M. performed research; E.L., A.G., D.S, D.V.D, V.K. and S.M. analyzed data; D.V.D. and S.M. wrote the paper.

References

Ambrose, J.C., Shoji, T., Kotzer, A.M., Pighin, J.A., and Wasteneys, G.O. (2007). The *Arabidopsis* CLASP gene encodes a microtubule-associated protein involved in cell expansion and division. Plant Cell **19,** 2763-2775.

Berkowitz, O., Jost, R., Pollmann, S., and Masle, J. (2008). Characterization of TCTP, the Translationally Controlled Tumor Protein, from Arabidopsis thaliana. The Plant Cell Online **20,** 3430-3447.

Boutte, Y., Frescatada-Rosa, M., Men, S., Chow, C.M., Ebine, K., Gustavsson, A., Johansson, L., Ueda, T., Moore, I., Jurgens, G., and Grebe, M. (2010). Endocytosis restricts Arabidopsis KNOLLE syntaxin to the cell division plane during late cytokinesis. EMBO J **29,** 546-558.

Buschmann, H., Sambade, A., Pesquet, E., Calder, G., and Lloyd, C.W. (2010). Chapter 20 - Microtubule Dynamics in Plant Cells. In Methods in Cell Biology, C. Lynne and T. Phong, eds (Academic Press), pp. 373-400.

Camilleri, C., Azimzadeh, J., Pastuglia, M., Bellini, C., Grandjean, O., and Bouchez, D. (2002). The *Arabidopsis TONNEAU2* gene encodes a putative novel protein phosphatase 2A regulatory subunit essential for the control of the cortical cytoskeleton. Plant Cell **14,** 833-845.

Cleary, A.L., and Smith, L.G. (1998). The *Tangled1* gene is required for spatial control of cytoskeletal arrays associated with cell division during maize leaf development. Plant Cell **10,** 1875-1888.

Cleary, A.L., Gunning, B.E.S., Wasteneys, G.O., and Hepler, P.K. (1992). Microtubule and F-Actin Dynamics at the Division Site in Living Tradescantia Stamen Hair-Cells. J. Cell Sci. **103,** 977-988.

Clough, S.J., and Bent, A.F. (1998). Floral dip: a simplified method for Agrobacterium-mediated transformation of Arabidopsis thaliana. Plant J **16,** 735-743.

De Rybel, B., Möller, B., Yoshida, S., Grabowicz, I., Barbier de Reuille, P., Boeren, S., Smith, Richard S., Borst, Jan W., and Weijers, D. (2013). A bHLH Complex Controls Embryonic Vascular Tissue Establishment and Indeterminate Growth in Arabidopsis. Developmental cell **24,** 426-437.

Dhonukshe, P., and Gadella, T.W., Jr. (2003). Alteration of microtubule dynamic instability during preprophase band formation revealed by yellow fluorescent protein-CLIP170 microtubule plus-end labeling. Plant Cell **15,** 597-611.

Earley, K.W., Haag, J.R., Pontes, O., Opper, K., Juehne, T., Song, K., and Pikaard, C.S. (2006). Gateway-compatible vectors for plant functional genomics and proteomics. The Plant Journal **45,** 616-629.

Endow, S.A., Kull, F.J., and Liu, H. (2010). Kinesins at a glance. Journal of Cell Science **123,** 3420-3424.

Geelen, D.N.V., and Inzé, D.G. (2001). A Bright Future for the Bright Yellow-2 Cell Culture. Plant Physiology **127,** 1375-1379.

Gorst, J., Wernicke, W., and Gunning, B.E.S. (1986). Is the preprophase band a of microtubules a marker of organization in suspension-cultures. Protoplasma **134,** 130-140.

Grefen, C., and Blatt, M.R. (2012). A 2in1 cloning system enables ratiometric bimolecular fluorescence complementation (rBiFC). Biotechniques **53,** 311-314.

Grefen, C., Donald, N., Hashimoto, K., Kudla, J., Schumacher, K., and Blatt, M.R. (2010). A ubiquitin-10 promoter-based vector set for fluorescent protein tagging facilitates temporal stability and native protein distribution in transient and stable expression studies. Plant J **64,** 355-365.

Gunning, B.E.S., and Wick, S.M. (1985). Preprophase Bands, Phragmoplasts, and Spatial Control of Cytokinesis. J. Cell Sci., 157-179.

Gutierrez, R., Lindeboom, J.J., Paredez, A.R., Emons, A.M., and Ehrhardt, D.W. (2009). Arabidopsis cortical microtubules position cellulose synthase delivery to the plasma membrane and interact with cellulose synthase trafficking compartments. Nat Cell Biol **11,** 797-806.

Karimi, M., Depicker, A., and Hilson, P. (2007). Recombinational Cloning with Plant Gateway Vectors. Plant Physiology **145**, 1144-1154.

Kirik, A., Ehrhardt, D.W., and Kirik, V. (2012). TONNEAU2/FASS Regulates the Geometry of Microtubule Nucleation and Cortical Array Organization in Interphase Arabidopsis Cells. The Plant Cell **24,** 1158-1170

Kirik, V., Herrmann, U., Parupalli, C., Sedbrook, J.C., Ehrhardt, D.W., and Hülskamp, M. (2007). CLASP localizes in two discrete patterns on cortical microtubules and is required for cell morphogenesis and cell division in Arabidopsis. Journal of Cell Science **120,** 4416-4425.

Kiyomitsu, T., and Cheeseman, Iain M. (2013). Cortical Dynein and Asymmetric Membrane Elongation Coordinately Position the Spindle in Anaphase. Cell **154,** 391-402.

Lau, S., Slane, D., Herud, O., Kong, J., and Jürgens, G. (2012). Early Embryogenesis in Flowering Plants: Setting Up the Basic Body Pattern. Annual Review of Plant Biology **63,** 483-506.

Lee, Y.R., and Liu, B. (2004). Cytoskeletal motors in Arabidopsis. Sixty-one kinesins and seventeen myosins. Plant Physiol **136,** 3877-3883.

Lipka, E., and Muller, S. (2012). Potential roles for Kinesins at the cortical division site. Front Plant Sci **3,** 158.

Marc, J., Granger, C.L., Brincat, J., Fisher, D.D., Kao, T., McCubbin, A.G., and Cyr, R.J. (1998). A GFP-MAP4 reporter gene for visualizing cortical microtubule rearrangements in living epidermal cells. Plant Cell **10,** 1927-1940.

Mineyuki, Y., and Palevitz, B.A. (1990). Relationship between Preprophase Band Organization, F-Actin and the Division Site in Allium - Fluorescence and

Morphometric Studies on Cytochalasin-Treated Cells. Journal of Cell Science **97,** 283-295.

Müller, S., Han, S., and Smith, L.G. (2006). Two kinesins are involved in the spatial control of cytokinesis in Arabidopsis thaliana. Curr Biol **16,** 888-894.

Paredez, A.R., Somerville, C.R., and Ehrhardt, D.W. (2006). Visualization of cellulose synthase demonstrates functional association with microtubules. Science **312,** 1491-1495.

Pickett-Heaps, J.D., and Northcote, D.H. (1966). Organization of microtubules and endoplasmic reticulum during mitosis and cytokinesis in wheat meristems. J Cell Sci **1,** 109-120.

Pietra, S., Gustavsson, A., Kiefer, C., Kalmbach, L., Hörstedt, P., Ikeda, Y., Stepanova, A.N., Alonso, J.M., and Grebe, M. (2013). Arabidopsis SABRE and CLASP interact to stabilize cell division plane orientation and planar polarity. Nature communications **4,** doi: 10.1038/ncomms3779

Rasmussen, C.G., Sun, B., and Smith, L.G. (2011). Tangled localization at the cortical division site of plant cells occurs by several mechanisms. J Cell Sci **124,** 270-279.

Rasmussen, C.G., Wright, A.J., and Müller, S. (2013). The role of the cytoskeleton and associated proteins in determination of the plant cell division plane. The Plant Journal **75,** 258-269.

Rodrigo-Peiris, T., Xu, X.M., Zhao, Q., Wang, H.-J., and Meier, I. (2011). RanGAP is required for post-meiotic mitosis in female gametophyte development in Arabidopsis thaliana. Journal of Experimental Botany **62,** 2705-2714.

Sano, T., Higaki, T., Oda, Y., Hayashi, T., and Hasezawa, S. (2005). Appearance of actin microfilament 'twin peaks' in mitosis and their function in cell plate formation, as visualized in tobacco BY-2 cells expressing GFP-fimbrin. Plant J **44,** 595-605.

Sasabe, M., Boudolf, V., De Veylder, L., Inzé, D., Genschik, P., and Machida, Y. (2011). Phosphorylation of a mitotic kinesin-like protein and a MAPKKK by cyclin-dependent kinases (CDKs) is involved in the transition to cytokinesis in plants. Proceedings of the National Academy of Sciences **108,** 17844-17849.

Schütze, K., Harter, K., and Chaban, C. (2009). Bimolecular Fluorescence Complementation (BiFC) to Study Protein-protein Interactions in Living Plant Cells. In Plant Signal Transduction, T. Pfannschmidt, ed (Humana Press), pp. 189-202.

Smith, L.G., Hake, S., and Sylvester, A.W. (1996). The tangled-1 mutation alters cell division orientations throughout maize leaf development without altering leaf shape. Development **122,** 481-489.

Spinner, L., Gadeyne, A., Belcram, K., Goussot, M., Moison, M., Duroc, Y., Eeckhout, D., De Winne, N., Schaefer, E., Van De Slijke, E., Persiau, G., Witters, E., Gevaert, K., De Jaeger, G., Bouchez, D., Van Damme, D., and Pastuglia, M. (2013). A protein phosphatase 2A complex spatially controls plant cell division. Nature communications **4,** 1863.

Suetsugu, N., Yamada, N., Kagawa, T., Yonekura, H., Uyeda, T.Q.P., Kadota, A., and Wada, M. (2010). Two kinesin-like proteins mediate actin-based chloroplast movement in Arabidopsis thaliana. Proceedings of the National Academy of Sciences **107,** 8860-8865.

Torres-Ruiz, R.A., and Jurgens, G. (1994). Mutations in the FASS gene uncouple pattern formation and morphogenesis in Arabidopsis development. Development **120,** 2967-2978.

Traas, J., Bellini, C., Nacry, P., Kronenberger, J., Bouchez, D., and Caboche, M. (1995). Normal differentiation patterns in plants lacking microtubular preprophase bands. Nature **375,** 676-677.

Tursun, B., Cochella, L., Carrera, I., and Hobert, O. (2009). A toolkit and robust pipeline for the generation of fosmid-based reporter genes in C. elegans. PLoS One **4,** e4625.

Van Damme, D. (2009). Division plane determination during plant somatic cytokinesis. Current Opinion in Plant Biology **12,** 745-751.

Van Damme, D., Van Poucke, K., Boutant, E., Ritzenthaler, C., Inze, D., and Geelen, D. (2004). In vivo dynamics and differential microtubule-binding activities of MAP65 proteins. Plant Physiol **136,** 3956-3967.

Vanstraelen, M., Van Damme, D., De Rycke, R., Mylle, E., Inze, D., and Geelen, D. (2006). Cell cycle-dependent targeting of a kinesin at the plasma membrane demarcates the division site in plant cells. Curr Biol **16,** 308-314.

Vos, J.W., Dogterom, M., and Emons, A.M. (2004). Microtubules become more dynamic but not shorter during preprophase band formation: a possible "search-and-capture" mechanism for microtubule translocation. Cell Motil Cytoskeleton **57,** 246-258.

Walker, K.L., Muller, S., Moss, D., Ehrhardt, D.W., and Smith, L.G. (2007). Arabidopsis TANGLED identifies the division plane throughout mitosis and cytokinesis. Curr Biol **17,** 1827-1836.

Wright, A.J., Gallagher, K., and Smith, L.G. (2009). discordia1 and alternative discordia1 function redundantly at the cortical division site to promote preprophase band formation and orient division planes in maize. Plant Cell **21,** 234-247.

Xu, X.M., Zhao, Q., Rodrigo-Peiris, T., Brkljacic, J., He, C.S., Muller, S., and Meier, I. (2008). RanGAP1 is a continuous marker of the Arabidopsis cell division plane. Proc Natl Acad Sci U S A **105,** 18637-18642.

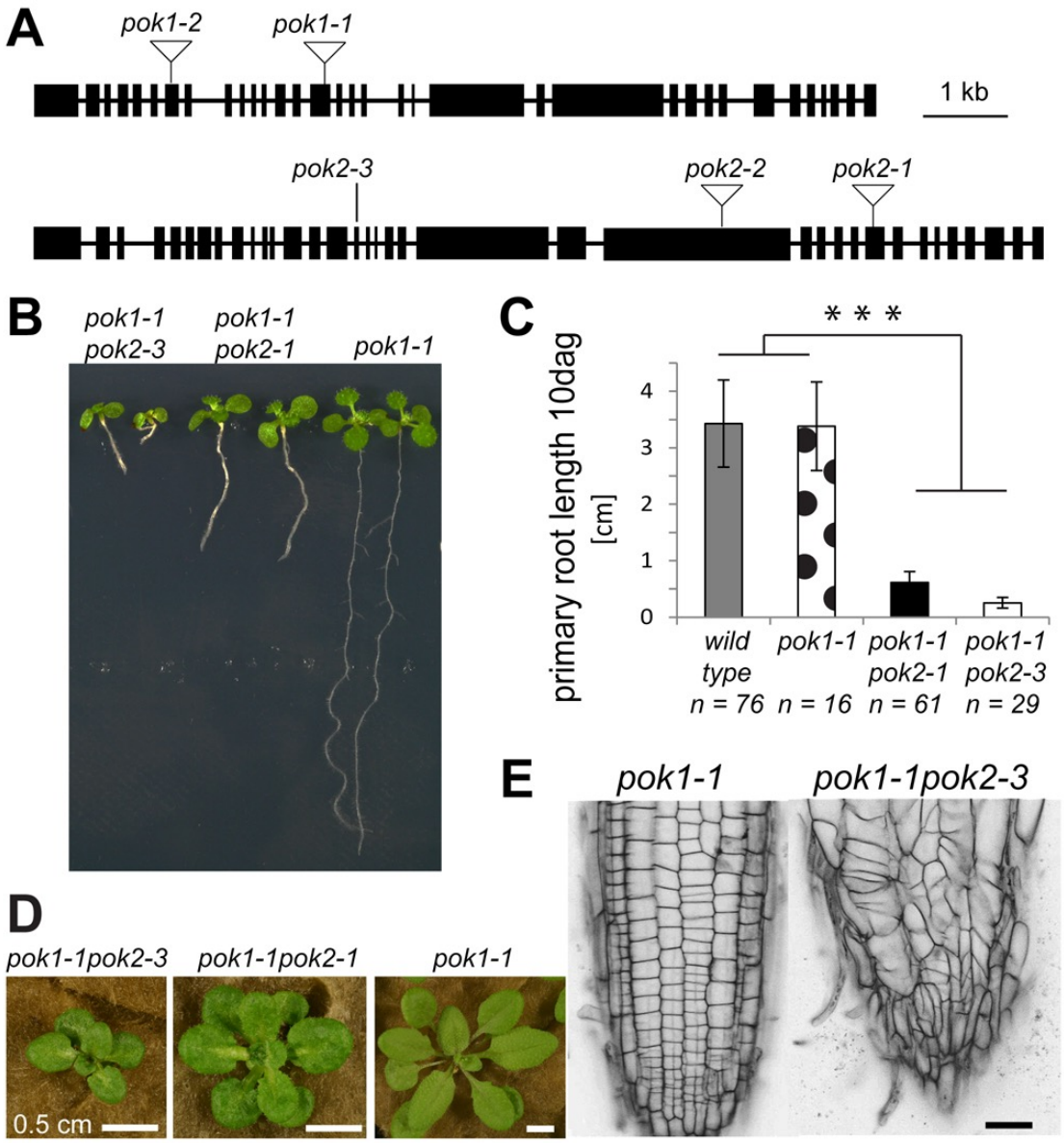

Figure 1: Mutant alleles and mutant phenotypes. (A) Schematic representation of *POK1* and *POK2* gene structure and position of mutations. SALK-TDNA insertions in alleles *pok1-1* (exon 15), *pok1*-2 (exon 7), *pok2-1* (exon 28) and *pok2-2* (exon 23) are indicated by triangles. The ethylmethansulfonate induced nonsense mutation in allele *pok2-3* is a C to T substitution (exon 16, at position 3845 bp), causing a premature Stop at amino acid 733 (Gln to *). Bars indicate exons. (B) Seedling phenotypes of (right to left) the *pok1-1* single mutant, *pok1-1 pok2-1* double mutant and *pok1-1 pok2-3* double mutant. (C) Comparison of average primary root length 10 days after germination (dag). Grey bar indicates wild type (3.4 cm ± 0.8), dotted bar indicates *pok1-1* (3.4 cm ± 0.8), black bar indicates *pok1-1pok2-1* (0.6 cm ± 0.2), grey bar indicates *pok1-1pok2-3* (0.25 cm ± 0.09). The average root length of *pok1-1 pok2-1* and *pok1-1 pok2-3* is significantly (***$P<<0.005$, Student's *t*-test) shorter than in wild type and *pok1-1*. Number of samples (n) is indicated. Error bars indicate ± SD. (D) Comparison of rosettes of three-week-old *pok1-1* single mutant, *pok1-1 pok2-3* double mutant and *pok1-1 pok2-1* double mutant plants. (E) Root meristems, stained with propidium Iodide to visualize cell walls. Whereas the *pok1-1* single mutant (left) shows a regular cell pattern of the root cell files, the *pok1-1 pok2-3* double mutant (right) cell pattern is completely disorganized. The scale bar in (B) equals 0.5 cm and 20 µm in (E).

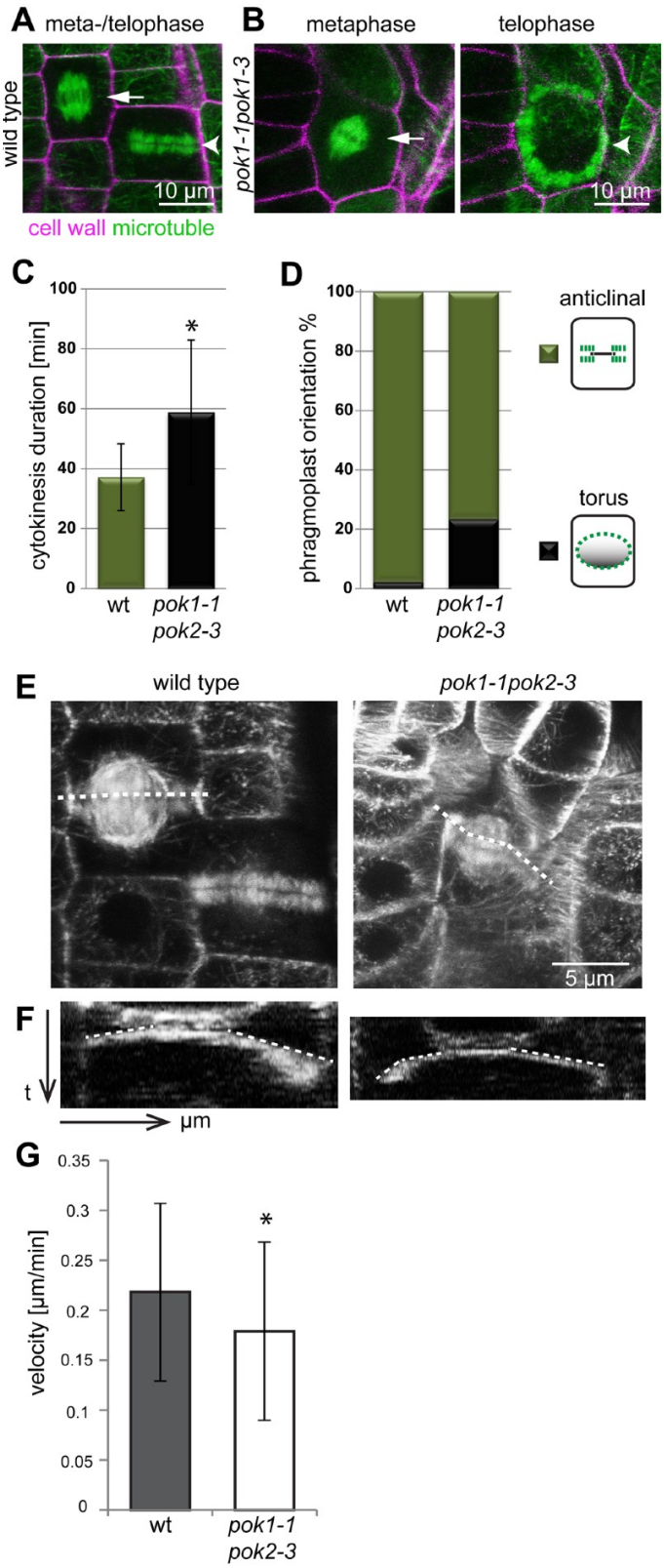

Figure 2: Duration of cytokinesis and orientation of phragmoplast expansion. Orientation of spindles (arrows) and phragmoplasts (arrowheads). (A) A wild type spindle and phragmoplast in a characteristic anticlinal orientation, with the phragmoplast expanding towards the lateral cell walls, perpendicular to the optical plane. (B) A *pok1-1pok2-3* mutant cell in metaphase (spindle) and the same cell during cytokinesis (phragmoplast). The spindle is slightly tilted. The phragmoplast expands in an oblique or periclinal orientation, thus presenting its torus. (C) The duration of phragmoplast expansion is significantly extended in *pok1-1 pok2-3* mutants (58 min ± 24, **P>0.01*, n= 17) compared to the wild type (wt, 37 min ± 11, n = 24). (D) In the wild type (wt, n = 49) 97.96% of the observed phragmoplasts displayed anticlinal orientation and only 2.04% were oriented with their torus parallel to the optical plane. In contrast, in *pok1-1 pok2-3* mutants (n = 43) the proportion of phragmoplasts presenting the torus (ring view) rises to 23.26%. (E) Projection of a time series throughout mitosis for wild type (45 min, 19 image stacks) and *pok1-1 pok2-3* mutants (60 min, 25 images). At 2.5 min intervals, image stacks were taken from mitotic cells at 1 µm z-intervals throughout the duration of mitosis. Maximum z-projections of each time point were projected for the depicted images. The white dotted lines indicate the selection for the kymograph analysis. (F) Space-time-plots (kymographs) of respective phragmoplasts depicted in (E). The x-coordinate depicts the distance in µm. The y-coordinate indicates the time t. The kymograph plugin in ImageJ was used to create kymographs and calculate the velocity of phragmoplast expansion. The slopes of the kymograph (contrast edge, selection is indicated by white dotted lines) are proportional to the velocity. In these examples, the two halves of the phragmoplasts expanded at different velocities. In addition, in one half the velocity decreased, indicated by the change in slope (2-phase expansion). (G) The average velocity of phragmoplast expansion is significantly reduced in *pok1-1 pok2-3* mutants (0.18 ± 0.09 µm/min; *P<0.02,* n = 22, Student *t*-test), compared to the expansion rate in the wild type (0.21 ± 0.09 µm/min; n = 43). Error bars indicate ± SD. Cell walls are stained with propidium iodide. Microtubules are visualized by GFP-MBD.

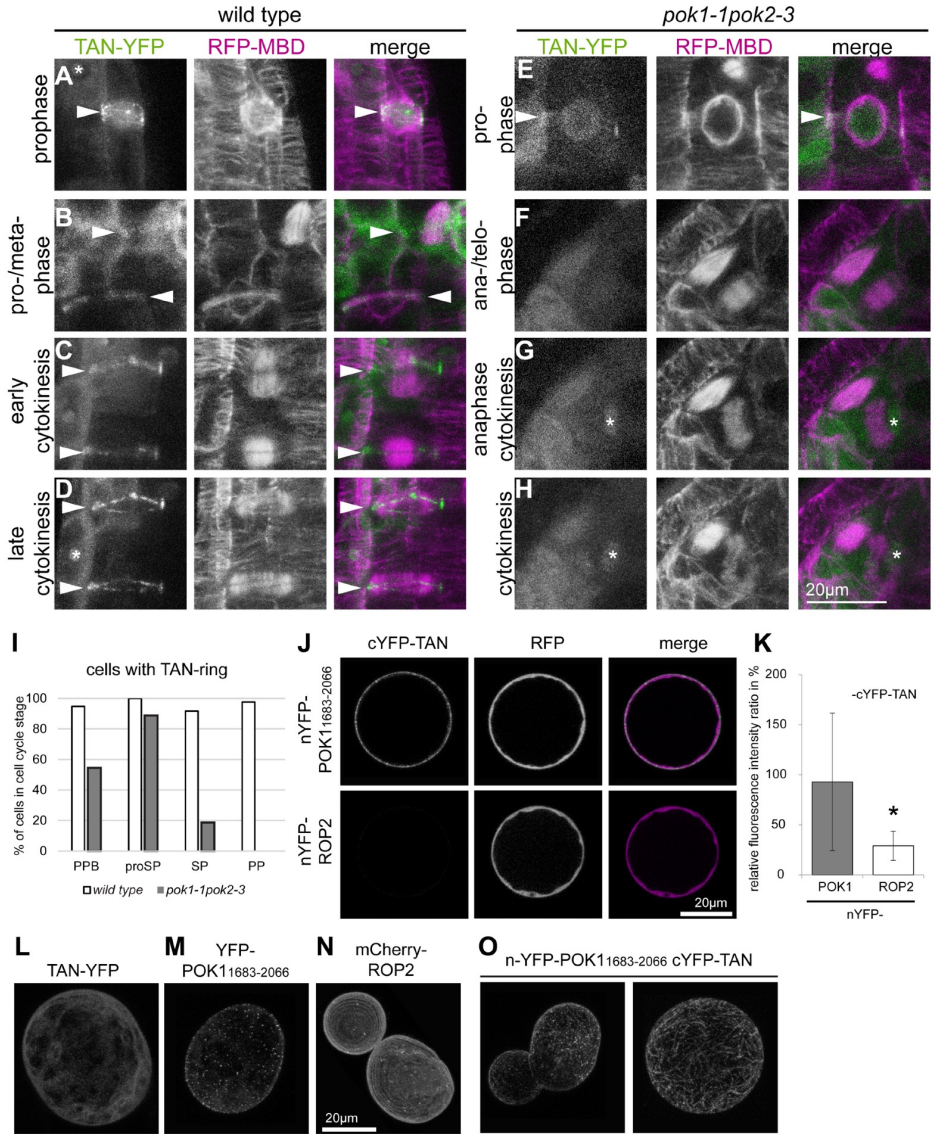

Figure 3: Loss of POK-dependent TAN localization at the cortical division zone correlates with PPB disassembly. TAN-YFP is recruited to the preprophase band in the wild type (A) and *pok1-1 pok2-3* double mutants (E). In the wild type, TAN-YFP rings co-exist with the preprophase band (A and B), pro-spindle (B), spindle (B), and early (C) and (D) late phragmoplasts. (E) Cell with pro-spindle displaying the TAN-YFP ring. (F) The spindle in the metaphase cell is not associated with cortical TAN-YFP, nor does the signal reappear during cytokinesis (F to H represent a time series). Images are z-projections of a varying number of images taken at 1 µm intervals. TAN-YFP rings are indicated by arrowheads. The nuclear localization of YFP-TAN is indicated by an asterisk. Scale bar is 10 µm. (I) Presence of TAN-YFP rings during the cell cycle in wild type and *pok1-1 pok2-3* mutants. (J to K) Interaction of TAN and the POK1 C-terminus, as determined by BiFC. (J) Confocal images of an *Arabidopsis thaliana* protoplast co-expressing nYFP-POK1$_{1683-2066}$ and cYFP-TAN, or nYFP-ROP2 and cYFP-TAN as negative controls. YFP fluorescence was specifically detected upon complementation of the fluorophore due to TAN and POK1$_{1683-2066}$ interaction in contrast to the control experiment. RFP, expressed from the same plasmid was used as an internal control. (K) Quantification of mean YFP fluorescence expressed as a ratio of mean RFP fluorescence. Data are means ± SD of 26 protoplasts per construct, each representing independent transformation events. The YFP/RFP ratio is significantly different (*P < 0.001, Student's *t*-test) between TAN/POK1$_{1683-2066}$ (interaction) and TAN/ROP2 (no interaction). (L to N) Localization of controls in protoplasts as indicated. Images are maximum z-projections of image stacks taken at 1 µm z-intervals. Scale bar indicates 20 µm. (L) Cytoplasmic localization upon expression of *Pro35S:TAN-YFP*. (M) Expression of *Pro35S:YFP-POK1$_{1613-2066}$* leads to punctate YFP signal in the plasma membrane similar to what is observed in *Arabidopsis thaliana* root meristem cells. (N) Expression of *pUB10:mCherry-ROP2*. (O) Examples of protoplasts co-expressing nYFP-POK1$_{1683-2066}$ and c-YFP-TAN. Images are maximum z-projections of images stacks taken at 1 µm z-intervals. Scale bar indicates 20 µm.

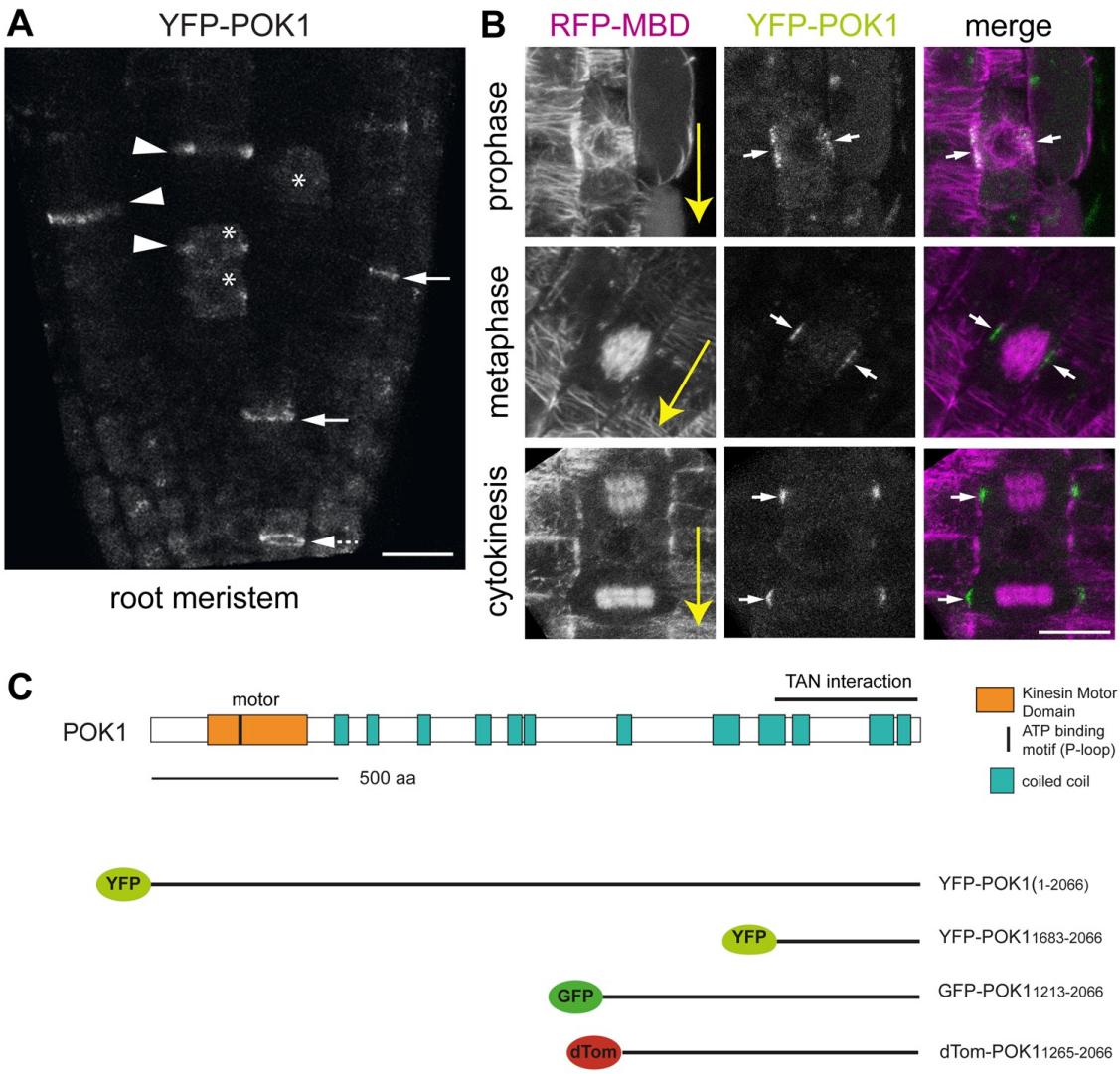

Figure 4: POK1 localizes at the cortical division zone/site. (A) Maximum z-projection of a root meristem expressing YFP-POK1. In cross sections, YFP-POK1 localizes as broad bands or dots (arrowheads) and sharp bands (arrows). Occasionally, YFP-POK1 rings are visible (arrow with dotted shaft). Some cells accumulate cytoplasmic YFP-POK1 (asterisk). (B) Co-expression of RFP-MBD and YFP-POK1 in different cell cycle stages in the root. YFP-POK1 co-localizes with the PPB in prophase and remains at the cell cortex throughout mitosis. Large yellow arrows indicate the longitudinal root axis. (C) POK1 domain organization as indicated in the legend and overview of fluorescent protein fusions used for localization studies. The $POK1_{1683-2066}$ fragment corresponds to the TAN-interacting fragment used in the BiFC experiment (Fig. 3J, 3K). Scale bar indicates 20 µm in (A) and 10 µm in (B).

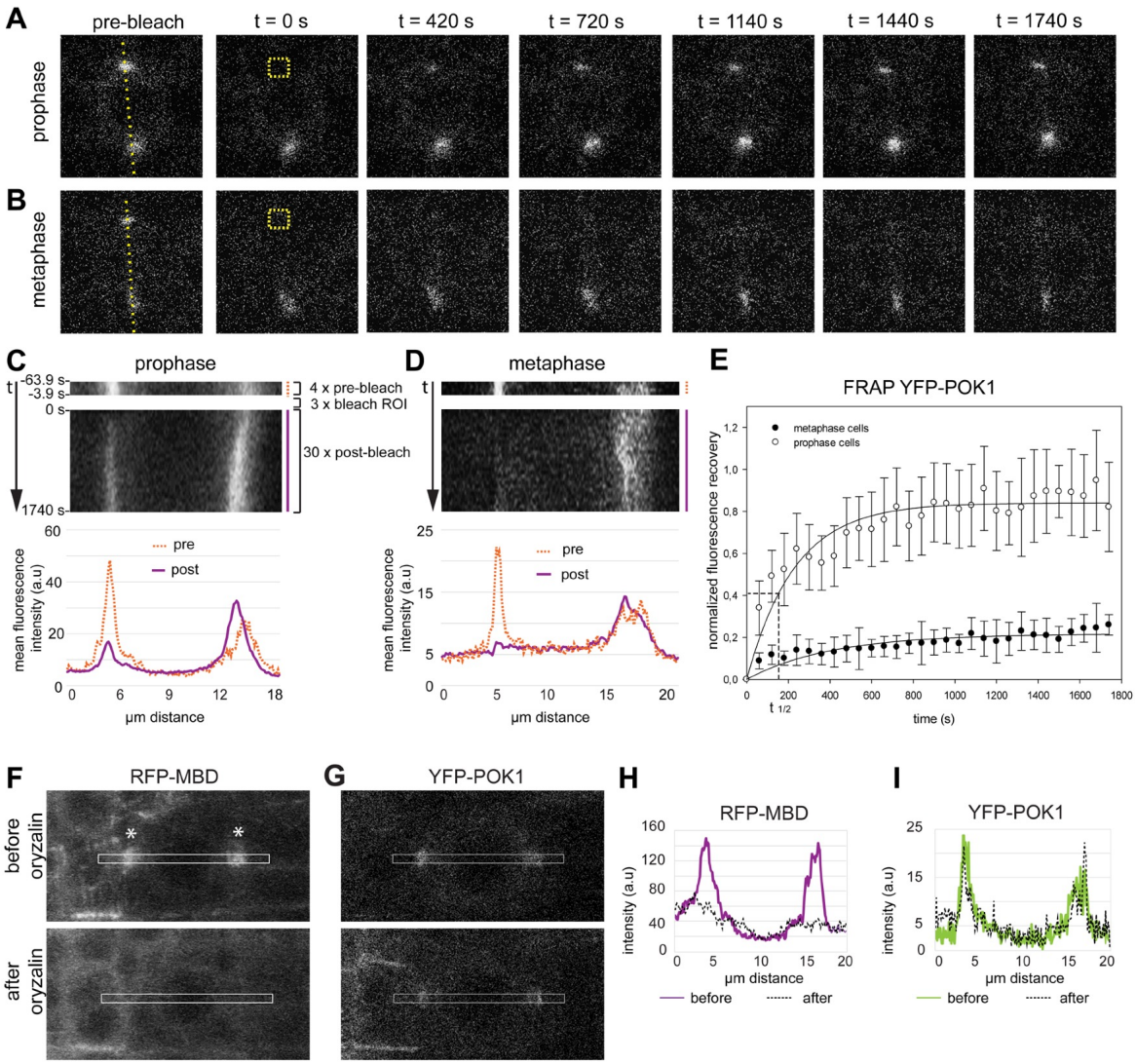

Figure 5: Differential POK1 dynamicity during mitosis. (A and B) Fluorescence Recovery After Photobleaching (FRAP) analysis of YFP-POK1. Representative time lapse of mitotic cells in the *Arabidopsis thaliana* root meristem. Transverse sections of (A) prophase and (B) metaphase cells recorded at different time points before (pre-bleach) and after photo-bleaching. Bleach regions are indicated by dashed square (region of interest, ROI) in first post-bleach images (t = 0 s). _Scale bar indicates 5µm. (C and D) Kymographs of pre-bleach and post-bleach time series corresponding to the dashed line selection as indicated in the pre-bleach images of (A) and (B). Pre-bleach kymograph (orange dashed line) of four pre-bleach images and post-bleach kymograph of 30 post-bleach images (magenta solid line) and corresponding profile plots are depicted. Profile plots show mean fluorescence intensities from the pre-bleach (orange dashed line) and post-bleach (magenta solid line) kymographs, respectively. Note the recovery of YFP signal in prophase. (E) An average of independent FRAP experiments is plotted to fit an exponential curve with rise to a maximum (y=a*(1-exp(-b*x))). In prophase cells (n=10), the YFP-POK1 signal recovers after photobleaching with a half time ($t_{1/2}$) of 154 s, while there is hardly any fluorescence recovery in metaphase cells (n=6). Error bars indicate ± SD. (F to I) POK1 localization at the cortical division zone is independent of microtubules (MT). Maximum z-projections of an *Arabidopsis thaliana* root meristem prophase cell co-expressing the microtubule (MT) reporter (F) RFP-MBD and (G) YFP-POK1 before and after treatment with 10 µM oryzalin. The PPB is indicated by asterisks. (F and G) Lower panels were recorded 15 min after oryzalin incubation and correspond to the cell in the upper panels. Due to MT de-polymerization, the RFP-MBD reporter localization becomes cytosolic, while the YFP-POK1 signal remains present at the CDZ. Scale bar indicates 10 µm. (H and I) Fluorescence intensity profile plots from a rectangular selection in (F and G) depicting (H) RFP-MBD signal distribution before oryzalin treatment (continuous, magenta line) and after oryzalin treatment (dashed, black line) and (I) YFP-POK1 signal distribution before (continuous, green line) and after (dashed, black line) oryzalin treatment. Note that the RFP-MBD peaks disappear after oryzalin treatment, while the YFP-POK1 peaks remain.

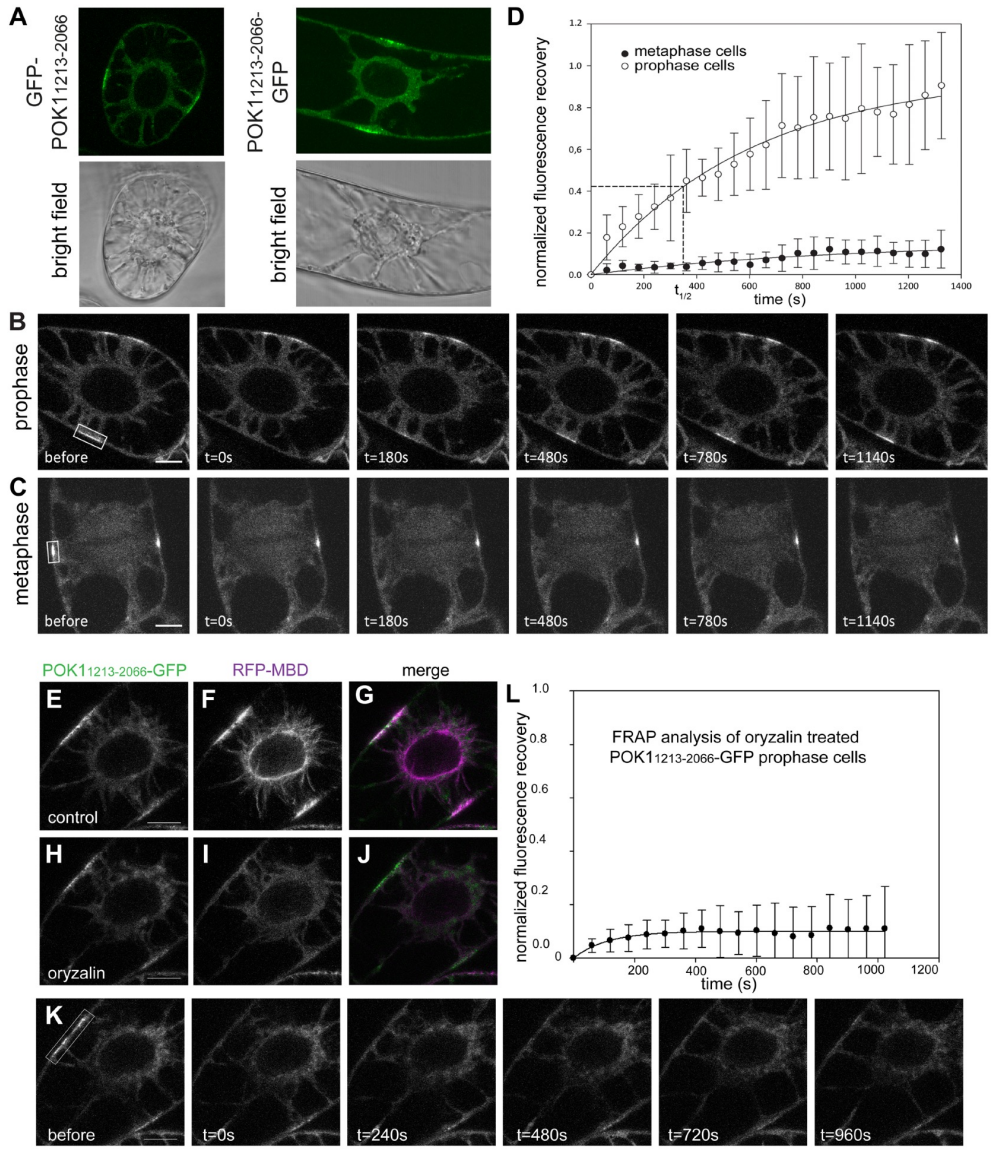

Figure 6: Changes of POK1 dynamicity during mitosis. (A) A tobacco BY-2 cell expressing *Pro35S:GFP-POK1*$_{1213-2066}$ and *Pro35S:POK1*$_{1213-2066}$-GFP) and the corresponding bright field image. Scale bar, 10 µm. (B to D) Fluorescence Recovery After Photobleaching (FRAP) analysis of GFP-POK1C. (B) Representative time lapse of a prophase BY-2 cell after photo-bleaching of GFP-POK1C at the preprophase band (PPB, white box indicates the bleached area). (C) Representative time lapse of a metaphase BY-2 cell after photobleaching the GFP-POK1 C-terminus at the cortical division zone (CDZ, indicated by white box). (D) Graph representing FRAP data for prophase and metaphase BY-2 cells overexpressing GFP-POK1$_{1213-2066}$. In prophase cells, the GFP-POK1 signal recovers slowly after photo-bleaching with a half time ($t_{1/2}$) of 362 s while there is hardly any fluorescence recovery in metaphase cells. An average of independent FRAP experiments is plotted to fit an exponential curve with rise to a maximum (y=a*(1-exp(-b*x))) (prophase cells: n=4; metaphase cells: n=7). Error bars indicate ± SD. (E to L) Recruitment of POK1C-GFP requires MTs, whereas PPB-localized POK1C-GFP statically associates with the CDZ independently of MTs in BY-2 cells. (E to J) Representative dividing BY-2 cell co-expressing the *Pro35S:RFP-MBD* MT marker and *Pro35S:POK1*$_{1213-2066}$*-GFP.* (E to G) POK1C-GFP co-localizes with the preprophase band (E, POK1C-GFP; F, RFP-MBD; G, merged image). (H to J) Upon oryzalin treatment, MTs depolymerize while POK1C-GFP remains associated with the CDZ (H, POK1C-GFP; I, RFP-MBD; J, merged image). (K) Representative time lapse of POK1C-GFP Fluorescence Recovery After Photobleaching (FRAP) performed on oryzalin-treated BY-2 cells in (E). In the absence of MTs, POK1C-GFP fluorescence did not recover at the bleached CDZ region. The bleached area is indicated by a white box. (L) Graph representing the FRAP experiments performed on oryzalin-treated prophase BY-2 cells co-expressing the *Pro35S:RFP-MBD* microtubule marker and *Pro35S:POK1*$_{1213-2066}$*-GFP* (n=6). GFP fluorescence did not recover at the CDZ upon MT depolymerization. Scale bar, 10 µm, error bars indicate ± SD.

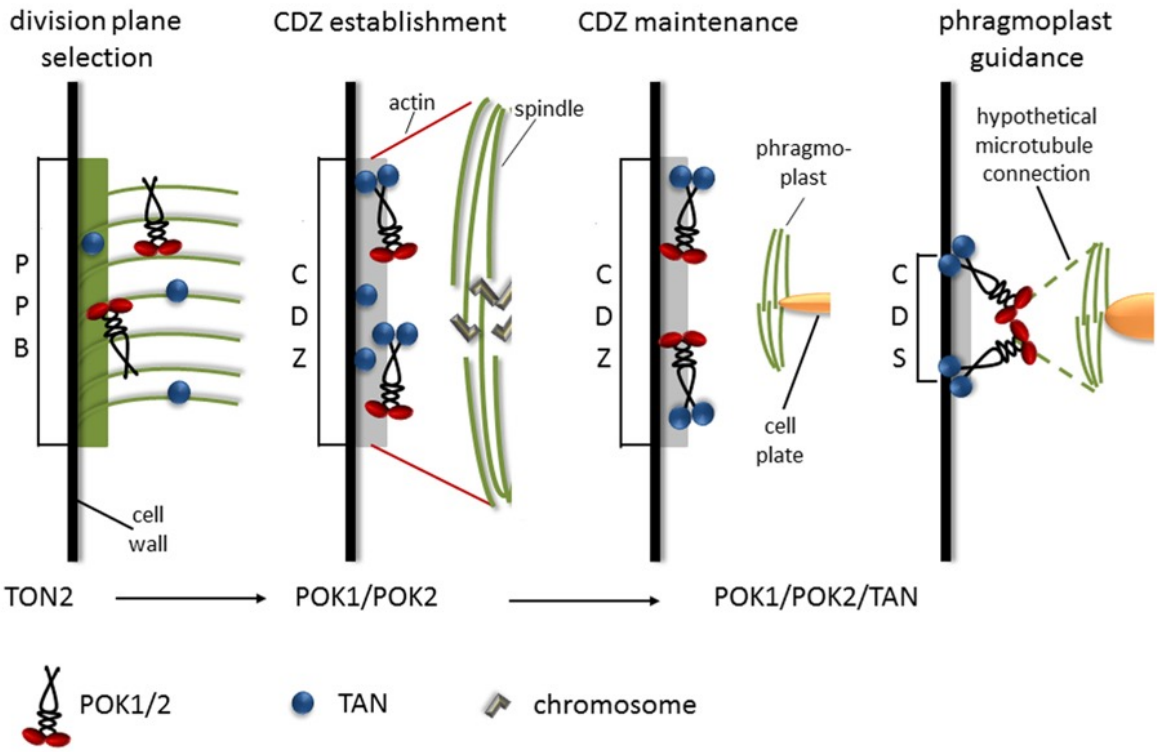

Figure 7: Schematic representation of cell cycle-dependent localization and function of POK1. In prophase cells, POK1 and TANGLED (TAN) are independently recruited to the TONNEAU (TON)2-dependent preprophase band (PPB). Upon metaphase, POK1 becomes immobilized at the cortical division zone (CDZ) and at the same time, TAN is tethered to the CDZ in a POK1/POK2-dependent manner, likely through direct binding to the C-terminus of POK1. Towards the end of cytokinesis, POK1 and TAN localization narrows to the exact site of cell plate anchoring at the parental wall, the cortical division site (CDS), via a yet unknown mechanism. Dashed line indicates hypothetical transient microtubules connecting the phragmoplast with the CDS at late cytokinesis (Supplemental Figure 6).

Table 1. Association of YFP-POK1 with the cortical division site is independent of microtubules. While microtubules disassembled, YFP-POK1 signal was not effected upon oryzalin treatment.

	RFP-MBD			YFP-POK1		
n = 8 roots	PPB	spindle	phragmoplast	PPB	spindle	phragmoplast
before oryzalin	10	5	15	8	4	20
after oryzalin	0	0	0	8	4	16

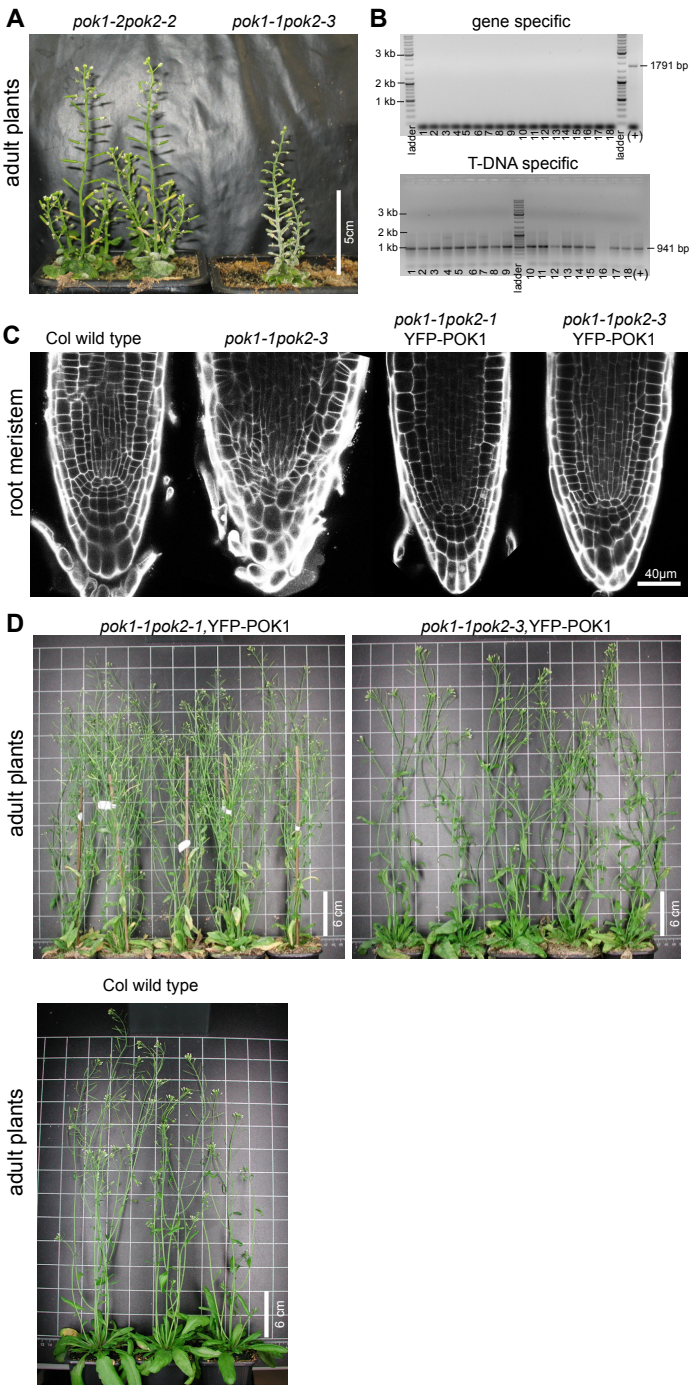

Supplementary Figure 1: Adult phenotype of *pok1pok2* and rescue with YFP- POK1. (A) Comparison of 8 week old dwarfed phenotypes of *pok1-2pok2-2* and *pok1-1pok2-3* double mutant plants showing the aggravated phenotype of the new allele combination. (B) Gel electrophoreses of Polymerase chain reaction (PCR) products. For PCR based genotyping of a segregating F2 population (*pok1-1pok2-3* x Col, BC1), DNA samples were prepared from phenotypically mutant plants. Presence of the 1791 bp PCR fragment using POK1-3491-F and POK1-SpeI-R (Table S1) indicates gene specific amplification of genomic *POK1*, while the amplification of the 941 bp PCR fragment using POK1-3491-F and LBa1 (Table S1) indicates the presence of the T-DNA insertion in the *POK1* locus. For all samples, except for # 16 which was of low quality, T-DNA specific, but not gene specific PCR fragments were amplified, indicating that the *pok1-1* T-DNA allele co-segregated with the mutant phenotype. (C) Confocal sections of seedling root meristems from different genotypes stained with Propidium iodide. Expression of *ProPOK1:YFP-gPOK1* (YFP- POK1) in double mutants *pok1-1pok2-1* and *pok1-1pok2-3* restores the (wild type) phenotype indicating functional redundancy between POK1 and POK2. (D) Adult *pok1-1pok2-1* and *pok1-1pok2-3* mutants expressing YFP-POK1 show normal growth and development, comparable to adult Col wild type plants.

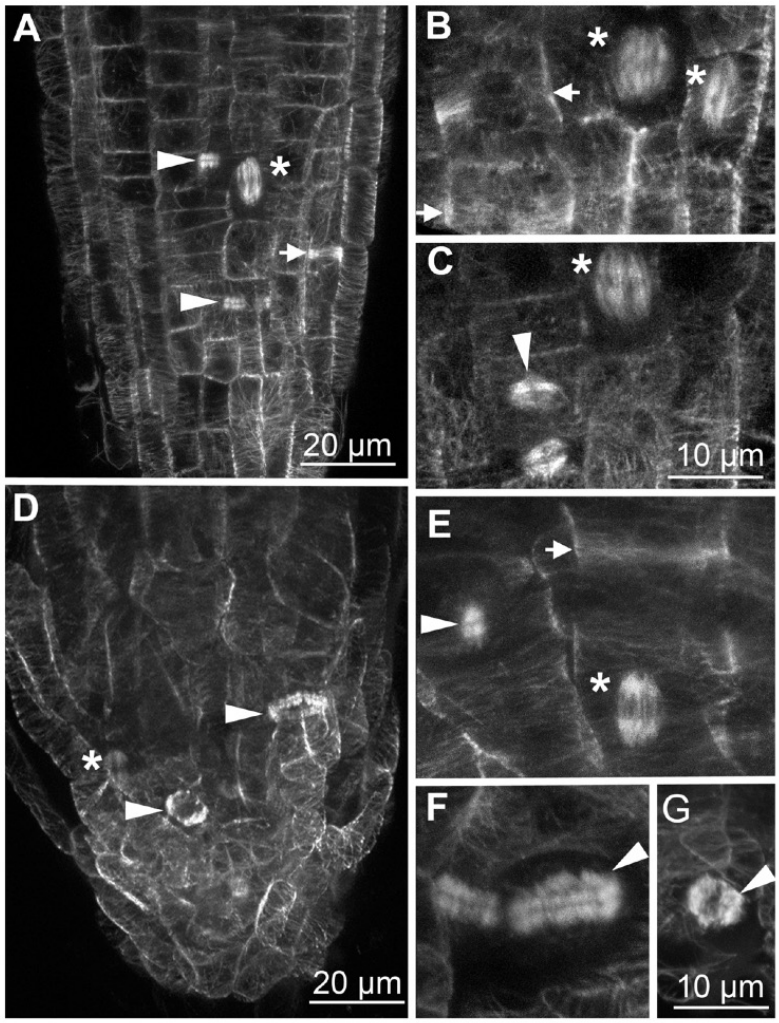

Supplementary Figure 2: Mitotic microtubule arrays in *pok1-1pok2-3* mutants
In vivo observations of mitotic microtubule (MT) arrays in wild type (A – C) and *pok1- 1pok2-3* mutants (D – F), expressing the MT reporter GFP-MBD. (A) Maximum Z- projection overview and (B, C) close up of mitotic cells in wild type. (D) Maximum Z- projection and (E to G) close up of mitotic *pok1-1pok2-3* cells. Arrows indicate preprophase bands (PPB). Spindles are indicated by asterisks and phragmoplasts are marked by arrow heads. Scale bars in (A) and (D) are 20 µm. Scale bars in (B, C, E, F) and (G) are 10 µm.

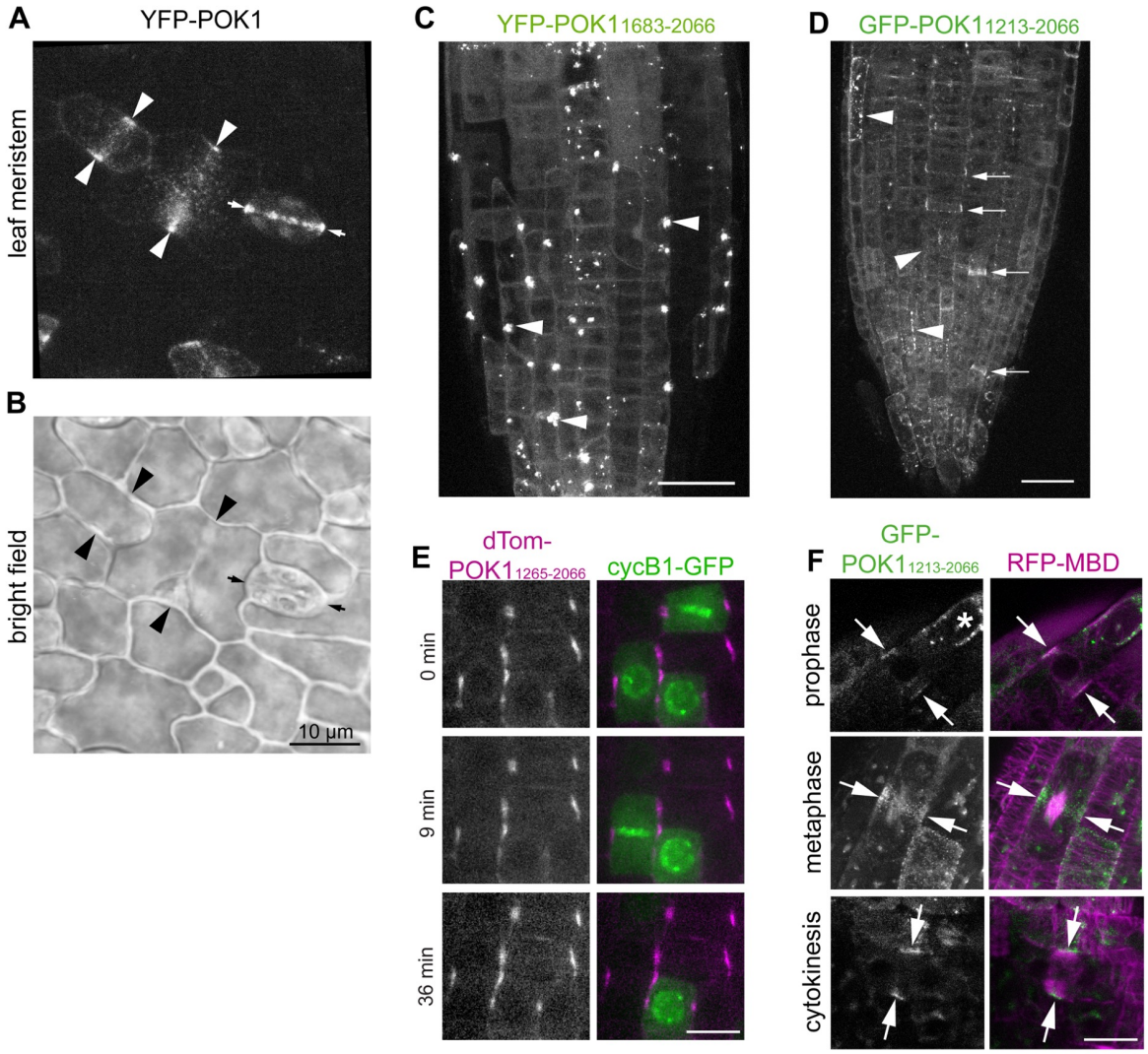

Supplementary Figure 3: (A and B) Expression of full length YFP-POK1 in young leaves. (A) Maximum z-projection of cells expressing full length YFP-POK1. Broad bands (arrow heads) and sharp bands (arrow) are distinguishable. (B) bright field image corresponding to (A). (C and D) Overview of root meristems expressing either (C) *Pro35S:YFP-POK1*$_{1683-2066}$ or (D) *Pro35S:GFP-POK1*$_{1213-2066}$. (C) Arrowheads indicate YFP-POK1$_{1683-2066}$ aggregates. (D) Arrows indicate GFP-POK1$_{1213-2066}$ localization in mitotic cells. Note that aggregates are less prominent and smaller (arrow heads). Scale bar is 50 µm. (E and F) POK1-C terminus is sufficient for localization at the cortical division zone/site. (E) Time series of cells co-expressing dTom-POK1$_{1265-2066}$ (magenta) and cycB1-GFP. cycB1-GFP associates with nuclei in prophase and with chromosomes in metaphase. During the time course, transition of cycB1-GFP fluorescence indicates cell cycle progression. dTom-POK1$_{1265-2066}$ is present at the cortical division zone at prophase and remains at the site beyond metaphase. (E) GFP-POK1$_{1213-2066}$ localization is similar like YFP-POK1. Left panel: Close up of prophase, metaphase and cytokinetic cells in cross sections, exhibiting characteristic fluorescent foci on lateral cell membranes (arrows). Right panel: Color merge of cells depicted in upper panel (green) and microtubule marker RFP-MBD (magenta). Asterisk indicates small aggregates present in the *Pro35S:GFP-POK1*$_{1213-2066}$ expressing line. Scale bar indicates 10 µm in (E and F).

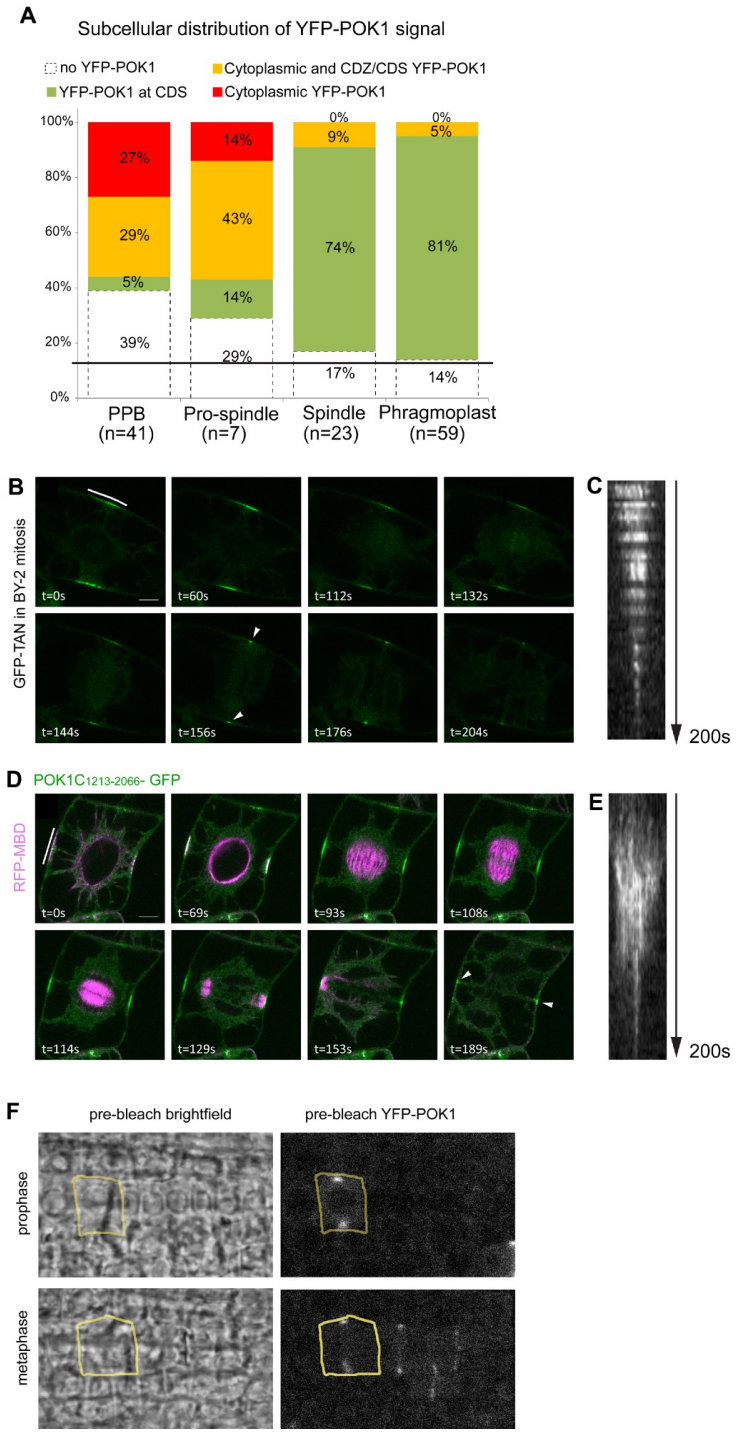

Supplementary Figure 4: Subcellular distribution of YFP-POK1 signal in *Arabidopsis* mitotic cells. YFP-POK1 subcellular signal shifts from cytoplasmic to CDZ/CDS associated during the course of mitosis; (n) indicates the number of observed cells per cell cycle stage. Cells with PPBs frequently displayed both cytoplasmic and cortical YFP-POK1 in the same cell (29 %), while a similar proportion (27 %) of prophase cells displayed solely cytoplasmic YFP-POK1. Only a minority of prophase cells exclusively displayed YFP-POK1 at the CDS (5%) and the majority of cells with PPBs did not show any YFP-POK1 (39%). In cells with pro- spindles, the co-occurrence of both, cytoplasmic and cortical YFP-POK1 rose to 43 %, concurrent with the proportion of cells displaying only CDZ YFP-POK1 (14 %). By contrast, fewer cells contained either cytoplasmic YFP-POK1 (14 %) or no YFP- POK1 signal (29 %). Cortical YFP-POK1 was prevalent in cells with spindles (74 %) and in cells with phragmoplasts (81 %), while in another 9% of cells with spindles and 5 % of cells with phragmoplasts cytosolic YFP-POK1 and cortical YFP-POK1 signal were observed concurrently. No YFP-POK1 signal was present in 17 % of cells with spindles and 14 % of cells containing phragmoplasts (15.5 % on average). We assume that this percentage reflects the margin of error for all cells that are expected to display YFP-POK1, but that we failed to detect due to low transgene expression or insufficient detection sensitivity. Data were collected from indirect immuno-localization experiments using anti-GFP (Invitrogen) and anti- tubulin (YL1/2, Abcam) and secondary antibodies anti-rabbit-Alexa488 (Invitrogen) and anti-rat-Cy3 (Jackson Immuno Research). Number of cells per cell cycle stage are indicated. Narrowing of TAN band width during BY-2 mitosis. (B) Time lapse of a dividing BY-2 cell expressing *Pro35S:GFP-TAN*. GFP-TAN accumulates at the CDZ from (pre)prophase to cytokinesis. As mitosis progresses, GFP fluorescence gradually narrows from a broad band at the CDZ to a punctate ring corresponding to the CDS (arrowheads), which is illustrated by a kymograph (C) along the CDZ membrane (white line in B). (D) Time lapse of a dividing BY-2 cell co-expressing the *Pro35S:POK1*$_{1213-2066}$-GFP (green) and the microtubule marker *Pro35S:RFP-MBD* (magenta). (D) POK1-GFP co-localizes with the preprophase band and persists at the CDZ membrane after PPB disassembly. POK1C-GFP fluorescence also gradually narrows from the CDZ to the CDS (arrowheads) upon cell plate anchoring, as demonstrated by a kymograph (E) along the plasma membrane (white line in D). Scale bar, 10 µm, error bars indicate ± STDV. (F) Maximum Z-projection of the pre- bleach images (bright field and YFP-POK1) taken during the FRAP experiments depicted in Figure 5A and 5B. The respective cells are outlined as indicated by the yellow selection in the images. Note that cells in interphase or prophase show distinct nuclei in brightfield.

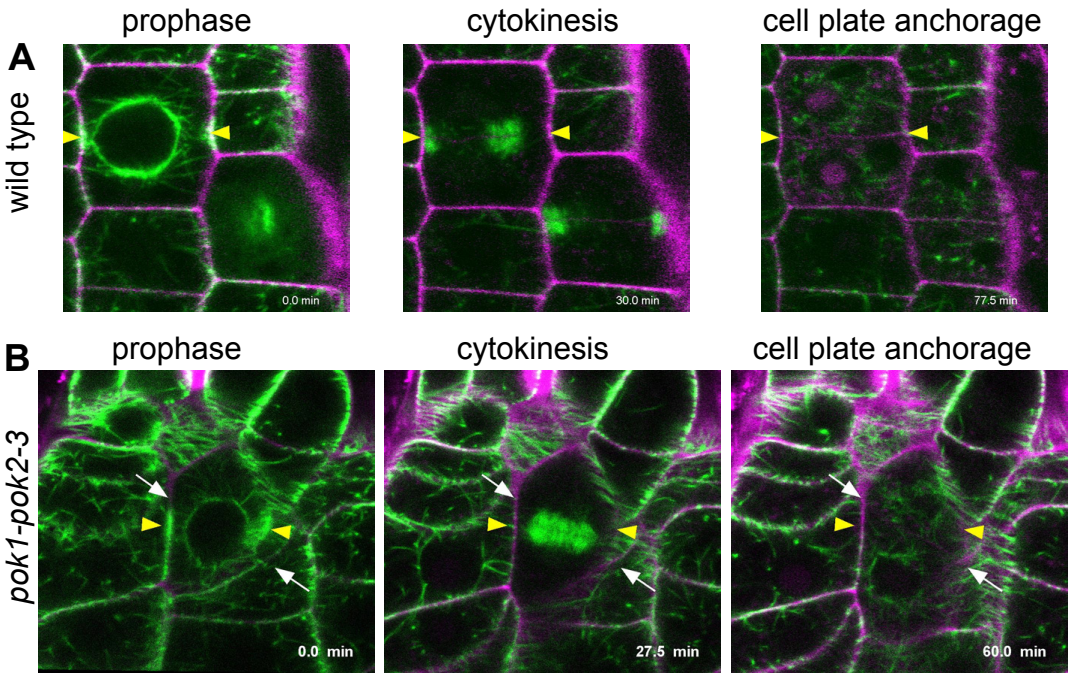

Supplementary Figure 5: Cell cycle progression. (A) Selected stages of cell cycle progression in wild type. Images correspond to Supplemental movie 1 as indicate by time stamps. Note, that the position of the preprophase band and the phragmoplast/cell plate co-align (yellow arrow heads). (B) Selected stages of cell cycle progression in *pok1-1pok2-3* double mutant. Images correspond to Supplemental movie 2 as indicate by time stamps. Note that the orientation of the preprophase band (yellow arrow heads) and the phragmoplast/cell plate (white arrows) do not match. Microtubules are visualized by GFP-MBD and indicated in green. Cell shape visualized by propidium iodide is shown in magenta.

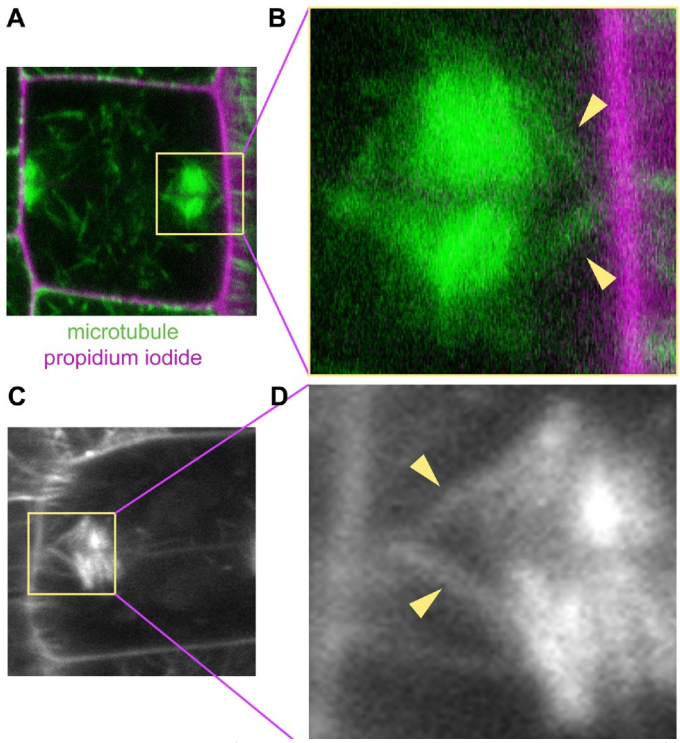

Supplementary Figure 6: Examples of transient microtubules reaching from the phragmoplast towards the putative cortical division site. (A and C) Cells in late cytokinesis with the phragmoplast approaching the parental cell wall (visualized with Propidium iodide in magenta in A and B and in gray scale in B and C). Microtubules originating from the phragmoplast extend towards the parental wall (indicated by arrowheads). (B and D) depict magnification of boxed areas in (A and C respecively).

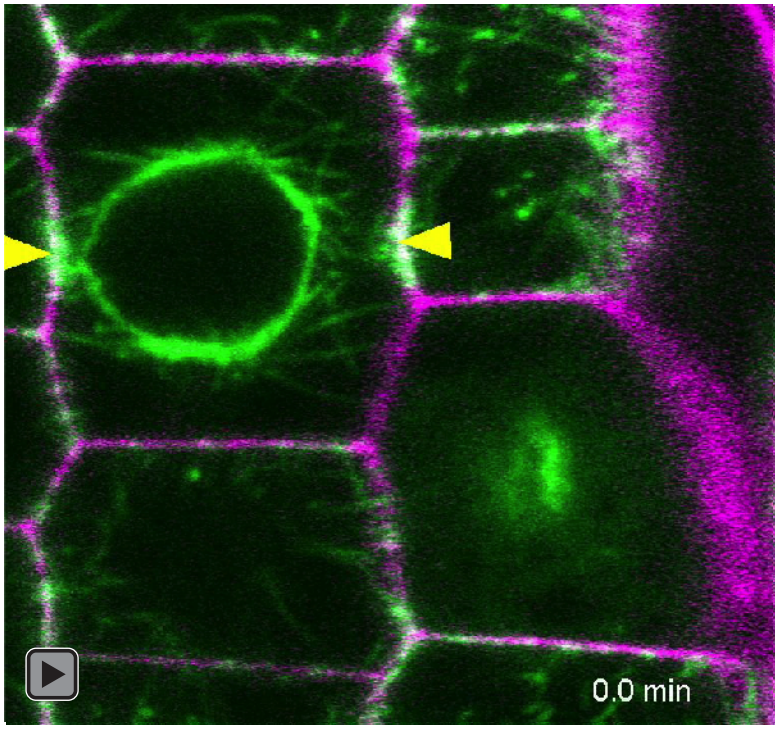

Supplemental movie 1: Time lapse of wild type cell division at 1.5 fps. Yellow arrowheads indicate position of PPB. The insertion of the cell plate at the end of cytokinesis corresponds with the position of the PPB. This movie corresponds to Supplementary Figure 5A.

Note: In order to see the movie you need to open this pdf with Adobe Acrobat DC

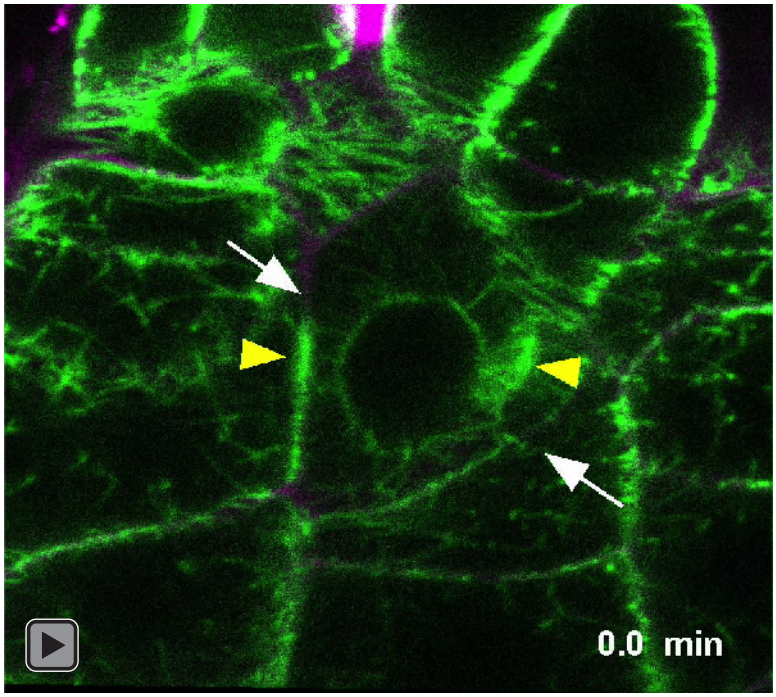

Supplemental movie 2: Time lapse of *pok1-1pok2-3* cell division at 1.5 fps. Yellow arrowheads indicate the position of the PPB. The white arrows indicate the cell plate insertion site, which deviates from the PPB position. This movie corresponds to Supplementary Figure 5B.

Note: In order to see the movie you need to open this pdf with Adobe Acrobat DC

Supplemental table 1. Primers used for cloning full-length YFP-POK1 and genotyping of *pok1-1*. POK1 homology sites are indicated in small italic font.

Oligo name	*5'-3'* sequence
Venus-FgF-POK1 F	*ttattcttcccggttggtgaaagagaccacaagctacttctcgatctacc*ATGGTGAGCAAGGGCGAGGAGCTGTTC
FgF-POK1 R	*aactcgttttcttccgattccggcatctctattctcggaacgtttcgggacat*GAAGTTCCTATTCTCTAGAAAGTATAGGAACTTCGCGGCCGC
p500-POK1	agttgatattattgacaccaccac
POK1-699-R	caagtgttcgttgatgctg
POK1-3491-F	gtcactgtcaggtgcataattc
POK1-SpeI-R	tcactagtgcacctctatcatag
LBa1	tggttcacgtagtgggccatcg

Supplemental table 2. List of primers used for cloning 2in1 plasmids. The attB recombination sites present in the oligo sequence are italicized.

Oligo name	*5'-3'* sequence
attB1 TAN	*ggggacaagtttgtacaaaaaagcaggctta*ATGGTTGCAAGAACCCCACAGAAGCA
attB4 TAN_r	*ggggacaactttgtatagaaaagttgggtg*CTACACTTTCCTGCTCTTCATTGGA
attB3 POK1Cshort	*ggggacaactttgtataataaagttgta*ATGGATGAAGAAGTAAAAAGGCATCGT
attB2 POK1C_r	*ggggaccactttgtacaagaaagctgggtt*TTACCGATATCTTGTACCAGAGCT
attB3 ROP2	*ggggacaactttgtataataaagttgta*ATGGCGTCAAGGTTTATAAAGTGT
attB2 ROP2 r	*ggggaccactttgtacaagaaagctgggtt*TCACAAGAACGCGCAACGGTTCTT

Supplemental table 3. List of primers used for cloning. The attB recombination sites present in the oligo sequence are indicated in italic.

Oligo name	*5'-3'* sequence
minB1F-TAN	*aaaaagcaggctccacc*ATGGTTGCAAGAACCCCACAGAAGC
minB2R-TAN stop	*agaaagctgggtc*CTACACTTTCCTGCTCTTCATTGG
minB2R-TAN no stop	*agaaagctgggtc*CACTTTCCTGCTCTTCATTGG
minB1F-POK1C	*aaaaagcaggctccacc*ATGGGTCTTATGCAGAGAATGG
minB2R-POK1C stop	*agaaagctgggtc*TTACCGATATCTTGTACCAGAGCT
minB2R-POK1C no stop	*agaaagctgggtc*CCGATATCTTGTACCAGAGCTCTG
B1F	GGGGACAAGTTTGTACAAAAAAGCAGGCTCCACC
B2R	GGGGACCACTTTGTACAAGAAAGCTGGGTC
TP1-B4-SE	GGGGACAACTTTGTATAGAAAAGTTGGTACCTACGTAGCCCAACACTCGAATCC
TP1-B1R-AN	*ggggctgctttttgtacaaacttgcgctagcggtcg*CTTATTGATTGTTTTCTCTCTCC
B2R-POK1C-1265	*ggggacagctttcttgtacaaagtggatc*ATGAAGAGTTAATAAGTAAGG
B3-POK1C-1265	*ggggacaactttgtataataaagttga*TTACCGATATCTTGTACCAGAG

7.1.2 Nitrosative stress triggers microtubule reorganization in *Arabidopsis thaliana*

Lipka, E. and Müller, S. Nitrosative stress triggers microtubule reorganization in *Arabidopsis thaliana*. *J. Exp. Bot.* **65:15**, 4177-4189 (2014).

Link: *http://jxb.oxfordjournals.org/content/65/15/4177*

Nitrosative stress triggers microtubule reorganization in *Arabidopsis thaliana*

Elisabeth Lipka and Sabine Müller*
ZMBP, Developmental Genetics, University of Tübingen, Auf der Morgenstelle 32, Tübingen, Germany
* corresponding author: sabine.mueller@zmbp.uni-tuebingen.de

Sabine Müller
University of Tübingen
Developmental Genetics, ZMBP
Auf der Morgenstelle 32
72076 Tübingen
Germany

Phone: 0049 (0)7071 2978888
Fax: 0049 (0)7071 2975797
e-mail: sabine.mueller@zmbp.uni-tuebingen.de

Running Title: Stress induced microtubule reorganization

Statement: Mimicking low level nitrosative stress by supplementing seedlings with nitrated tyrosin induced subtle, reversible changes in root growth and in microtubule organization suggesting that nitric oxid signaling targets the cytoskeleton.

Abstract
Microtubules are essential components of the cytoskeleton and fulfill multiple cellular functions in developmental processes readily responding to intrinsic and external cues. Nitric oxide signaling is well established in plants and the microtubule cytoskeleton emerges as one of its potential targets. To mimic low level nitrosative stress, we supplemented 3-nitro-L-tyrosine (NO_2-Tyr), a nitrated form of the amino acid tyrosine with the growth medium and observed concentration dependent changes in root growth rate and a reduction in cell division frequencies in *Arabidopsis thaliana*. In addition, we report that exposure to low NO_2-Tyr concentrations were not detrimental to plant health and caused subtle and reversible defects. In contrast, growth defects caused by high NO_2-Tyr concentrations could not be reversed. Live cell imaging of a microtubule reporter line revealed that low concentration NO_2-Tyr treatment correlated with disorganized cortical MT arrays and associated non-polar cell expansion in the elongation zone. NO_2-Tyr treatment antagonized taxol and oryzalin effects further supporting NO_2-Tyr association with MTs. Furthermore, oblique division plane orientations were observed which were likely induced prior to cytokinesis.

Keywords: cytoskeleton dynamics, microtubule, nitrosative stress; phragmoplast

Introduction
Nitric oxide (NO) and its reactive derivatives act as intra- and intercellular signaling molecules in a variety of organisms (Besson-Bard *et al.*, 2008). In plants NO is a key molecule triggering signaling cascades during development and in response to abiotic stresses (Neill *et al.*, 2002; He *et al.*, 2005; Neill *et al.*, 2008; Lombardo *et al.*, 2006; Lombardo and Lamattina, 2012, León *et al.,* 2013). The NO concentrations for signaling during plant development are low while high levels of NO induce

programmed cell death (PCD) (Bai *et al.*, 2012). NO signaling acts upon diverse cellular responses including changes in gene expression levels via mitogen activated protein kinase (MAPK) signaling cascades and regulation of transcription factors, as well as direct post-translational protein modifications (Neill *et al.*, 2002). The nitration of the amino acid tyrosine (n-tyr) is a highly specific product of NO signaling, although post-translational nitration does not affect all proteins to the same extend (Abello *et al.*, 2009). The impacts of n-tyr incorporation into proteins include changes in enzymatic activity, alterations in proteolytic degradation, effects on protein phosphorylation, immunogenicity and implications in disease (Abello *et al.*, 2009).
The cytoskeleton is a common downstream target of multiple signaling pathways leading to its extensive reorganization and consequent changes in cell morphology. Tubulin isoforms and many microtubule (MT) associated proteins (MAPs) are conserved throughout the plant and animal kingdom. Increasing evidence in the literature suggests that the cytoskeleton might be a direct target of NO signaling in mammals as well as in plants. For instance, in mouse brain tissue α- and β- tubulin isoforms were identified in a protein fraction enriched for n-tyr (Zhang *et al.*, 2007). Similarly, α- and β- tubulin isoforms from *Arabidopsis thaliana (A. thaliana)* were immuno-purified with anti-3nitroY antibody (Lozano-Juste *et al.*, 2011). Furthermore, n-tyr containing proteins immuno-precipitated with anti-tubulin antibodies demonstrating the incorporation of n-tyr into tubulin isoforms (Yemets *et al.*, 2011). In mammalian cells n-tyr was incorporated into the extreme C-terminus of α-tubulin by tubulin-tyrosine-ligase (TTL) likely disturbing the tyrosination/detyrosination cycle of α-tubulin (Eiserich *et al.*, 1999). Substitution of the C-terminal tyrosine by n-tyr correlated with MT disorganization and changes in cell morphology. The modification of the extreme C-terminus of α-tubulin by reversible enzymatically catalyzed addition and removal of tyrosine is one of a number of well characterized post-translational tubulin modifications (PTMs) in mammalian cells and in plants, although in plants the respective enzymes have not been identified conclusively (Westermann and Weber, 2003; Verhey and Gaertig, 2007; Smertenko *et al.*, 1997; Giannoutsou *et al.*, 2012).
The significance of PTMs for MT functions however, is not fully elucidated. Most PTMs occur at the C-terminal tail of tubulins and associate with sub-populations of MTs with distinct functions and subcellular localizations. Furthermore, immuno-localization of PTMs using a variety of PTM specific antibodies revealed that combinations of different PTMs were present on individual MTs in mammalian and in tobacco cells (Smertenko *et al.*, 1997; Janke and Kneussel, 2010; Quinones *et al.*, 2011). Thus, it was suggested that different PTMs might serve as road maps to ensure accurate cargo delivery (Verhey and Hammond, 2009). MAPs and more specifically kinesins emerged as possible targets of tyrosine signaling and PTM sensing (Gurland and Gundersen, 1995).
In plants, the MT cytoskeleton enables diverse cellular functions and is an integral constituent of developmental processes. In directionally expanding interphase cells cortical MTs arrange in parallel bundles, transverse to the axis of expansion and guide plasma membrane resident cellulose synthase complexes (Chan *et al.*, 2007; Gutierrez *et al.*, 2009). In mitotically active cells of higher plants, the cytoskeletal preprophase band is indicative of the future site of cell division. During cytokinesis the phragmoplast facilitates the synthesis and fusion of the cell plate at the site formerly occupied by the preprophase band (Müller, 2012; Rasmussen *et al.*, 2013).
Recently it has been proposed that n-tyrosinylation of the α-tubulin C-terminus might play a role in plant cell division (Jovanović et al. 2010). Rice seedlings and tobacco suspension culture cells were grown in the presence of 3-nitro-L-tyrosine (NO_2-Tyr) as an exogenous source of n-tyr, to irreversibly add n-tyr to the C-terminus of α-

tubulins. Upon treatment, tobacco cell culture cells exhibited mitotic inhibition and obliquely orientated cross walls, supporting the idea of direct impact of NO_2-Tyr on prominent MT functions. In a recent report growth defects of NO_2-Tyr were investigated in *A. thaliana* (Blume *et al.,* 2013). Here we report on growth defects and associated MT reorganization in *A. thaliana* seedlings grown in the presence of NO_2-Tyr. We directly monitored changes in MT organization, using live cell imaging of MTs, visualized by a fluorescent MT reporter. In a concentration dependent manner, NO_2-Tyr decreased mitotic activity and caused cell swelling due to re-organized cortical MT arrays, however effects of oryzalin or taxol were less pronounced in combination with NO_2-Tyr. Thus, we provide *in vivo* evidence that modulation of NO signaling allows for the reorganization of the MT cytoskeleton that might be relevant for development.

Material and Methods

Plant material and growth conditions

Throughout this study we used transgenic *A. thaliana* plants, accession Columbia (Col) and Col expressing Green Fluorescent Protein (GFP) MAP4 (Marc et al., 1998) unless indicated otherwise. Seeds were surface sterilized, plated on standard medium plates containing 1x Murashige and Skoog salt mixture, (pH 5.7) and 1% agar and were stratified for two to four days at 4°C. In the growth chamber, plates were positioned vertically and seedlings grew for four days at 22°C temperature and continuous light (standard conditions). Under sterile conditions, seedlings were then transferred onto nutrient agar plates containing different concentrations of 3-nitro-L-tyrosine (NO_2-Tyr, Sigma-Aldrich). Treatment plates were prepared from standard medium supplemented with varying amounts of NO_2-Tyr from 1 mM NO_2-Tyr stock solution dissolved in 50 µM HCl or DMSO. Mock controls contained 0.5 µM HCl and 10 µM tyrosine (Tyr).

Construction of XFP-fusion proteins

TUA6 cDNA was synthesized as described elsewhere (Muller *et al*., 2006). Primers TUA6 F 5'-*ggtacc*ATGAGAGAGTGCATTTCGATCCA-3' and TUA6 R 5'-*ctcgag*TTAGTATTCCTCTCCTTCATCAT-3' were used to amplify the TUA6 coding sequence flanked by KpnI and XhoI restriction sites (indicated in *italic*). Subsequently, cTUA6 was cloned into pGEM T (Promega), sequence-verified and transferred into into pENTR3C via cloning into the KpnI and XhoI sites. Primers TUA6-Y224A-F 5'-AACATTGAGAGACCTACC**gcc**ACCAA-3' and TUA6-Y224_R 5'-TTGAGGTTGGT**ggc**GGTAGGTCTCTCAAT-3' were used for site directed mutagenesis to create pENTR-cTUA6 Y224A. To create pENTR cTUA6 Y450A, primer TUA6 F was used with TUA6-Y450A R 5'-*ctcgag*TTA**Ggc**TTCCTCTCCTTCATCAT-3' for amplification of a PCR fragment which was digested with restriction enzymes EcoRI (TU6 internal site) and XhoI to exchange the respective fragment in pENTR cTUA6. Finally, pENTR-clones were recombined with pFK-241 pGreenIIS destination vector using LR clonase (Invitrogen).

The MT binding domain MBD contained in destination vector pEG104-*35S*::mCherry-MBD (Gutierrez et al., 2009) was recombined into pDONR207 by BP clonase reaction (Invitrogen). Subsequently, an LR clonase reaction (Invitrogen) was performed with the destination vector *pUBN*:RFP containing the *Arabidopsis* Ubiquitin10 promoter (*pUB*)(Grefen et al., 2010).

Imaging and data analysis

Microscopic images were either acquired on a Leica SP2 upright confocal microscope

using either a 20 x, n.a. = 0.70 water-immersion objective lens or a 63 x, n.a. = 1.20, water-immersion objective lens. Imaging of mitotic MT arrays was performed on a Leica SP8 inverted confocal microscope, 40 x, n.a. = 1.10, water-immersion objective lens, equipped with a resonant scanner. GFP was excited with the 488 nm emitting line of Argon lasers. Cell wall patterns were visualized by staining with Propidium Iodide (10 µM, Sigma-Aldrich) which was excited with a 561 nm HeNe laser. Images were acquired using Leica AF software. Image analysis and processing was performed in ImageJ http://rsbweb.nih.gov/ij/) and Adobe Photoshop CS5, respectively. Figures were assembled in Adobe Illustrator CS5.
The density of MT bundles per µm was determined as described previously in (Tanou *et al.*, 2012). In brief, Z-projections were assembled in ImageJ and grey values of Plot Profiles were measured and background corrected by subtracting the mean grey values of cortex areas without MTs. Along the plot profile, peaks were defined as grey values which were at least 10 units higher than the grey values of both neighboring pixels, using Excel. Six intensity classes were deduced and the numbers of peaks were counted for each intensity class. Peaks are indicative of MT bundles.
Intensity of cytosolic GFP-MBD signal in root cells of the elongation zone was determined in maximum projections of 21 optical sections at 0.5 µm intervals. Fluorescence intensities of areas between cortical MTs, corresponding to unbound cytosolic GFP-MBD, were measured. Averaged grey values per cell were background-substracted and plotted in Excel.
The Kymograph Plugin (http://www.embl.de/eamnet/html/body_kymograph.html) was used to determine MT plus end dynamicity and measurements were used to calculate average growth and shortening velocities in Excel. Pearsons correlation coefficient was calculated using the Colocalization Finder Plugin in ImageJ (http://rsb.info.nih.gov/ij/plugins/colocalization-finder.html).
Statistical significance of differences in measurements was determined with Student's t test.

Results

Effects of nitro-tyrosine on root growth

To mimic nitrosative stress conditions in our experiments *A. thaliana* seedlings were exposed to different 3-nitro-L-tyrosine supplemented in the growth medium, designated NO_2-Tyr to distinguish from intracellular/endogenous (n-tyr) concentrations. Then, the effects of n-tyr imbalance on seedling development were assessed. Therefore, four day old seedlings expressing the microtubule (MT) reporter GFP-MBD were transferred to growth media containing varying concentrations of NO_2-Tyr (0.1 µM, 0.25µM, 0.5 µM 1 µM, 5 µM and 10 µM) and grown for an additional 36 hours (1.5 days). Control seedlings were transferred to standard medium, or medium containing either 0.5 µM HCl, 10 µM Tyr, or both (mock controls).
Analysis of root length before and after treatment revealed a dramatic reduction in growth upon NO_2-Tyr exposure compared to the non-treated and the mock control seedlings (Figure 1A). The reduction in root length was significant and further decreased with increasing NO_2-Tyr concentrations (Figure 1A). In contrast, root growth of untreated controls and mock treated seedlings (0.5 µM HCl, 10 µM Tyr) did not vary (Figure 1A, Supplemental Figure 2A). In addition, the use of either HCl or DMSO as the solvent did not make a difference in growth responses (Supplemental Figure 2B). As well, upon NO_2-Tyr treatment the growth response of wild type plants (Col) and GFP-MBD transgene plants was comparable (Supplemental Figure 3A and 3B).
Seedlings grown on NO_2-Tyr exhibited altered tip organization. At low concentrations

of NO_2-Tyr (0.5 µM and 1 µM) cells in the elongation zone displayed non-polar expansion (Figure 1B). Intriguingly, high concentrations (5 µM, 10 µM) did not induce morphological alterations, suggesting that high amounts of NO_2-Tyr rapidly interfered with cellular functions. Moreover, a concentration dependent reduction of the meristem and elongation zone was apparent between the root tip and the first root hair (Figure 1B and Supplemental Figure 1A). In addition the elongation of root hairs was affected at NO_2-Tyr concentrations ≥1 µM, (Figure 1B).

Mitosis is inhibited in nitro-tyrosine treated seedlings

Observations on rice seedlings and tobacco Bright Yellow (BY)-2 suspension culture cells suggested that NO_2-Tyr treatment inhibited cell division (Jovanović *et al.*, 2010). Expression of the MT reporter GFP-MBD allowed the evaluation of mitotic activity in living *A. thaliana* seedlings (Supplemental Figure 1B). The number of mitotic cells between quiescent center and epidermis was counted in image stacks at 2 µm z-intervals (Supplemental Figure 1B). In control plants, on average 25.5 mitotic MT structures were observed per image stack (Figure 1C and Supplemental Figure 1B). In contrast, equivalent image stacks of NO_2-Tyr treated seedlings revealed a significant reduction in mitotic activity. At 0.5 µM NO_2-Tyr the mean number of mitotic MT structures dropped to 6.1 and at a concentration of 1 µM NO_2Tyr only 1.3 mitotic cells were observed on average. Mitotic activity was entirely inhibited at 5 µM NO_2-Tyr. These results confirmed a concentration dependent inhibition of cell divisions upon NO_2-Tyr treatment in *A. thaliana* seedlings.

NO_2Tyr induced growth inhibition effects are reversible at low concentrations

Since high concentrations of NO_2Tyr had dramatic effects on root growth, we investigated whether low concentrations or extended treatment periods were harming cellular functions to a similar extent and whether NO_2-Tyr induced effects on root growth could be reversed. As described above, seedlings grew under standard conditions for four days and were subsequently transferred onto NO_2-Tyr-containing medium for an additional 1.5 days. Then, the root length was measured, and half of the seedlings were retransferred onto standard medium for 4.5 more days (Figure 2, black lines, designated as “ret” for retransfer) to test whether root growth defects were reversed. The remaining half of the seedlings was transferred onto freshly prepared treatment plates of the respective NO_2-Tyr concentration (Figure 2, red lines indicating continuous NO_2-Tyr treatment).

The root length of seedlings under different treatment conditions was plotted over time and regression equations for each treatment were calculated as a reference for growth performance (Figure 2). Based on similarities of the regression equations the samples were grouped into four classes (I to IV). Controls (class I) were set to 100 %, representing the full growth potential. Class II included low NO_2-Tyr samples that were retransferred to standard medium (0.25 µM ret and 0.5 µM ret) attaining 72 % recovery of potential growth. In addition, the 1 µM ret sample was grouped with class II, still displaying 55 % of the potential growth. In contrast, samples that continuously grew on low NO_2-Tyr concentrations (0.25 µM and 0.5 µM) fell into class III possessing only between 30 % to 16 % of controls growth potential. Finally, class IV comprised all high concentration samples (5 µM, 10 µM continuous NO_2-Tyr and retransferred 5 µM ret, 10 µM ret), all of which displayed severely reduced growth (1% growth). In addition, class IV also held samples continuously grown on 1µM NO_2-Tyr (7 % growth). The clustering of samples into distinct groups indicated that high concentrations of NO_2-Tyr irreversibly harmed seedlings even during the initial short term treatment (1.5 days). On the other hand, low NO_2-Tyr concentrations caused mild, non-toxic effects

which were reversible during the same treatment period. Remarkably, continuous treatment with 0.25 µM NO_2-Tyr still allowed 30% of growth while short term treatment with 1 µM NO_2-Tyr could still be reversed to about half (55%) of the potential growth.

Cortical microtubule arrays are disordered upon NO_2-Tyr treatment

Low concentrations of NO_2-Tyr (0.5 µM) caused non-polar cell expansion in the elongation zone after 1.5 days of treatment while cell division and cell expansion ceased at concentrations above 1 µM NO_2-Tyr (Figure 1B and Figure 1C). Non-polar cell expansion is typically related to alterations in MT organization. Indeed, in NO_2-Tyr treated plants, the characteristic parallel alignment of the cortical MT array was disturbed in cells with obvious expansion defects (Figure 1B, 3A). Rather, cortical MT arrays occurred disordered and appeared less dense than in control cells (Figure 3A). Intensity based quantification of MT bundles along the long axis of cells (as indicated by the yellow lines in Figure 3A and corresponding blot profiles in Supplemental Figure 4A) revealed an overall reduction of thick and thin MT bundles in 0.5 µM NO_2-Tyr treated cells (Supplemental Figure 4B). The average number of MT bundles per µm was significantly smaller in treated cells (1.05 ± 0.12, *$P<0.05$) compared to control cells (1.32 ± 0.18, Supplemental Figure 4C). Consistent with the reduction of thick and thin MT bundles, the intensities of cytosolic GFP-MBD fluorescence increased upon increasing concentration of NO_2-Tyr (Supplemental Figure 4D). To assess the degree of disorder, angles between MT bundles and the cell long-axis (as depicted in Figure 3A, red angle symbol) were measured. In cells of treated seedlings the mean direction of MT bundles (86.8 ± 34.6°) deviated significantly (*$P=0.0003$) from the mean MT angle calculated for control cells (94.6 ± 19.6°). Moreover, the high standard deviation indicated a larger variability in the data set for NO_2-Tyr treated cells (Figure 3B) which became more obvious when the frequencies of angles were blotted in 10 degree bins (Figure 3C). In controls the majority of MT angles (67.1 %) ranged between 80 to 110 degrees. However, upon NO_2-Tyr treatment only 35.5 % of cortical MTs displayed angles between 80 to 110 degrees while the number of higher and lower angles increased. Noteworthy, the distribution across the 10 degree bins in the control resembled a normal curve of distribution with a distinct peak, while the angle distribution in NO_2-Tyr treatment displayed a more homogeneous, flat distribution across the degree bins. In reversibility experiments, parallel MT array organization was restored at NO_2-Tyr low concentrations (data not shown).

In order to determine whether loss of cortical MT organization was caused by altered MT dynamicity, we measured growth velocities (indicative of MT polymerization) and shortening velocities of MT plus ends (indicative of MT de-polymerization) in epidermal cells of the elongation zone. Interestingly, no significant differences were observed between growth velocities in control (3.04 ± 1.46 µm/min), in 0.5 µM NO_2-Tyr treated (3.44 ± 1.14 µm/min) and in 1 µM NO_2-Tyr treated seedlings (3.15 ± 0.82 µm/min) or for shortening velocities in control (10.91 ± 4.31 µm/min), in 0.5 µM NO_2-Tyr treated (12.63 ± 5.89 µm/min) and in 1 µM NO_2-Tyr treated seedlings (11.48 ± 5.43 µm/min) (Figure 3D).

Low concentrations of NO_2-Tyr counteracts responses to taxol and oryzalin

Both, oryzalin and taxol stimulate non-polar cell expansion through their interaction with tubulin (Baskin *et al.,* 1994). By combining 0.5 µM NO_2-Tyr with different concentrations of either taxol or oryzalin, we observed changes in growth rate and MT organization in seedlings exposed to the drug treatment as described before.

taxol alone had little (11 % for 1 µM taxol) or similar effects (54 % for 10 µM taxol) on growth inhibition (as a percentage of control) compared to 0.5 µM NO_2-Tyr alone

(56%) (Figure 4A and D). Growth inhibition of taxol in combination with NO_2-Tyr (55 % and 77 %) was mostly attributed to NO_2-Tyr effects (Fig 4B, C and D). On cellular levels, taxol induced stabilization of MT (Fig 4G and 4I) was counteracted by NO_2-Tyr when both drugs were present in the growth medium (Fig 4H). High levels of taxol combined with NO_2-Tyr caused pronounced cell expansion defects and NO_2-Tyr-induced re-organization of MTs (Fig. 4J) indicating that taxol effects on MTs were overridden by NO_2-Tyr.

Oryzalin treatment disrupted MTs causing irregular expansion of cells and inhibition of mitosis, both contributing to concentration dependent reduction in growth rate (Figure 4E, 4K and 4L). Effects of 1 µM oryzalin on growth inhibition (74 %) were more severe than 0.5 µM NO_2-Tyr alone (65%) (Fig. 4E). However, in combination with 0.5 µM NO_2-Tyr, the oryzalin effect on growth rate inhibition increased only to 78% (Figure 4E and M). Consistently, the addition of 0.5 µM NO_2-Tyr reduced the oryzalin dependent destabilization of MTs (Figure 4 M) suggesting that oryzalin binding to tubulin might be less efficient in the presence of NO_2-Tyr.Single mutations in helix 7 (H7) of alpha-tubulins were reported to render plants and protozoa resistant to oryzalin (Anthony *et al.,* 1998, Morrisette *et al.,* 2004, Supplemental Figure 5). Therefore, we mutated tyrosine at the beginning of H7 to alanine (Y224A) in TUA6 (Figure 5A), which was identified among nitrotyrosinated proteins in *A. thaliana*. (Lozano-Justo *et al.*, 2011, Supplemental Figure 5 A) and expressed it as GFP-fusion in *A. thaliana* protoplasts. Similarly, we mutated the C-terminal tyrosine in TUA6 the putative target of the tyrosination/detyrosination cycle to alanine (Y450A) (Figure 5A). Wild type TUA6 (TUA6 WT) and mutant GFP-fusion proteins were co-expressed with RFP-MBD to visualize MTs (Figure 5B and 5D). While TUA6 WT (Figure 5B, 5C and 5F) and the TUA6 Y450A mutant showed co-localization with RFP-MBD (Figure 5F), TUA6 Y224A was not efficiently incorporated into MTs as determined by Pearsons correlation coefficient (Figure 5D, 5E and 5F) supporting a critical role of Y224 for the integrity of the tubulin molecule.

Long term, low concentration NO_2-Tyr treatment affects division plane orientation in root meristems

In BY-2 cells NO_2-Tyr treatment altered division planes (Jovanović *et al.*, 2010). We wondered whether similar defects occurred in the tissue context of *A. thaliana* root meristems. In short term (1.5 day) experiments, cell wall positioning was normal, but under high NO_2-Tyr concentrations (1 µM to 10 µM), mitosis was almost abolished and already reduced at 0.5 µM NO_2-Tyr (Figure 1C, Supplemental Figure 1B). Therefore, cell wall positions in the root meristem were visualized by Propidium Iodide staining and were analyzed in seedlings exposed to 0.5 µM NO_2-Tyr for six days. We reasoned that in our hands cell divisions still occurred at this concentration (Figure 1C) and thus might permit the accumulation of cell wall positioning defects over time. Indeed, we observed a low number of oblique cell walls in primary (Figure 6B) and lateral root meristems (Figure 6F) compared to wild type (Figure 6A, 6E).

However, positioning defects in NO_2-Tyr treated plants were modest compared to mutants exhibiting defects in this pathway, such as the double mutant of *PHRAGMOPLAST ORIENTING KINESIN(POK)1* and *2* (Muller *et al.*, 2006). While *pok* single mutants are phenotypically wild type, *pok1pok2* double mutants display severely misplaced cell walls due to a failure in phragmoplast guidance (Muller *et al.*, 2006). Thus, we investigated whether *pok1* and *pok2* single and *pok1pok2* double mutants were hypersensitive to NO_2-Tyr and whether cell wall positioning defects in these plants were induced at lower NO_2-Tyr concentrations than in GFP-MBD plants. As in previous experiments, we exposed seedlings to different NO_2-Tyr concentrations

and assessed the growth performance. Both, *pok1pok2* double mutants and *pok1* single mutants, as well as *pok2* single mutants expressing GFP-MBD (*pok2;*GFP-MBD), showed NO_2-Tyr induced growth reduction similar to GFP-MBD transgenic plants (Supplemental Figure 4). Furthermore, cell wall positioning defects were comparable to wild type plants (data not shown). Thus we concluded that NO_2-Tyr had no effect on either *pok1*, or *pok2;*GFP-MBD or *pok1pok2* double mutants (Supplemental Figure 6) and that NO_2-Tyr induced oblique cell walls were not a result of interference with phragmoplast guidance.

Discussion

In all organisms investigated so far including plants, the abundance of nitric oxide (NO) and its derivatives such as free 3-nitro-L-tyrosine (NO_2-Tyr) is regarded as a reporter of nitrosative stress under pathological conditions (Besson-Bard *et al.*, 2008; Foissner *et al.*, 2000; Halliwell *et al.*, 1999; Moreau *et al.*, 2010). In plants, biotic and abiotic stress conditions lead to nitric oxide imbalance and provoke nitrosative responses preceding physiological and developmental changes (Neill *et al.*, 2008; Lombardo *et al.*, 2006; Tanou *et al.*, 2012; Corpas *et al.*, 2011). A solid understanding of NO biosynthesis and the *in vivo* effects of NO signaling is emerging in the plant field (Besson-Bard *et al.*, 2008; Moreau *et al.*, 2010). However, the detection of low, physiologically and developmentally relevant concentrations of reactive nitrogen species remains challenging (Halliwell *et al.*, 1999; Berton *et al.*, 2012). In the present study we evaluated the impacts of different concentrations of exogenously supplied NO_2-Tyr on root growth, root tip morphology, MT organization and phragmoplast guidance in *A. thaliana* seedlings.

A recent study in *A. thaliana* roots reported that NO stress, induced by sodium nitroprussid (SNP), caused programed cell death (PCD) at high SNP levels, but triggered cell cycle arrest in G1 phase at medium SNP levels, which were still above the reported developmentally relevant concentrations (Bai *et al.*, 2012). Consistent with our findings in response to different NO_2-Tyr concentrations, root growth was reduced and meristem cell number decreased upon SNP treatment (Bai et al., 2012). In our experiments the number of cell divisions decreased significantly at high NO_2-Tyr concentrations indicative of cell cycle arrest. Although we did not analyze parameters such as DNA damage it is plausible that DNA damage induced at high NO_2-Tyr concentrations was responsible for the observed irreversible arrest of plant growth. Our reversibility experiments are consistent with a recent study reporting reversibility of growth inhibiting effects (Blume *et al.*, 2013) at NO_2-Tyr concentrations similar to this study. While we observed stunted and moderately depolarized root hairs, 10-fold higher NO_2-Tyr caused ectopic and distorted root hairs (Blume *et al.*,2013) reflecting the broad morphological impact of nitrosative stress.

NO is a developmentally important signaling molecule in plants (Moreau *et al.*, 2010). For instance, NO signaling targets root development via signal transduction to a MAPK signaling cascade (Wang *et al.*, 2010). NO is also a significant intermediate of abscisic acid induced signaling in the control of stomatal aperture (He *et al.*, 2005; Ribeiro *et al.*, 2009). In this context NO targets the protein phosphatase 2C ABI1, but whether NO directly modifies the ABI1, as it has been shown for H_2O_2 is unclear (Desikan *et al.*, 2002; Meinhard and Grill, 2001).

Yet, direct modification of cytoskeletal proteins might represent one disposition of NO signal propagation. In mammalian cells, n-tyr is incorporated into the C-terminus of α-tubulin under pathological conditions, strongly suggesting that the cytoskeleton might be one target of NO signaling (Eiserich *et al.*, 1999). Moreover, in BY-2 cells NO_2-Tyr treatment correlated with a decrease in the relative amount of de-tyrosinated α-tubulin

isoforms (Jovanović *et al.*, 2010).
Several recent studies reported about cytoskeletal targets of NO signaling or nitrosative stress. In protein extracts from BY-2 cells, antibodies against NO_2-Tyr preferentially decorated proteins of about 55 kDa molecular weight, similar to anti-tubulin antibodies and precipitated tubulin cross-reacted with anti-tubulin antibodies, in support of the proposed incorporation of NO_2-Tyr into cytoskeletal proteins (Yemets *et al.*, 2011). Indeed, recently *in vivo* evidence for extensive nitrotyrosination was provided by immuno-localization of n-tyr along mitotic MT arrays in BY-2 cells (Blume *et.al.*, 2013), indicating that n-tyr might have specific affinity to highly dynamic MTs.Furthermore, a proteome approach identified the *A. thaliana* tubulin A6 as a target of nitrogen starvation, which lead to MT de-polymerization in transgenic lines overexpressing GFP-TUA6 (Wang *et al.*, 2012). Finally, several tubulin isoforms were identified as putative *in vivo* targets of nitrotyrosination by immuno-purification of proteins with anti-nitrotyrosine antibodies and subsequent mass spectrometry from *A. thaliana* seedlings (Lozano-Juste *et al.*, 2011).
Recent reports implicate that reactive oxygen species (ROS) signaling targets the MT cytoskeleton causing MT de-polymerization, abnormal MT organization and inhibition of cell cycle progression (Livanos *et al.*, 2012; Yao *et al.*, 2012). As well, de-polymerization of MTs was observed, following the treatment with *Verticillium dahlia* toxins, which was shown to effect H_2O_2 and downstream NO homeostasis (Yao *et al.*, 2012). Finally, drug induced disturbance of ROS homeostasis resulted in the formation of MT paracrystals and abnormally bent MT bundles (Livanos *et al.*, 2012). These reports support the direct modifications of the MT cytoskeleton by nitrosative stresses and the possible incorporation of n-tyr into tubulin and MTs. However, in contrast to the above mentioned studies, we observed subtle and significant changes in the organization of the interphase MT array that were reversible. Thus, we provide evidence that developmentally relevant low concentration NO signaling might act via delicately controlled modulation of MT organization. Consistently, exposure to SNP as an exogenous NO source also caused reorganization of the cortical MT array into randomly distributed MT bundles in *A. thaliana* epidermis cells of the differentiation zone (Yemets *et al.,* 2009), further correlating NO signaling and cytoskeletal organization. Intriguingly, guard cell function correlated with quantifiable changes in MT clustering or bundling within guard cells (Eisinger *et al.*, 2012a) and abscisic acid induced guard cell aperture closure was accompanied by the reduction in MT structures (Eisinger *et al.*, 2012b). Although the causal relation between NO signaling, which acts downstream of abscicic acid, and MT bundling in guard cell function has not been demonstrated, the experimental evidence is suggestive that this relation indeed exist.
Structural modeling of the interaction between plant alpha tubulin and dinitroanilins suggested that slight changes in tubulin primary structure could provoke changes in binding activity of dinitroanilins (Blume *et. al.,*2003). Combined treatment with oryzalin and NO_2-Tyr showed multiplicative growth inhibition of BY-2 cells (Jovanovic *et al.,* 2010) and *Arabidopsis* (this study), supporting the notion these drugs share a common target. Oryzalin binding to a conserved pocket of alpha tubulin containing Thr239, just below the N-loop might interfere with lateral binding to the M-loop of the adjacent dimer thereby disrupting MTs and their polymerization (Morrissette *et al.*, 2004). Mutation of Thr239 to Ile in alpha-tubulin conferred resistance to oryzalin in goosegras (Mudge *et al.,* 1984) and expression of the respective tubulin mutant Thr239Ile in maize suspension culture also conferred oryzalin resistance (Antony *et al.,* 1998). Oryzalin induced MT depolymerization is diminished in the presence of NO_2-Tyr, implying that NO_2-Tyr might interfere with efficient oryzalin binding at its

target site. Mutation of tyrosine 224 to alanine (Y224A) in *A. thaliana* TUA6, one of the tubulins that precipitated with anti- NO_2-Tyr antibody (Lozano-Juste *et al*., 2011) interferes with efficient incorporation into MTs when expressed in protoplasts, revealing the essential role of this tyrosin. Nevertheless, the observed effects of the Y224A mutant may not be related to failure of n-tyr incorporation, but rather reflect other structural characteristics of TUA6. A similar observation in transgenic *A. thaliana* expressing the phosphomimic mutant $TUA6^{T349D}$ (Fujita *et al.,* 2013) further demonstrates how post-translational tubulin modifications contribute to the establishment of the MT cytoskeleton.

Likewise, NO_2-Tyr appeared to override Taxol effects on growth inhibition and MT organization. Taxol binding stabilizes the beta-tubulin M-loop which interacts with N-loops from adjacent tubulin dimers to form lateral contacts (Snyder *et al.,* 2001, Morrisette *et al.,* 2004). Since potential nitrotyrosination could interfere with the conformation of the N-loop, lateral binding of dimers might be destabilized even in the presence of taxol, consistent with our observations. As expected expression of the GFP-TUA6 Y450A, replacing the C-terminal tyrosine did not alter MT incorporation efficiency noteable, consistent with the detection of detyrosinated Tubulin isoforms along MTs in plants (Smertenko *et al.*, 1997).

Computer simulations that modeled the α-tubulin C-terminus in three potential configurations predicted the reorganization of the cortical MT cytoskeleton and changes in cell morphology as a consequence of conformational changes of the C-terminus (Blume *et al.*, 2005, Blume *et al.*, 2013). According to these models, a C-terminal tyrosine would increase dynamicity of the MT polymer. In contrast, removal of the C-terminal tyrosine would cause conformational changes that could contribute to MT polymer stability. The addition of NO_2-Tyr at the C-terminus would result in an intermediate MT polymer behavior in this model. Consistent with the computer predictions, we did observe changes in MT organization and corresponding alterations of cell morphology upon NO_2-Tyr treatment. Notably, simulation and modeling of tubulin C-termini dynamics also suggested that dynamic interactions between tubulin tails and the MT surface might influence MT polymerization and MT conformation and thus flexibly alter the interaction of the MT with ligands (Freedman *et al.*, 2011). Indeed, removal of the α-tubulin C-terminal tail altered efficiency and pH-dependency of colchicine binding to tubulin (Chakraborty *et al.*, 2004). Similarly, the anions of glutamate-rich extreme C-termini of tubulin were involved in the regulation of vinblastine-induced tubulin polymerization (Rai and Wolff, 1998). Thus, NO_2-Tyr at the C-terminus might lead to conformational changes of the tubulin dimer and in consequence Oryzalin and taxol binding might be inefficient, consistent with our observations. Taken together, these findings further encourage the idea that NO signaling targets the MT cytoskeleton via post-translational modification (PMT) of α-tubulin isoforms by direct incorporation of NO_2-Tyr.

In animal systems it is well established that the balance between tyrosinated and de-tyrosinated α-tubulin in the MT cytoskeleton might reflect the developmental status of cells depending on whether they divide or differentiate (Quinones *et al.*, 2011). Within distinct MT subpopulations entire filaments may consist of tubulin subunits containing α-tubulins pre-dominantly in their tyrosinated or de-tyrosinated form. These subpopulations might also be associated with multiple other PTMs at the same time, adding to the level of regulation (Verhey and Gaertig, 2007; Quinones *et al.*, 2011). It has been recognized that stable MTs were associated with an increased degree of detyrosination, while highly dynamic MTs are mostly tyrosinated. Since MTs in most cells are usually very dynamic, the tyrosination cycle provides an effective way to modulate MT organization, for example during transitions between cell cycle phases

(Janke and Kneussel, 2010).
In our experiments, cortical MT array organization in the elongation zone appeared less well ordered upon low level NO_2-Tyr treatment. MT arrays displayed fewer bundles and oblique angles relative to the longitudinal axis of the cell (Figure 3) consistent with a recent study reporting the reorganization of cortical and endoplasmic MTs in the root apex, the transition and elongation zone at concentrations > 50 µM NO_2-Tyr within 2 hours of treatment (Blume *et al*., 2013). Although concentration and treatment period vary, our results are comparable with Blume *et al*., 2013.
The changes in cortical array organization could not be attributed to changes in MT plus end dynamicity. However, analysis of a small data set suggested that frequencies of transitions between MT growth, shortening, and/or pausing might be altered upon NO_2-Tyr treatment (Supplemental Figure 4D). Nevertheless, our results are consistent with observations from guard cells, where the organization of MTs changed, despite unaltered MT dynamicity of the MT plus end (Eisinger *et al.*, 2012b). Changes in transition rates were also reported for a mutant of the MT Plus-End binding protein AUGMIN subunit8 which is defective in MT re-organization, in addition to altered MT plus end shrinkage rate (Cao *et al.*, 2013), implying that changes in transition rates are regulated by MT associated proteins (MAPs) and contribute to MT reorganization. We propose that MAPs might be responsible for the cortical MT array reorganization. Consistent with this idea, we observed changes in cytosolic GFP-MBD upon NO_2-Tyr treatment (Supplemental Figure 4E). Indeed, it was proposed that MAPs might be direct targets of posttranslational tubulin modifications (PTMs), that as road maps to regulate MAP and motor protein trafficking along MTs (Verhey and Gaertig, 2007).
In BY-2 cells NO_2-Tyr treatment readily altered the orientation of the division plane and it was hypothesized that kinesins required for phragmoplast expansion and vesicle transport were specific targets of de-tyrosinated α-tubulins (Jovanović *et al.*, 2010). However, defects in phragmoplast expansion and vesicle transport typically result in incomplete cell walls and multinucleated cells (Jurgens, 2005) which were not observed in BY-2 cells (Jovanović *et al.*, 2010), indicating that mechanisms different from phragmoplast expansion and vesicle transport are the targets of NO signaling via incorporation of n-tyr. As well, division plane orientations were altered in *A. thaliana* seedlings root meristems upon long term, low concentration NO_2-Tyr treatment (Figure 5). Nevertheless, NO_2-Tyr treatment did not produce more pronounced defects in *pok* single and double mutants and did not induce hypersensitive responses in *pok* mutants suggesting that the mechanisms of phragmoplast guidance, which is disturbed in *pok* mutants (Müller et al., 2006) was not specifically effected upon NO_2-Tyr treatment. Thus, we propose that NO_2-Tyr affects the MT cytoskeleton and associated MAPs already during prophase when the division plane is selected and established (Müller, 2012; Rasmussen *et al.*, 2011). Therefore, NO_2-Tyr treatment might become a useful tool to induce oblique division planes to study the underlying molecular mechanism.
In summary our results support the hypothesis that incorporation of n-tyr into the C-terminus of α-tubulins interferes with the α-tubulin tyrosination/detyrosination cycle, leading to MT reorganization via MAPs that differentially recognize PTMs at the C-terminus of α-tubulins. Thus, we assume that MAPs that might be the prime targets of developmentally relevant NO signaling, transduce the NO signal by reorganizing the MT cytoskeleton.

Supplementary data may be found at JXB online
Supplementary Figure 1. (A) Reduction of root tip size. **(B)** Representative, inverted confocal images depict single optical sections of the root meristem.

Supplemental Figure 2. Growth response curves of seedling roots under different control conditions.
Supplementary Figure 3. Growth response of *A. thaliana* Columbia wild type (Col wt) roots upon 3-nitro-L-tyrosine (NO_2-Tyr) treatment.
Supplementary Figure 4. Quantification of organization and dynamic of cortical microtubule (MT) arrays in epidermal cells at the elongation zone.
Supplementary Figure 5. (A) Alignment of TUA6 isoforms. *Arabidopsis thaliana* (*A. th.*) TUA6 (At4g14960), goosegrass TUA1 (AAC05717), *Zea mays* TUA1 (P14641), Toxoplasma gondii TUA1 (AAA30145). **(B)** 3D model (CDD structure model, http://www.ncbi.nlm.nih.gov/Structure/cdd/cddsrv.cgi?uid=100015), of nucleotide binding site in alpha tubulin.
Supplementary Figure 6. Growth responses to 3-nitro-L-tyrosine (NO_2-Tyr) in *A. thaliana* seedlings grown on standard medium for four days and subsequent exposure to different NO_2-Tyr treatments for 6 additional days.

Acknowledgement
We thank Frank Küttner for sharing unpublished plasmid pFK-241 pGreenIIS. We would like to acknowledge generous support from the Department of Developmental Genetics and Prof. Gerd Jürgens. This work was supported by a grant from Deutsche Forschungsgemeinschaft to S.M. (DFG MU 3133/1-1).

The authors declare no conflict of interest.

References
Abello N, Kerstjens HAM, Postma DS, Bischoff R. 2009. Protein Tyrosine Nitration: Selectivity, Physicochemical and Biological Consequences, Denitration, and Proteomics Methods for the Identification of Tyrosine-Nitrated Proteins. *Journal of Proteome Research* **8**, 3222-3238.
Anthony RG, Waldin TR, Ray JA, Bright SWJ, Hussey PJ. 1998. Herbicide resistance caused by spontaneous mutation of the cytoskeletal protein tubulin. *Nature* **393**, 260-263.
Bai S, Li M, Yao T, Wang H, Zhang Y, Xiao L, Wang J, Zhang Z, Hu Y, Liu W, He Y. 2012. Nitric oxide restrain root growth by DNA damage induced cell cycle arrest in Arabidopsis thaliana. *Nitric Oxide* **26**, 54-60.
Baskin TI, Wilson JE, Cork A, Williamson RE. 1994. Morphology and Microtubule Organization in Arabidopsis Roots Exposed to oryzalin or taxol. *Plant and Cell Physiology* **35**, 935-942.
Berton P, Domínguez-Romero J, Wuilloud R, Sánchez-Calvo B, Chaki M, Carreras A, Valderrama R, Begara-Morales J, Corpas F, Barroso J, Gilbert-López B, García-Reyes J, Molina-Díaz A. 2012. Determination of nitrotyrosine in Arabidopsis thaliana cell cultures with a mixed-mode solid-phase extraction cleanup followed by liquid chromatography time-of-flight mass spectrometry. *Anal Bioanal Chem* **404**, 1495-1503.
Besson-Bard A, Pugin A, Wendehenne D. 2008. New Insights into Nitric Oxide Signaling in Plants. *Annual Review of Plant Biology* **59**, 21-39.
Blume Y.B., Nyporko AY, Yemets AI, Baird WV. 2003. Structural modeling of the interaction of plant alpha-tubulin with dinitroaniline and phosphoroamidate herbicides. Cell Biol Int. **27**, 171-4.
Blume YB, Nyporko AY, Demchuk O. 2005. Nitrotyrosination of plant alpha-tubulin: potential mechanisms of influence on cellular processes. *BMC Plant Biology* **5**, S26.
Blume, YB, Krasylenko, YA, Demchuk, O.M. and Yemets, A.I. 2013 Tubulin

tyrosine nitration regulates microtubule organization in plant cells. *Frontiers in Plant Science*, doi: 10.3389/fpls.2013.00530.

Cao L, Wang L, Zheng M, Cao H, Ding L, Zhang X, Fu Y. 2013. Arabidopsis AUGMIN Subunit8 Is a Microtubule Plus-End Binding Protein That Promotes Microtubule Reorientation in Hypocotyls. *The Plant Cell Online* **25**, 2187-2201.

Chakraborty S, Gupta S, Sarkar T, Poddar A, Pena J, Solana R, Tarazona R, Bhattacharyya B. 2004. The B-ring substituent at C-7 of colchicine and the α-C-terminus of tubulin communicate through the "tail–body" interaction. *Proteins: Structure, Function, and Bioinformatics* **57**, 602-609.

Chan J, Calder G, Fox S, Lloyd C. 2007. Cortical microtubule arrays undergo rotary movements in Arabidopsis hypocotyl epidermal cells. *Nat Cell Biol* **9**, 171-175.

Corpas FJ, Leterrier M, Valderrama R, Airaki M, Chaki M, Palma JM, Barroso JB. 2011. Nitric oxide imbalance provokes a nitrosative response in plants under abiotic stress. *Plant Science* **181**, 604-611.

Desikan R, Griffiths R, Hancock J, Neill S. 2002. A new role for an old enzyme: Nitrate reductase-mediated nitric oxide generation is required for abscisic acid-induced stomatal closure in Arabidopsis thaliana. *Proceedings of the National Academy of Sciences* **99**, 16314-16318.

Eiserich JP, Estevez AG, Bamberg TV, Ye YZ, Chumley PH, Beckman JS, Freeman BA. 1999. Microtubule dysfunction by posttranslational nitrotyrosination of alpha-tubulin: a nitric oxide-dependent mechanism of cellular injury. *Proc Natl Acad Sci U S A* **96**, 6365-6370.

Eisinger W, Ehrhardt D, Briggs W. 2012b. Microtubules Are Essential for Guard-Cell Function in Vicia and Arabidopsis. *Molecular Plant* **5**, 601-610.

Eisinger WR, Kirik V, Lewis C, Ehrhardt DW, Briggs WR. 2012a. Quantitative Changes in Microtubule Distribution Correlate with Guard Cell Function in Arabidopsis. *Molecular Plant* **5**, 716-725.

Foissner I, Wendehenne D, Langebartels C, Durner J. 2000. In vivo imaging of an elicitor-induced nitric oxide burst in tobacco. *The Plant Journal* **23**, 817-824.

Freedman H, Luchko T, Luduena RF, Tuszynski JA. 2011. Molecular dynamics modeling of tubulin C-terminal tail interactions with the microtubule surface. *Proteins: Structure, Function, and Bioinformatics* **79**, 2968-2982.

Fujita S, Pytela J, Hotta T, Kato T, Hamada T, Akamatsu R, Ishida Y, Kutsuna N, Hasezawa S, Nomura Y, Nakagami H, Hashimoto T. 2013. An Atypical Tubulin Kinase Mediates Stress-Induced Microtubule Depolymerization in Arabidopsis. Current Biology, **23,** 1969-1978.

Giannoutsou E, Galatis B, Zachariadis M, Apostolakos P. 2012. Formation of an endoplasmic reticulum ring associated with acetylated microtubules in the angiosperm preprophase band. *Cytoskeleton* **69**, 252-265.

Gurland G, Gundersen GG. 1995. Stable, detyrosinated microtubules function to localize vimentin intermediate filaments in fibroblasts. *J Cell Biol* **131**, 1275-1290.

Gutierrez R, Lindeboom JJ, Paredez AR, Emons AM, Ehrhardt DW. 2009. Arabidopsis cortical microtubules position cellulose synthase delivery to the plasma membrane and interact with cellulose synthase trafficking compartments. *Nat Cell Biol* **11**, 797-806.

Halliwell B, Zhao K, Whiteman M. 1999. Nitric oxide and peroxynitrite. The ugly, the uglier and the not so good: a personal view of recent controversies. *Free Radic Res* **31**, 651-669.

He J, Xu H, She X, Song X, Zhao W. 2005. The role and the interrelationship of hydrogen peroxide and nitric oxide in the UV-B-induced stomatal closure in broad bean. *Functional Plant Biology* **32**, 237-247.

Janke C, Kneussel M. 2010. Tubulin post-translational modifications: encoding functions on the neuronal microtubule cytoskeleton. *Trends in Neurosciences* **33**, 362-372.
Jovanović AM, Durst S, Nick P. 2010. Plant cell division is specifically affected by nitrotyrosine. *Journal of Experimental Botany* **61**, 901-909.
Jurgens G. 2005. Cytokinesis in higher plants. *Annu. Rev. Plant Biol.* **56**, 281-299.
León, J., Castillo, M.C., Coego, A., Lozano-Juste, J. and Mir, R. (2013) Diverse functional interactions between nitric oxide and abscisic acid in plant development and responses to stress. *Journal of Experimental Botany.* doi:10.1093/jxb/ert454.
Livanos P, Galatis B, Quader H, Apostolakos P. 2012. Disturbance of reactive oxygen species homeostasis induces atypical tubulin polymer formation and affects mitosis in root-tip cells of Triticum turgidum and Arabidopsis thaliana. *Cytoskeleton* **69**, 1-21.
Lombardo MC, Graziano M, Polacco JC, Lamattina L. 2006. Nitric Oxide Functions as a Positive Regulator of Root Hair Development. *Plant Signaling & Behavior* **1**, 28-33.
Lombardo MC, Lamattina L. 2012. Nitric oxide is essential for vesicle formation and trafficking in Arabidopsis root hair growth. *Journal of Experimental Botany* **63**, 4875-4885.
Lozano-Juste J, Colom-Moreno R, León J. 2011. In vivo protein tyrosine nitration in Arabidopsis thaliana. *Journal of Experimental Botany* **62**, 3501-3517.
Marc, J., Granger, C.L., Brincat, J., Fisher, D.D., Kao, T., McCubbin, A.G., and Cyr, R.J. (1998). A GFP-MAP4 reporter gene for visualizing cortical microtubule rearrangements in living epidermal cells. *Plant Cell* **10**, 1927-1940.**Grefen, C., Donald, N., Hashimoto, K., Kudla, J., Schumacher, K., and Blatt, M.R. (2010).** A ubiquitin-10 promoter-based vector set for fluorescent protein tagging facilitates temporal stability and native protein distribution in transient and stable expression studies. *The Plant Journal* **64**, 355-365.
Meinhard M, Grill E. 2001. Hydrogen peroxide is a regulator of ABI1, a protein phosphatase 2C from Arabidopsis. *FEBS Letters* **508**, 443-446.
Moreau M, Lindermayr C, Durner J, Klessig DF. 2010. NO synthesis and signaling in plants – where do we stand? *Physiologia Plantarum* **138**, 372-383.
Morrissette NS, Mitra A, Sept D, Sibley LD. 2004. Dinitroanilines bind alpha-tubulin to disrupt microtubules. *Mol Biol Cell* **15**, 1960-1968.
Mudge C, Gossett BJ, Murphy TR. 1984. Resistance of goosegrass (*Eleusine indica*) to dinitroaniline herbicides. *Weed Sci.* **32**, 591–594.
Müller S, Han S, Smith LG. 2006. Two kinesins are involved in the spatial control of cytokinesis in Arabidopsis thaliana. *Curr Biol* **16**, 888-894.
Müller S. 2012. Universal rules for division plane selection in plants. *Protoplasma* **249**, 239-253.
Neill S, Barros R, Bright J, Desikan R, Hancock J, Harrison J, Morris P, Ribeiro D, Wilson I. 2008. Nitric oxide, stomatal closure, and abiotic stress. *Journal of Experimental Botany* **59**, 165-176.
Neill SJ, Desikan R, Clarke A, Hurst RD, Hancock JT. 2002. Hydrogen peroxide and nitric oxide as signalling molecules in plants. *Journal of Experimental Botany* **53**, 1237-1247.
Quinones GB, Danowski BA, Devaraj A, Singh V, Ligon LA. 2011. The posttranslational modification of tubulin undergoes a switch from detyrosination to acetylation as epithelial cells become polarized. *Mol. Biol. Cell* **22**, 1045-1057.
Rai SS, Wolff J. 1998. The C terminus of beta-tubulin regulates vinblastine-induced tubulin polymerization. *Proceedings of the National Academy of Sciences of the*

United States of America **95**, 4253-4257.
Rasmussen CG, Humphries JA, Smith LG. 2011. Determination of symmetric and asymmetric division planes in plant cells. *Annu Rev Plant Biol* **62**, 387-409.
Rasmussen CG, Wright AJ, Müller S. 2013. The role of the cytoskeleton and associated proteins in plant cell division plane determination. *The Plant Journal*, doi: 10.1111/tpj.12177.
Ribeiro DM, Desikan R, Bright JO, Confraria ANA, Harrison J, Hancock JT, Barros RS, Neill SJ, Wilson ID. 2009. Differential requirement for NO during ABA-induced stomatal closure in turgid and wilted leaves. *Plant, Cell & Environment* **32**, 46-57.
Smertenko A, Blume Y, Viklický V, Opatrný Z, Dráber P. 1997. Post-translational modifications and multiple tubulin isoforms in *Nicotiana tabacum* L. cells. *Planta* **201**, 349-358.
Snyder JP, Nettles JH, Cornett B, Downing KH, Nogales E. 2001. The binding conformation of taxol in β-tubulin: A model based on electron crystallographic density. *Proceedings of the National Academy of Sciences*, **98,** 5312-5316.
Tanou G, Filippou P, Belghazi M, Job D, Diamantidis G, Fotopoulos V, Molassiotis A. 2012. Oxidative and nitrosative-based signaling and associated post-translational modifications orchestrate the acclimation of citrus plants to salinity stress. *The Plant Journal* **72**, 585-599.
Verhey KJ, Gaertig J. 2007. The Tubulin Code. *Cell Cycle* **6**, 2152-2160.
Verhey KJ, Hammond JW. 2009. Traffic control: regulation of kinesin motors. *Nat Rev Mol Cell Biol* **10**, 765-777.
Wang P, Du Y, Li Y, Ren D, Song C-P. 2010. Hydrogen Peroxide–Mediated Activation of MAP Kinase 6 Modulates Nitric Oxide Biosynthesis and Signal Transduction in Arabidopsis. *The Plant Cell* **22**, 2981-2998.
Wang X, Bian Y, Cheng K, Zou H, Sun SS-M, He J-X. 2012. A Comprehensive Differential Proteomic Study of Nitrate Deprivation in Arabidopsis Reveals Complex Regulatory Networks of Plant Nitrogen Responses. *Journal of Proteome Research* **11**, 2301-2315.
Westermann S, Weber K. 2003. Post-translational modifications regulate microtubule function. *Nat Rev Mol Cell Biol* **4**, 938-948.
Yao LL, Pei BL, Zhou Q, Li YZ. 2012. NO serves as a signaling intermediate downstream of H 2O 2 to modulate dynamic microtubule cytoskeleton during responses to VD-toxins in Arabidopsis. *Plant Signal Behav* **7**, 174-177.
Yemets AI, Krasylenko YA, Lytvyn DI, Sheremet YA, Blume YB. 2011. Nitric oxide signalling via cytoskeleton in plants. *Plant Science* **181**, 545-554.
Yemets AI, Krasylenko YA, Sheremet YA, Blume YB. 2009. Microtubule reorganization as a response to implementation of NO signals in plant cells. *Cytology and Genetics* **43**, 73-79.
Zhang Q, Qian W-J, Knyushko TV, Clauss TRW, Purvine SO, Moore RJ, Sacksteder CA, Chin MH, Smith DJ, Camp DG, Bigelow DJ, Smith RD. 2007. A Method for Selective Enrichment and Analysis of Nitrotyrosine-Containing Peptides in Complex Proteome Samples. *Journal of Proteome Research* **6**, 2257-2268.

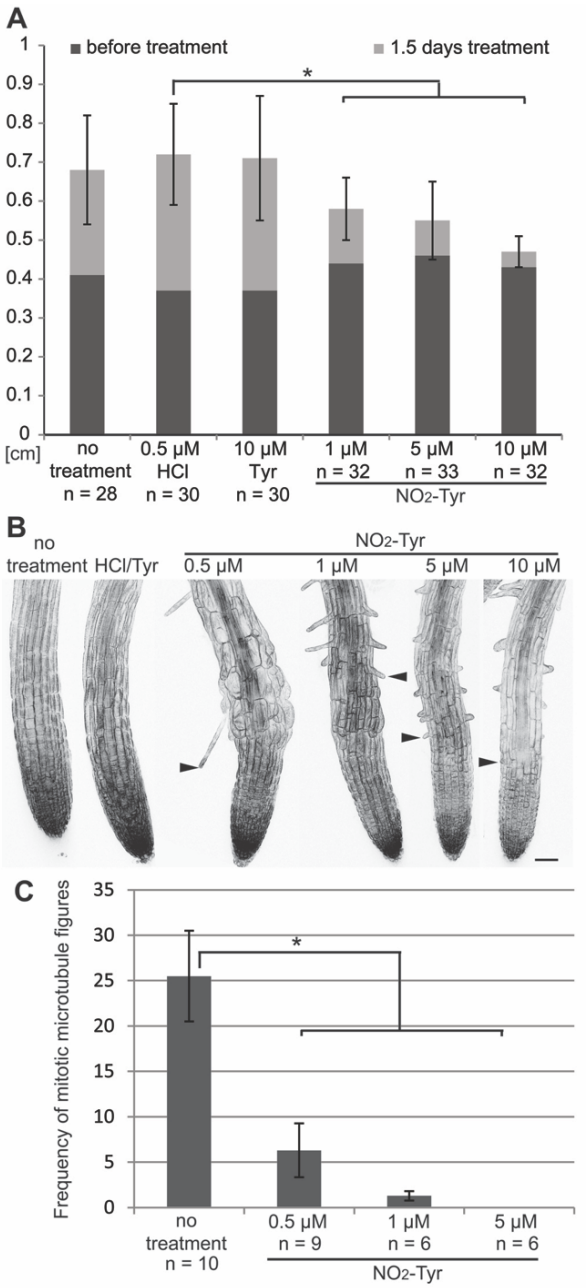

Figure 1. *Arabidopsis thaliana s*eedling root growth and root tip morphology. **(A)** Average root length of seedlings at 4 days after germination (dark grey bar) and subsequently after 1.5 days of exposure to different amounts of 3-nitro-L-tyrosine (NO_2-Tyr) in the growth medium (light grey bar). Root growth during the 1.5 day treatment (light grey bars) is significantly deminished on NO_2-Tyr containing medium (1 µM NO_2-Tyr 0.14 ± 0.08 cm, 5 µM NO_2-Tyr 0.09 ± 0.01 cm, 10 µM NO_2-Tyr 0.04 ± 0.04 cm, **P* ≤ 0.015) compared to controls, which show insignificant differences in root growth (no treatment 0.27 ± 0.14 cm, 0.5 µM HCl 0.35 ±0.13 cm, 0.34 ± 0.16 cm *P* ≥ 0.21). Sample sizes (n) for each treatment are given. Error bars indicate ± standard deviation (SD). **(B)** Confocal images of seedling root tips expressing the microtubule reporter GFP-MBD. Images are maximum intensity z-projections of image stacks taken at 10 µm intervals; the number of images per stack varies. Seedlings grown under control conditions (10 µM Tyr, 0.5 µM HCl) did not exhibit changes in root morphology. Seedlings exposed to NO_2-Tyr displayed moderate cell expansion defects in the root elongation zone (0.5 µM and 1 µM NO_2-Tyr) and short root hairs (1 µM, 5 µM and 10 µM NO_2-Tyr) as indicated by arrowheads. Scale bar is 50 µm. **(C)** Exposure of seedlings to different amounts of NO_2-Tyr inhibits mitotic activity in the root meristems. Frequency of mitotic microtubule arrays (preprophase band, spindle and phragmoplast) dropped significantly (**P* <0.01) in NO_2-Tyr treated seedlings. The numbers (n) of analyzed root meristems are indicated for each individual treatment. Bars represent mean quantities of mitotic microtubule arrays. Error bars indicate ± SD.

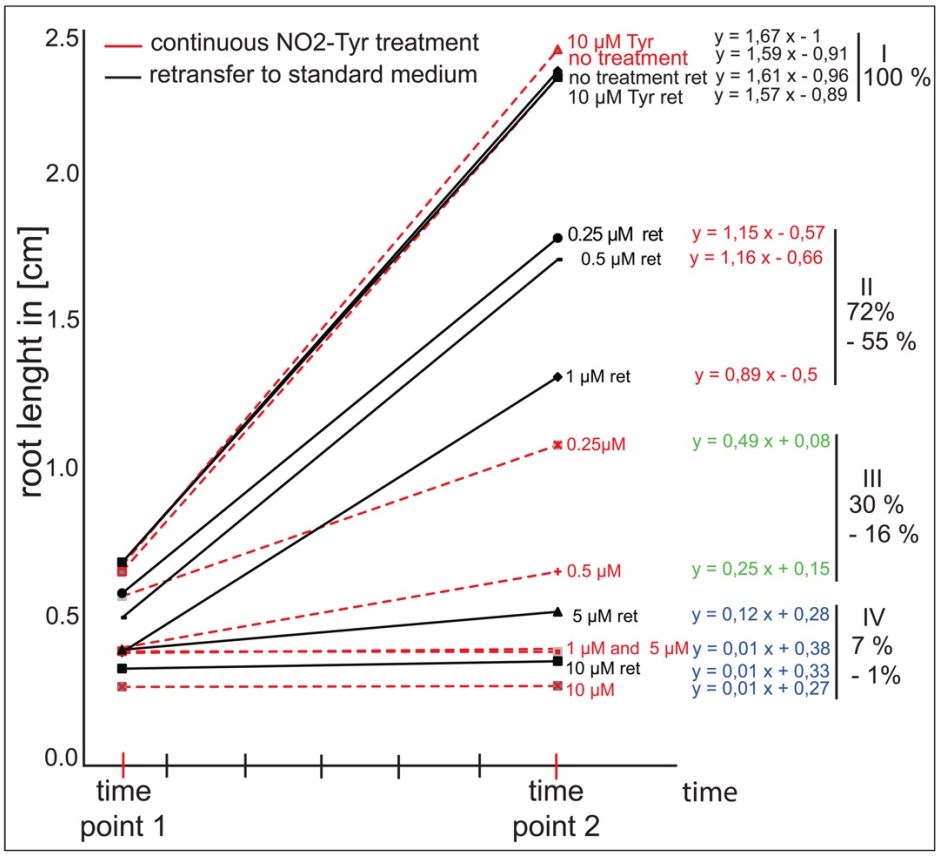

Figure 2. Growth effects induced by 3-nitro-L-tyrosine (NO_2-Tyr) concentrations are reversible. Seedlings grow on standard medium for four days and are subsequently transferred to growth medium containing different NO_2Tyr concentrations as indicated for 1.5 days (time point 1). Then, half of the seedlings are re-transferred to standard medium for additional 4.5 days (time point 2). Root length before (time point 1) and 4.5 days after retransfer (time point 2) is blotted over time. Black curves (continuous line) indicate samples retransferred onto standard medium plates and red curves (dashed lines) indicate samples that were transferred to freshly prepared NO_2Tyr medium (continuous NO_2Tyr treatment). Equations of linear regression curves are indicative of growth rate performance and are given for each treatment. The equation are grouped into four classes (I to IV) based on the similarity of their slope. Class (I) contains non-transferred and retransferred control samples and represent 100% of the growth rate potential. Class (II) comprises samples retransferred from low NO_2-Tyr concentrations (0.25 µM ret, 0.5 µM ret and 1 µm ret). Class (III) contains samples, continuously treated with low NO_2-Tyr concentrations (0.25 µM, 0.5 µM). Class (IV) includes high NO_2-Tyr concentrations (1 µM, 5 µM, 10 µM and 5 µM ret, 10 µM ret). Percentage ranges indicate growth performance as achieved in each class as a means to illustrate growth recovery relative to the potential growth as measured for controls (100%).

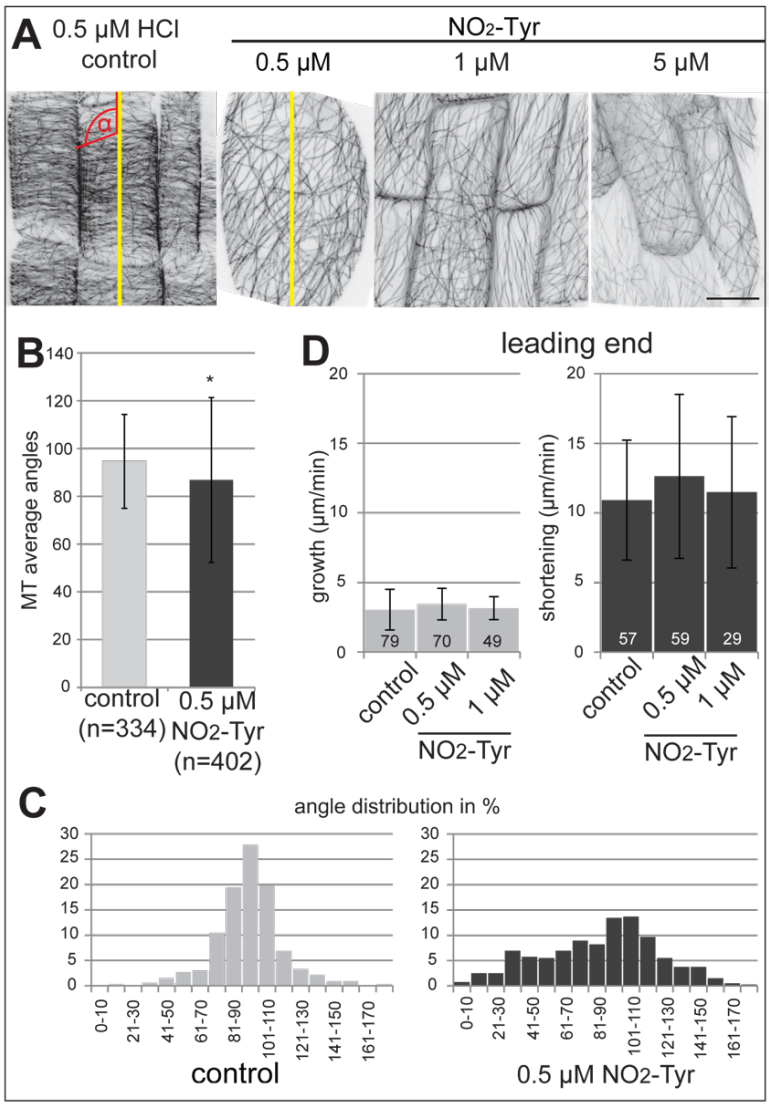

Figure 3. Organization of cortical microtubule (MT) arrays in epidermal cells at the elongation zone. **(A)** In controls, interphase cells show characteristic parallel alignment of cortical MTs. Low concentrations of 3-nitro-L-tyrosine (NO_2-Tyr, 0.5 µM) disrupt the cortical MT array organization and cells show signs of non-polarized expansion. Representative, inverted images are maximum intensity z-projections of image stacks, taken at 1 µm z-intervals; stacks encompass optical sections from the surface to a median cross section through the cells. The number of optical sections per stack varies. Scale bar is 10 µm. **(B – D)** Distribution of microtubule (MT) angles and the dynamicity of MT plus (leading) ends in epidermal cells of the elongation zone; **(B)** MT angles (red angle symbol in Figure 3A) were determined counter clock wise, relative to the long axis of the cell (indicated by the yellow lines in Figure 3A). The average angle of MTs (86.8 ± 34.6°) in 3-nitro-L-tyrosine (NO_2-Tyr) cells differs significantly from the average angle in control cells (94.6 ± 19.6°). The total number (n) of evaluated MT angles is given. Results represent the average angle of n = 8 cells calculated from eight plants for controls and the average angle calculated from n=7 cells of seven plants for 0.5 µM NO_2-Tyr. The average angle of cortical MTs upon NO_2-Tyr treatment is significantly different form the transverse angle observed in controls (**P=0.0003)*. It is noteworthy that the standard deviation is rather large for NO_2-Tyr. **(C)** Distribution histogram of MT angles observed in relation to the long axis of the cell in **(A)**, the x-axis represents MT angles in 10 degree bins and the y-axis depicts the frequency of measurements for each bin. **(D)** Growth (polymerization) and shortening (de-polymerization) velocities were determined for MT plus (leading) ends. No significant differences in MT dynamicity were observed between no treatment controls and NO_2-Tyr treated cells. MT growth and shortening velocities were measured in controls (n= 23 cells from 10 roots), 0.5 µM NO_2-Tyr treated (n= 28 cells from 11 roots) and 1 µM NO_2-Tyr treated (n= 21 cells from 8 roots) plants. The numbers of analyzed plus ends are indicated in the bar diagram. Results represent the average velocities of two independent experiments. Error bars indicate ± standard deviation.

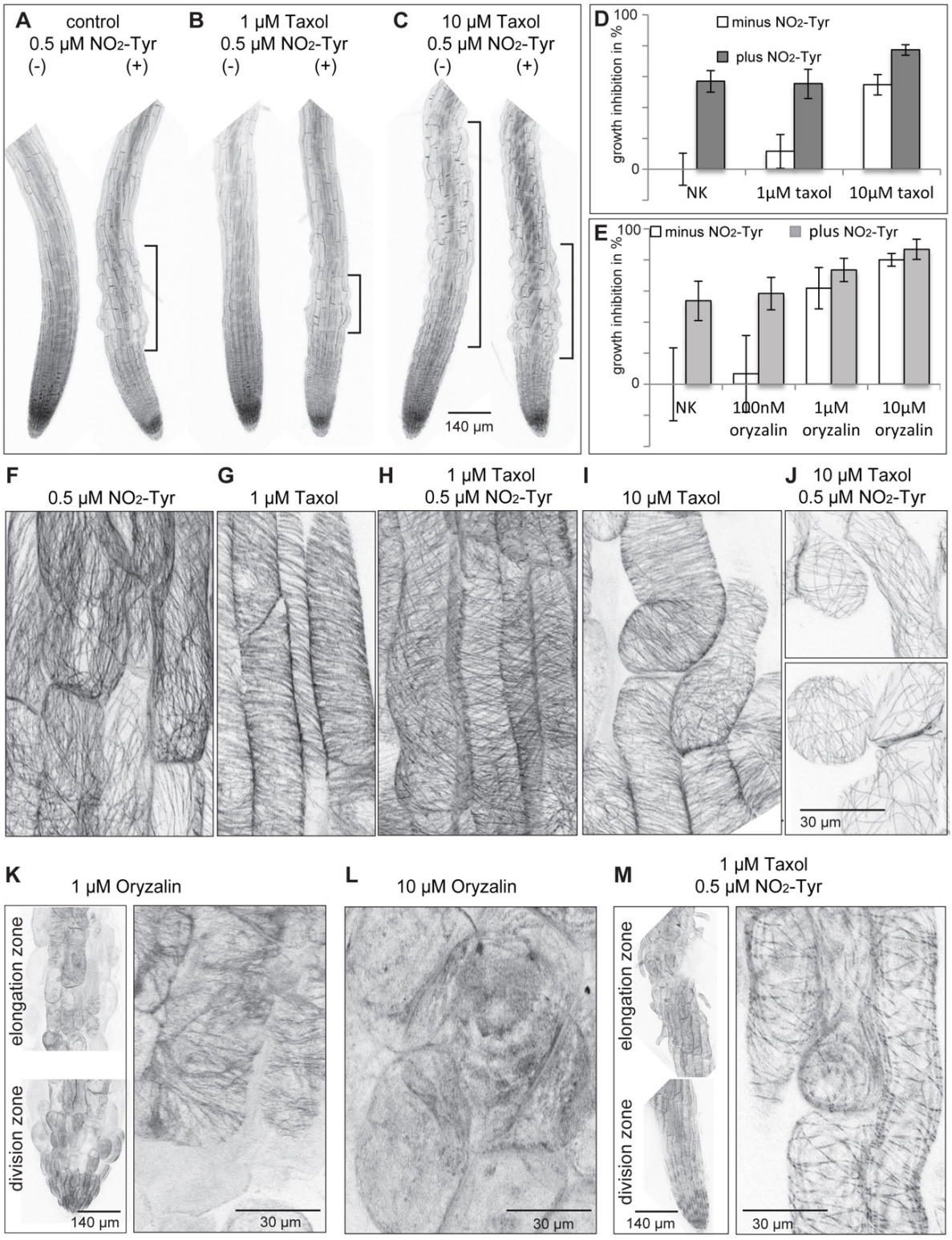

Figure 4. Effects of NO_2-Tyr in combination with taxol or oryzalin. **(A to C)** Seedling morphology of **(A)** control without (-) and with (+) 0.5 µM NO_2-Tyr, **(B and C)** taxol treatment as indicated without (-) and with (+) 0.5 µM NO_2-Tyr. **(D and E)** Growth inhibition is displayed as a percentage of untreated controls. **(D)** White columns show growth inhibition with taxol only. Grey columns show growth inhibition in the presence of 0.5 µM NO_2-Tyr. Error bars indicate ± standard deviation (n ≥ 24). **(E)** Normalized growth inhibition as a percentage of control. White columes show growth inhibition with oryzalin only. Grey columes show growth inhibition in the presence of 0.5 µM NO_2-Tyr. Error bars indicate ± standard deviation (n ≥ 27). **(F to M)** Microtubule (MT) organization in the presence of drugs as indicated. **(K and M)** Left panel: Morphology of elongation zone and division zone upon drug treatment as indicated.

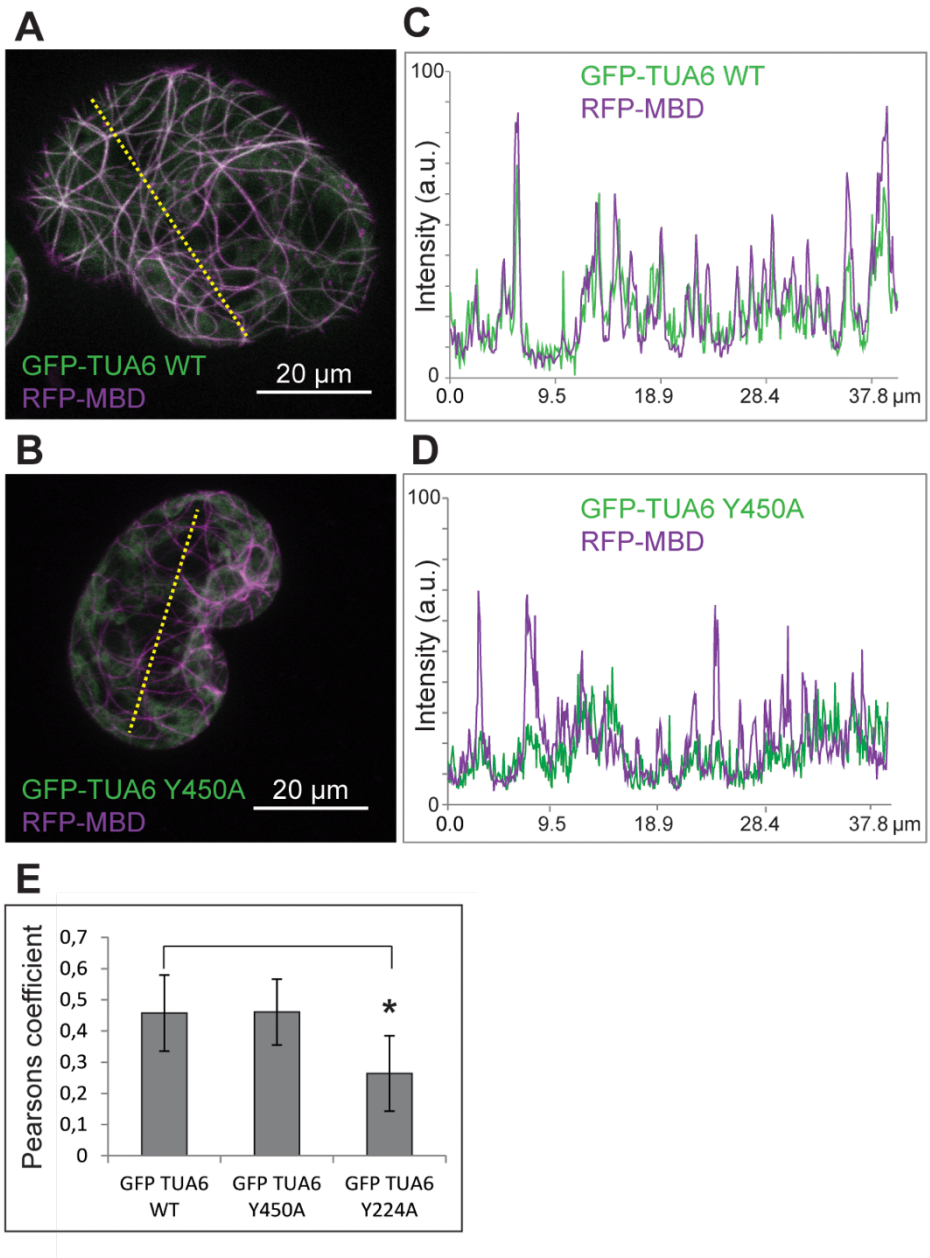

Figure 5. *Arabidopsis thaliana* protoplasts co-expressing TUA6 *p35S:GFP-TUA6* (green) and *p35S:RFP-MBD* (magenta). **(A)** Protoplast co-expressing *p35S:GFP-TUA6 WT* and *p35S: RFP-MBD*. **(C)** Plot profile of fluorescent signal intensities along the dotted line in (A). (B) Protoplast co-expressing *p35S:GFP-TUA6 Y450A* and *p35S: RFP-MBD*. **(D)** Plot profile of fluorescent signal intensities along the dotted line in **(B)**. (**E)** Mean Pearsons correlation coefficient determined for GFP and RFP in protoplasts co-expressing *p35S:RFP-MBD* together with either *p35:GFP-TUA6 WT* (0.45 ± 0.12, n=14) or mutant *p35:GFP-TUA6 Y450A* (0.46 ± 0.10, n=14) and *p35:GFP-TUA6 Y224A* (0.26 ± 0.12, n=14, **P* > 0.001).

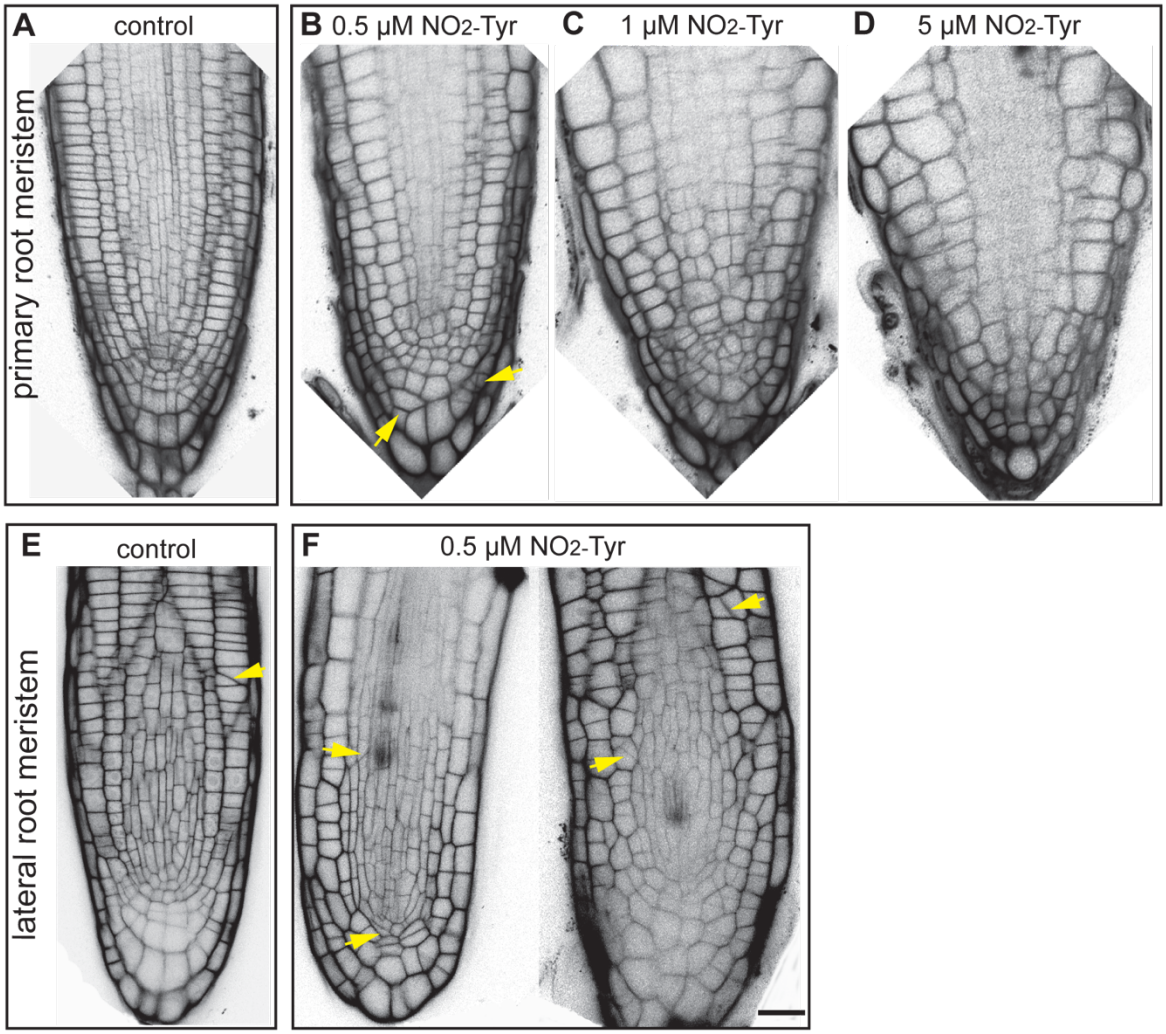

Figure 6. Long term treatment at low 3-nitro-L-tyrosine (NO_2-Tyr) concentrations moderately effects division plane orientation in root meristems. Confocal images show cell wall patterns of root meristems stained with Propidium Iodide. **(A** and **E)** no treatment controls display regular stereotypic cell division patterns. **(B, C, F)** Low amounts of NO_2-Tyr (0.5 µM and 1 µM) have modest effects on cell wall positioning, exhibiting low frequency of oblique cell walls (arrows). **(D)** No oblique walls were observed in 5 µM NO_2-Tyr treated meristems due to the inhibition of mitotic activity at high NO_2-Tyr concentrations.

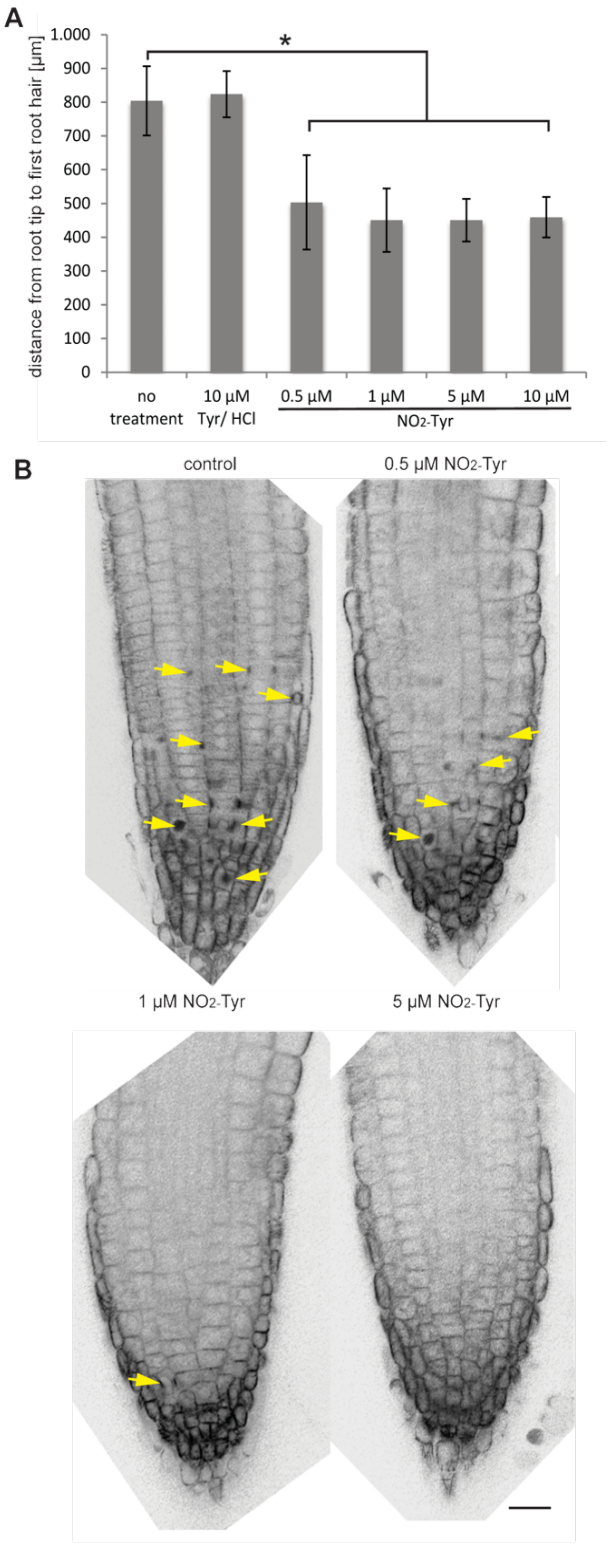

Supplementary Figure 1

Supplemental Figure 1. (A) Reduction of root tip size. The distance between root tip and first root hair is significantly shorter in 3-nitro-L-tyrosine (NO_2-Tyr) treated plants (**P* < 0.001, n=10) compared to control plants (n=10). **(B)** Representative, inverted confocal images depict single optical sections of the root meristem. On average multiple mitotic microtubule (MT) arrays are visible in single optical sections of control meristems. Considerably fewer mitotic MT arrays are present in single sections of NO_2-Tyr treated samples (see also Figure 1C). Mitotic figures (preprophase band, spindle, phragmoplast) in cross section are indicated by arrows. Scale bar is 20 µM.

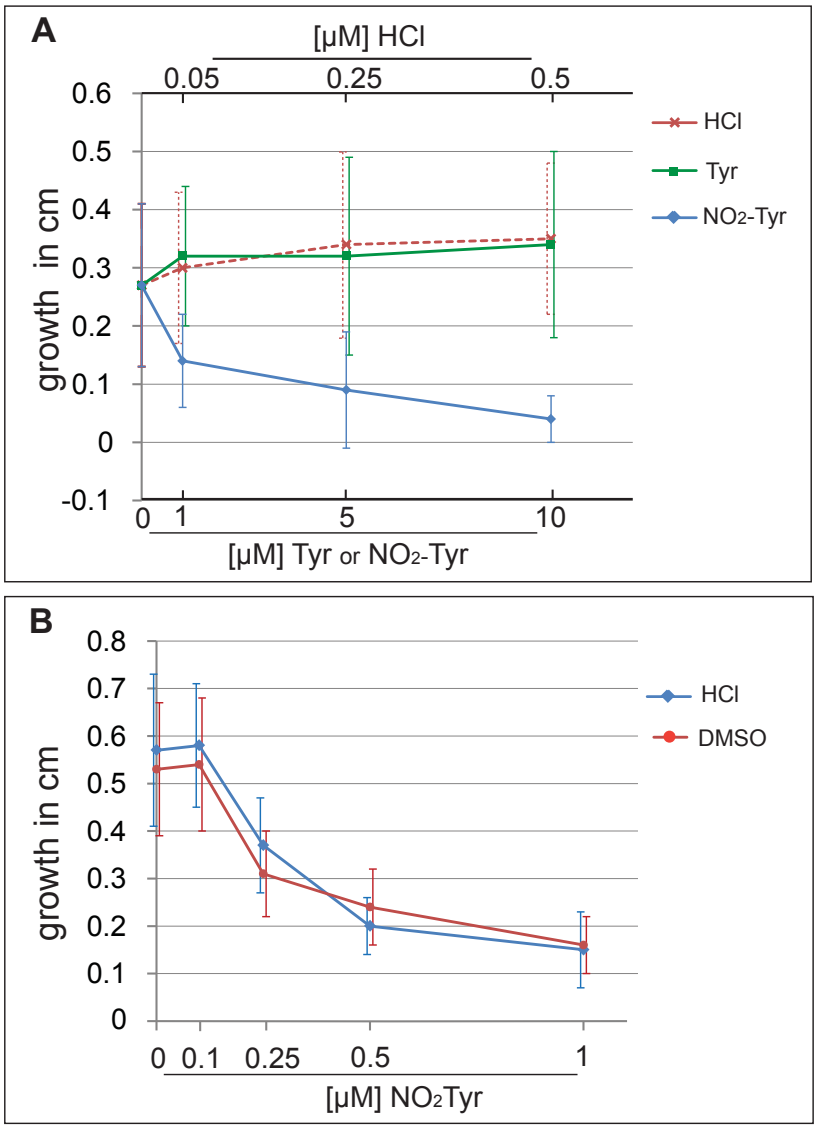

Supplemental Figure 2. Growth response curves of seedling roots under different control conditions. Seedlings were grown on standard medium for four days and subsequently subjected to different treatments for 1.5 additional days. **(A)** Different 3-nitro-L-tyrosine (NO_2-Tyr) concentrations were compared with tyrosine (Tyr) concentrations supplemented in the medium. While seedlings grown on NO_2-Tyr showed dramatic decrease in growth rate, the corresponding Tyr controls showed a steady growth rate, similar to seedlings grown on medium supplemented with different HCl concentrations as mock (solvent only) control (n ≥ 27 plants). The lower abscissae represent different Tyr or NO_2-Tyr concentrations while the abscissae on the top, indicates HCl concentrations. **(B)** HCl supports the stability of the NO_2-Tyr solution, but is not a widely used solvent. To ensure that HCl by itself had no effect on plant growth we compared plant growth on plates prepared from NO_2-Tyr stock solution dissolved in 1 mM HCl or dissolved in DMSO. No significant differences were observed (n ≥ 19 plants) indicating that HCl had no effect.

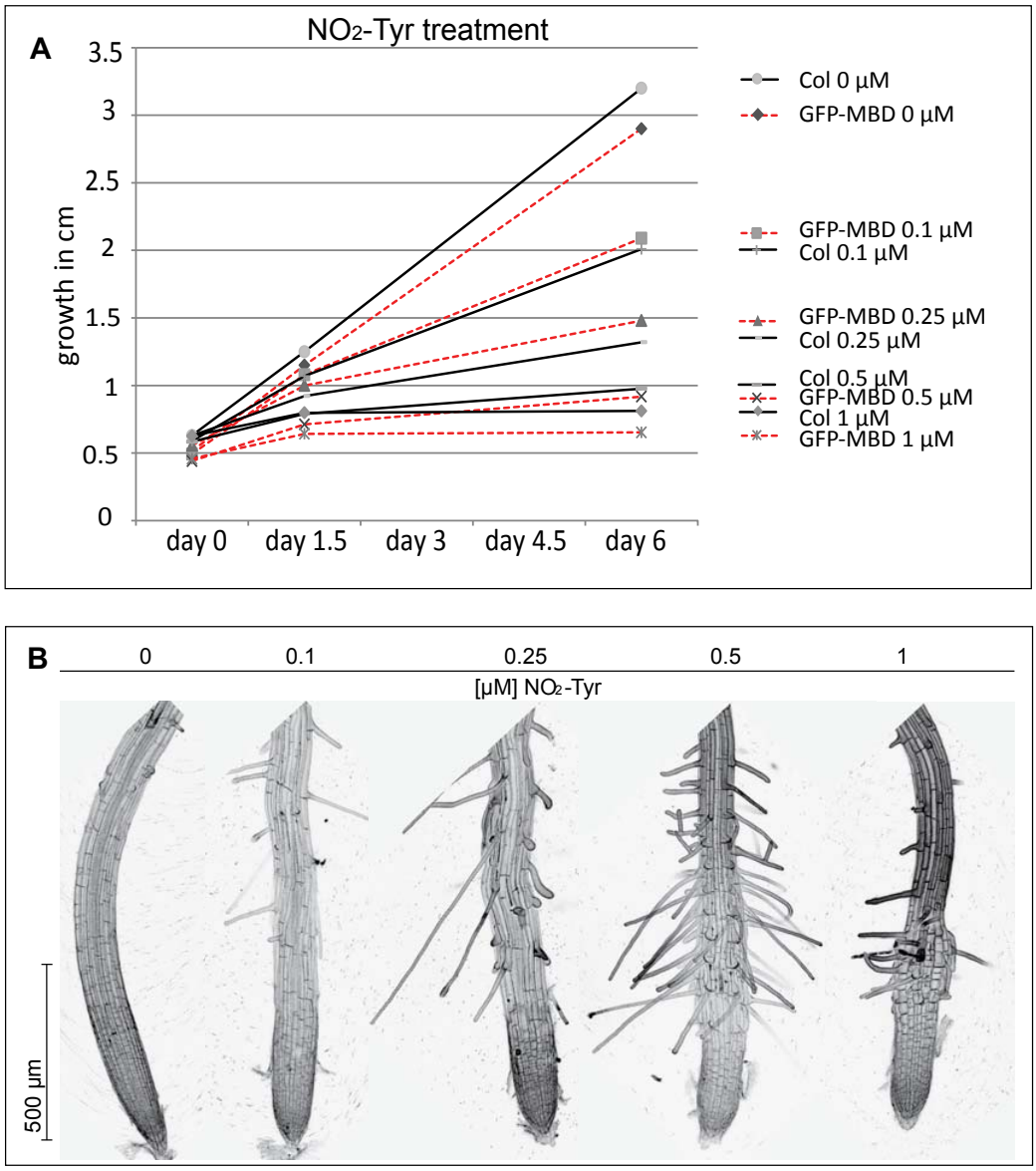

Supplemental Figure 3. Growth response of *A. thaliana* Columbia wild type (Col wt) roots upon 3-nitro-L-tyrosine (NO_2-Tyr) treatment. **(A)** Comparison of root growth of Col wt (black, continuous line) and the microtubule reporter line GFP-MBD (red, dashed line). No significant differences were observed during the treatment and the overall trend of growth inhibition is similar for Col wt and the GFP-MBD line (n ≥ 19 plants for each data point). Seedlings were germinated and grown on standard medium for four days. Then root growth was evaluated (day 0) immediately before treatment with different concentrations of NO_2-Tyr (0 µM, 0.1 µM, 0.25 µM, 0.5 µM and 1 µM) started. After 1.5 days (day 1.5) and six days (day 6) of treatment root growth was measured and blotted over time. Note that root length between Col wt and GFP-MBD differ before treatment (day 0), but that slopes of growth rate are very similar, indicating that growth response to NO_2-Tyr treatment is comparable between Col wt and GFP-MBD. **(B)** Root tip morphology of Col wt plants on different NO_2-Tyr concentrations after six days of treatment.

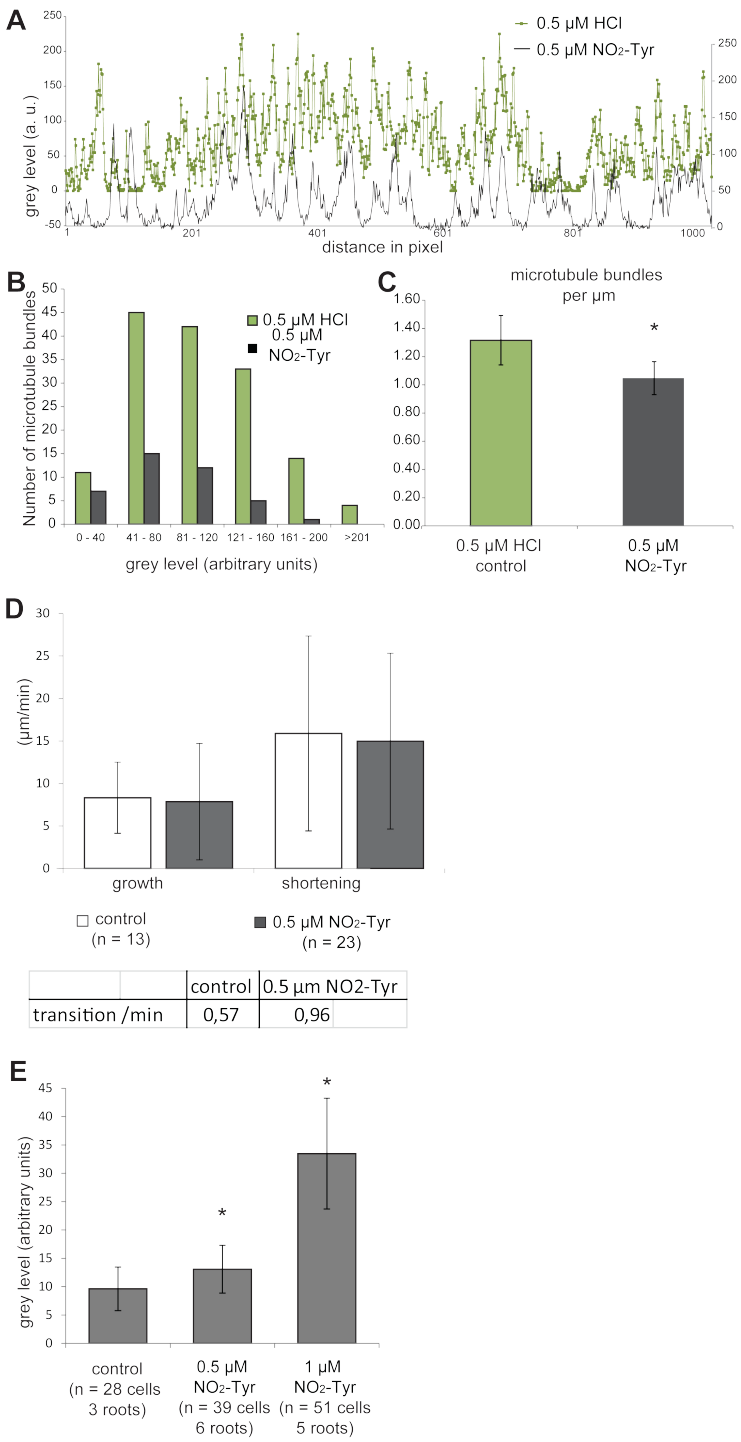

Supplemental Figure 4. (A) Representative fluorescence intensity (arbitrary units, a.u.) profile plots, along the yellow lines in (A) are depicted as green line with squares for 0.5 µM HCl (control) and continuous black line for 0.5 µM NO_2-Tyr treated samples (the y-axis is shifted by 50 arbitrary units). Intensity values are background subtracted. **(B)** The distribution of intensity peaks into six fluorescence intensity classes for intensity blot profile in (B) is depicted. NO_2-Tyr treatment reduced the frequency of fluorescence peaks (black bars) throughout the different intensity classes (x-axis) compared to the control (green boxed bar). Values for NO_2-Tyr treatment are 7 (0-40), 15 (41-80), 12 (81-120), 5 (121-160), 1 (161-200) and 0 (>201). Values for controls are 11 (0-40), 45 (41-80), 42 (81-120), 33 (121-160), 14 (161-200) and 4 (>201). **(C)** Mean values for total numbers of MT bundles (defined as peaks) per µm in control (n = 9 cells from 6 roots) and treated samples (**P*<0.05, n = 10 cells from 6 roots). Error bars indicate ± standard deviation. **(D)** Growth (polymerization) and shortening (de-polymerization) velocities for microtubule (MT) plus ends and transition rates. No significant differences in MT dynamicity were observed between controls (n= 13 microtubules) and 0.5 µM NO_2-Tyr treated (n= 23 microtubules) cells. Transition frequencies between growth, shortening and pausing increase to 0.96 transitions/min in 0.5 µM NO_2-Tyr compared to 0.57 transitions/min in controls. Error bars indicate ± standard deviation. **(E)** Increase of cytosolic GFP-MBD determined by increase of fluorescent signal intensity upon increasing NO_2-Tyr concentrations. Number of cells and roots are indicated (**P*≤0.001).

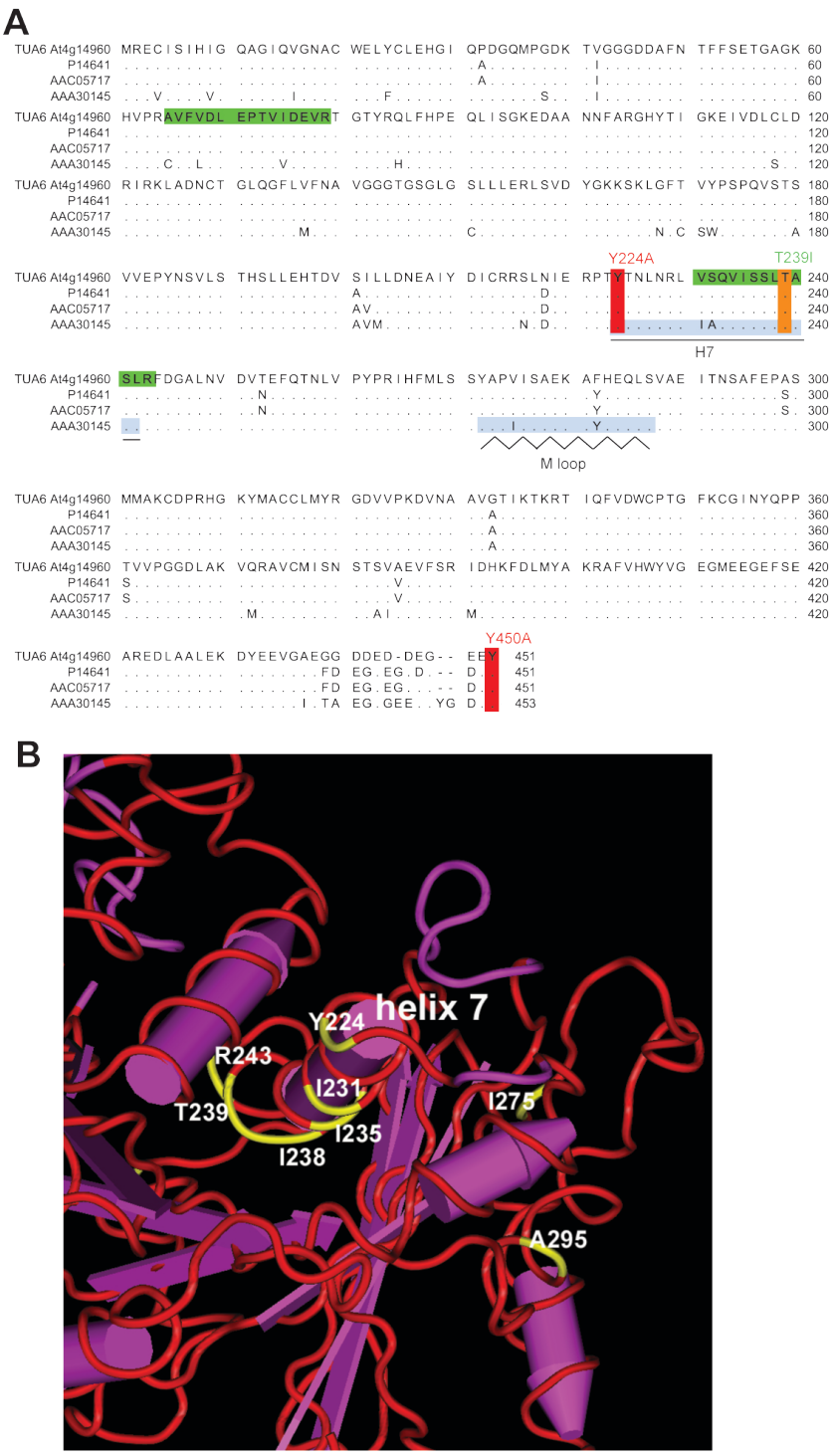

Supplemental Figure 5. (A) Alignment of TUA6 isoforms. *Arabidopsis thaliana* (*A. th.*) TUA6 (At4g14960), goosegrass TUA1 (AAC05717), *Zea mays* TUA1 (P14641), Toxoplasma gondii TUA1 (AAA30145). Identical amino acids are indicated by dots. Green boxes indicate peptide sequences identifying *At.h.* TUA6 as a target of nitro-tyrosination (Lozano-Justo *et al.*, 2011). Blue boxes indicate helix 7 (H7) and M-loop which build the oryzalin binding pocket (Morrisette *et al.*, 2004). Mutation of Threonin 239 to Isoleucin in the H7 confers oryzalin resistance in goosegrass (Mudge *et al.,* 1984) and *Zea mays* (Anthony *et al.* 1998). Mutation in tyrosine 224 (Y224A) and tyrosine 450 (Y450A) mutants used in this study are indicated. Alignment was created with Alignment tool in CLC Main Workbench 6.8.4. **(B)** 3D model (CDD structure model, http://www.ncbi.nlm.nih.gov/Structure/cdd/cddsrv.cgi?uid=100015), of nucleotide binding site in alpha tubulin. Positions of Y224 and amino acids which confer oryzalin resistance when mutated are labelled in yellow. Note that Y224 maps to the same face of H7 as mutated amino acids identified in oryzalin resistant lines.

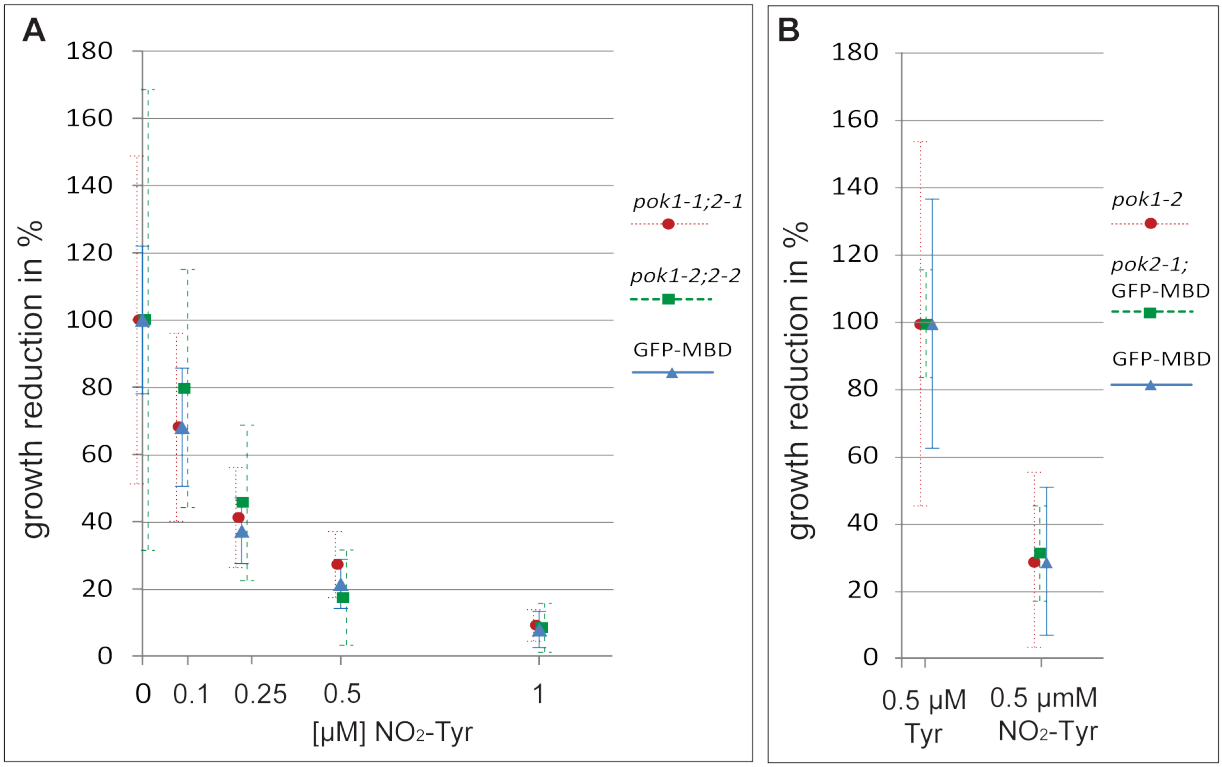

Supplemental Figure 6. Growth responses to 3-nitro-L-tyrosine (NO_2-Tyr) are similar for wild type, *pok1* and *pok2* single and *pok1pok2* double mutants. As in previously described experiments, the *A. thaliana* seedlings were grown on standard medium for four days but then exposed to different NO_2-Tyr treatments for 6 additional days. **(A)** The decline in root growth upon different concentrations of NO_2-Tyr treatment does not differ significantly for GFP-MBD (indicated by blue triangle and continuous line) plants and two different allele combinations of *pok1pok2* double mutants (*pok1-1pok1-2* indicated by red circle and dotted line and *pok1-2pok2-2* indicated by green square and dashed line). The number of plants analyzed for each data point is n ≥ 15. **(B)** *pok* sinlge mutants and GFP-MBD control showed similar growth response to 0.5 µM NO_2-Tyr treatment. GFP-MBD is indicated by blue triangle and continuous line, *pok1-2* is indicated by the red circle and dotted line and *pok2-1*;GFP-MBD (*pok2-1* in GFP-MBD background) is indicated by green square and dashed line. The number of plants analyzed for each genotype is n ≥ 15. Root length on control plates is set to 100% for each genotype.

7.2 Review articles

7.2.1 Potential roles for Kinesins at the cortical division site

Lipka, E., and Müller, S. Potential roles for Kinesins at the cortical division site. *Frontiers in plant science* **3**, 158 (2012).

Link: *http://journal.frontiersin.org/article/10.3389/fpls.2012.00158/abstract*

frontiers in
PLANT SCIENCE

MINI REVIEW ARTICLE
published: 13 July 2012
doi: 10.3389/fpls.2012.00158

Potential roles for kinesins at the cortical division site

Elisabeth Lipka and Sabine Müller*

Cell and Developmental Genetics, Center for Plant Molecular Biology, University of Tuebingen, Tuebingen, Germany

Edited by:
Luis Vidali, Worcester Polytechnic Institute, USA

Reviewed by:
Pankaj Dhonukshe, Utrecht University, Netherlands
Giampiero Cai, Università degli Studi di Siena, Italy

***Correspondence:**
Sabine Müller, Cell and Developmental Genetics, Center for Plant Molecular Biology, University of Tuebingen, Auf der Morgenstelle 3, D-72076 Tuebingen, Germany. e-mail: sabine.mueller@zmbp.uni-tuebingen.de

Spatial control of cytokinesis is critical for cell and plant morphology. The plane of cell division is established at G2/M transition and is initially demarcated at the cortex of the cell by the cytoskeletal preprophase band (PPB) and subsequently throughout mitosis by the cortical division zone (CDZ). Few kinesins, belonging to different classes of the superfamily, either display a distinct spatio-temporal localization at the PPB and CDZ, or genetic evidence proposes a specific function there. Protein phosphorylation and degradation are likely directing the cell cycle-dependent localization and activity of some of these kinesins, as indicated by mutation of respective conserved motifs. Furthermore, kinesins are required for continuous recruitment of CDZ identity markers to the CDZ. This review summarizes the limited current knowledge of kinesins potentially involved in the steps required for correctly oriented division planes, considering localization patterns and genetic evidence, and discussing kinesin function in context with interaction partners and cell cycle regulation.

Keywords: kinesin, cell division, cortical division site, preprophase band, phragmoplast

INTRODUCTION

The cytoskeleton is a major facilitator of cell division and cell expansion in all organisms. In cellulose-enfolded plant cells, specific cytoskeletal arrays are responsible for the selection of the division plane in pre-mitotic cells and the formation of the cell plate to partition cytoplasmic contents of daughter cells during cytokinesis. The preprophase band (PPB), composed of microtubules (MTs), F-actin, and endoplasmic reticulum delineates the plane of cell division at the cell cortex. The transition from the interphase cortical MT array to the mitotic PPB involves local changes in MT dynamic behavior, regulated by the activity of MT-associated proteins (MAPs; Dhonukshe and Gadella, 2003; Vos et al., 2004). Minute detail is known about the regulation of PPB assembly; however, genes encoding MT nucleation factors TONNEAU (TON)1A and TON1B and a protein phosphatase PP2A subunit TON2/DCD1/ADD1 are strictly required for PPB formation in *Arabidopsis*, *Physcomitrella* and maize, respectively, since knockout mutants lack PPBs and exhibit mis-positioned division planes (Camilleri et al., 2002; Azimzadeh et al., 2008; Wright et al., 2009; Spinner et al., 2010). The PPB's spatial information is preserved throughout mitosis by proteins, distinctly recruited to the cortical division zone (CDZ), formerly occupied by the PPB, and by proteins selectively depleted from the CDZ. Thus, the CDZ is tagged by positive and negative identity markers. Progressive confinement of the CDZ during cytokinesis specifies the precise site of cell plate fusion, the cortical division site (CDS).

Among the 61 predicted kinesins in *Arabidopsis*, only about one-third were up-regulated during mitosis (Menges et al., 2003; Lee and Liu, 2004; Vanstraelen et al., 2006a) and even fewer were implicated in division plane selection and maintenance (Zhu and Dixit, 2011).

DIVISION PLANE SELECTION AND PPB FORMATION

The position of the nucleus is informative for division plane orientation (Muller, 2011; Rasmussen et al., 2011a). Displacement of the prophase nucleus in protonemata leads to the formation of a new PPB, encircling the dislodged nucleus (Murata and Wada, 1991). Prior to proliferative, symmetric divisions in pre-mitotic cells, the nucleus is centered presumably by MT length-dependent forces (Goodbody et al., 1991; Besson and Dumais, 2011).

Recently, members of the KCH subgroup of kinesin-14 class were implicated in nuclear migration. A number of KCH proteins tested so far displayed actin binding activity conferred by the conserved Calponin homology (CH) domain (**Figure 2**) potentially linking the MT and the actin cytoskeleton (Frey et al., 2009; Buschmann et al., 2011; Klotz and Nick, 2012). A study revealed the existence of motile, MT-associated NtKCH populations at the cell cortex, and non-motile peri-nuclear populations associating with actin in interphase of tobacco BY-2 cells (Klotz and Nick, 2012). Consistent with overexpression of its *Arabidopsis* homolog AtKinG in BY-2 cells and with other kinesins in that class, NtKCH motility was MT minus end directed (Lee and Liu, 2004; Buschmann et al., 2011). Furthermore, motile NtKCH associated with a subset of MTs, bridging the nucleus with the cell cortex. Thus, it was suggested that KCH might act in the positioning of the nucleus involving a combination of MT dynamics and actin anchored KCH sliding toward MT minus ends (Klotz and Nick, 2012). Indeed, pre-mitotic nuclear migration was significantly delayed in tobacco BY-2 cells overexpressing GFP-KCH1 from rice (OsKCH1; Frey et al., 2010).

Kinesin-14 class members ATK1 and KCBP and kinesin-5 AtKRP125c co-localized with the PPB, but also with interphase and mitotic MT arrays supporting a more general role in MT bundling (Bowser and Reddy, 1997; Marcus et al., 2003; Bannigan et al., 2007). Although *atk1* mutants display wider PPBs indicating a role in PPB formation, an impact on the CDZ or cell wall positioning was not reported (Marcus et al., 2003).

The function of the negative CDZ marker, kinesin KCA1 remains enigmatic (Vanstraelen et al., 2006b). KCA1 accumulated at the plasma membrane at high levels during mitosis, but

remained absent from the CDZ, presenting a KCA1 depleted site and resembling aspects of F-actin distribution (**Figure 1**). As indicated by MT-depolymerization experiments, formation of the KCA1 depleted site depended on prior PPB assembly and absence of the KCA1 depleted site lead to mis-positioning of cell plates. Similarly, drug induced depolymerization of F-actin before formation of the actin depleted zone/microfilament twin peaks (ADZ/MFTP) disturbed proper cell plate positioning in BY-2 cells (Hoshino et al., 2003; Sano et al., 2005). In contrast, KCA1 localization did not alter upon actin depolymerization (Vanstraelen et al., 2006b). Interestingly, *kca1kca2* double mutants were defective in light-induced chloroplast movement (Suetsugu et al., 2010), a process known to be actin dependent. It is likely that the CDZ requires an environment of reduced motility to recruit and maintain a certain suite of proteins (Panteris, 2008). Experiments pertaining to the temporal relations between KCA1 and other CDZ markers should help elucidate the significance of differential KCA1 localization.

KCA1 and its homolog KCA2 were initially identified as CDKA;1 interaction partners (Vanstraelen et al., 2004). The KCAs shared a conserved domain structure with N-terminal motor domain. However, the motor domain was most similar to that of C-terminal kinesins and preceded by a neck-linker and therefore, KCAs were placed within the kinesin-14 subfamily (Vanstraelen et al., 2004). The subsequent stalk domain-mediated homo- and hetero-dimerization *in vitro* (Vanstraelen et al., 2004) and the C-terminal tails of KCA1 and KCA2 featured three and two CDKA;1 phosphorylation sites, respectively. Site directed mutagenesis indeed reduced binding to CDKA;1 *in vitro* and intramolecular folding of the tail onto the stalk was obstructed. Thus, KCA activity might be regulated depending on their phosphorylation status, which might be addressed by expression of phospho-mimic mutants in plants.

Progression through the cell cycle depends on the timely degradation of cell cycle regulatory proteins, to ensure synchronization of chromatin condensation and mitotic cytoskeletal array formation. Recently, the kinesin AtKINUa/ARK3 was proposed to act as a synchronizer (Sakai et al., 2008; Malcos and Cyr, 2011). AtKINUa is a member of a small ungrouped class of kinesins, present in plants and protists. Their domain structure is unique, comprising

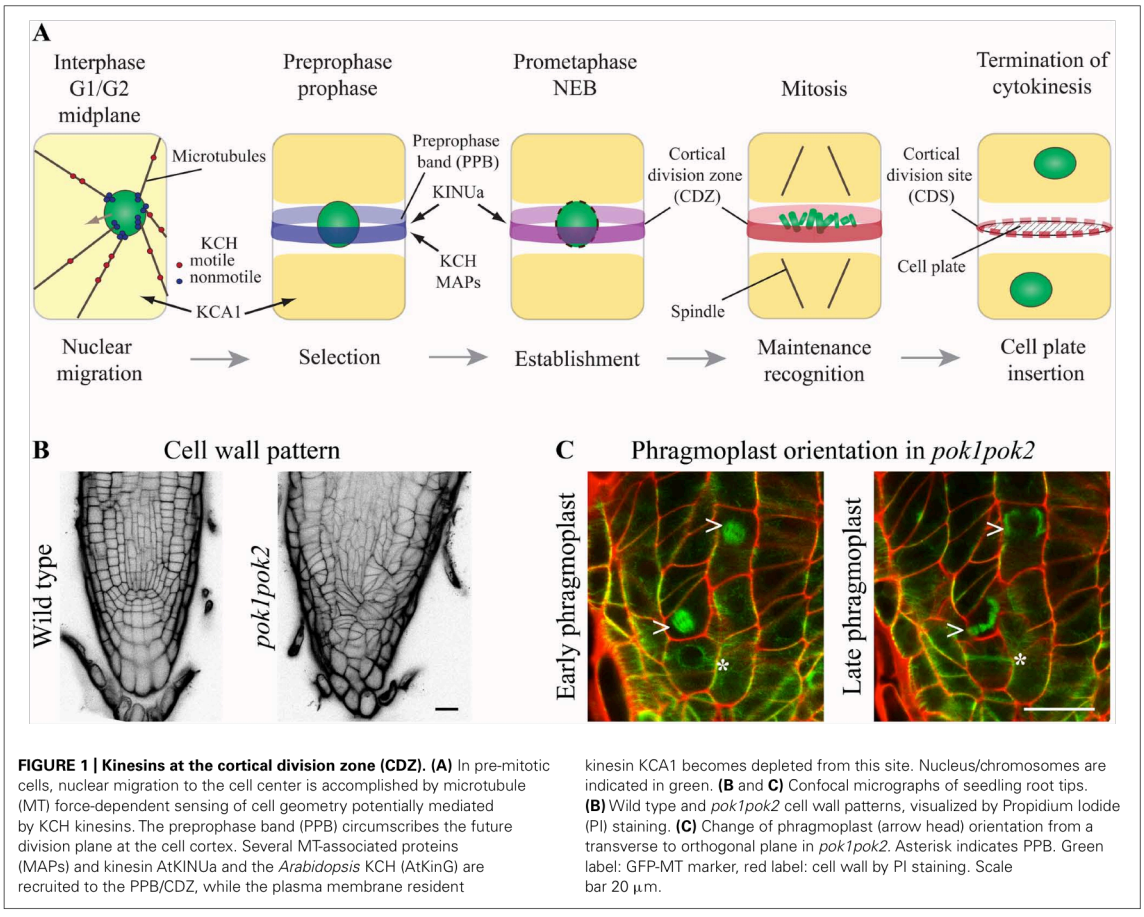

FIGURE 1 | Kinesins at the cortical division zone (CDZ). (A) In pre-mitotic cells, nuclear migration to the cell center is accomplished by microtubule (MT) force-dependent sensing of cell geometry potentially mediated by KCH kinesins. The preprophase band (PPB) circumscribes the future division plane at the cell cortex. Several MT-associated proteins (MAPs) and kinesin AtKINUa and the *Arabidopsis* KCH (AtKinG) are recruited to the PPB/CDZ, while the plasma membrane resident kinesin KCA1 becomes depleted from this site. Nucleus/chromosomes are indicated in green. **(B** and **C)** Confocal micrographs of seedling root tips. **(B)** Wild type and *pok1pok2* cell wall patterns, visualized by Propidium Iodide (PI) staining. **(C)** Change of phragmoplast (arrow head) orientation from a transverse to orthogonal plane in *pok1pok2*. Asterisk indicates PPB. Green label: GFP-MT marker, red label: cell wall by PI staining. Scale bar 20 μm.

a non-conserved N-terminal motor domain and a variable number of armadillo repeats at their C-terminus, however, lacking a characteristic neck-linker (Malcos and Cyr, 2011). Furthermore, these kinesins contain a conserved destruction box (D-BOX) motif, serving as a potential target for proteasome-mediated degradation. AtKINUa associated with cortical MTs in interphase, but became highly enriched at the PPB in prophase and eventually disappeared upon nuclear envelope breakdown (NEB) in metaphase. Intriguingly, not only AtKINUa degradation at the NEB depended on the D-BOX motif, but also the protein's association with PPB MTs. The mutation of a conserved residue within the D-BOX motif resulted in diffuse accumulation of AtKINUa-GFP at the PPB, as well as at the spindle and phragmoplast, indicating that timely degradation of the fusion protein was obstructed (Malcos and Cyr, 2011). Immediately succeeding the D-BOX is a putative CDKA phosphorylation site, however, its significance for AtKINUa localization was not evaluated so far. AtKINUa was distinctly expressed in embryos and cells of the stomatal lineage in *Arabidopsis*, but, genetic evidence for specific function of AtKINUa during cell division is not available yet (Sakai et al., 2008; Malcos and Cyr, 2011).

The confined spatio-temporal localization pattern of AtKINUa and its protein domains narrow the number of potential interaction partners to several PPB-associated MAPs such as MOR1, CLASP, AIR9, or MAP65s (Buschmann et al., 2006; Kawamura et al., 2006; Ambrose et al., 2007) and above mentioned kinesins ATK1, KCBP, and AtKRP125c. TON2/DCD1, however, showed a spatio-temporal distribution very similar to AtKINUa (Wright et al., 2009) making it a probable interaction partner. Indeed, recently shown genetic interaction between *TON2* and *MOR1* and *TON2* and *TON1* further validated the involvement of these proteins in division plane placement (Kirik et al., 2012). Most likely, TON2-dependent dephosphorylation modulates the activity of MOR1 and TON1 in MT array organization. Thus, functional aspects of AtKINUa might be revealed by investigating localization of endogenous and AtKINUa phosphomutants in mutants defective in PPB formation and cell wall positioning.

DIVISION PLANE MAINTENANCE

PHRAGMOPLAST ORIENTING KINESIN (POK) 1 and 2 were required for the preservation and/or recognition of spatial information conveyed by the PPB. POKs belonged to the kinesin-12 class based on their N-terminal motor domain and were the largest predicted kinesins in *Arabidopsis* (**Figure 2**; Lee and Liu, 2004). Despite their significant size difference (**Figure 2**) and overlapping, yet distinct gene expression patterns, POK1 and POK2 exhibited functional redundancy. While single mutants were indistinguishable from wild-type, double mutants of T-DNA insertion alleles displayed dwarfed overall morphology and pronounced mis-orientation of cell walls in root meristems, deviating from the regular pattern characteristic for wild-type (**Figure 1B**; Muller et al., 2006).

The plant-specific MAP TANGLED and the Ran regulatory protein RanGAP1, both positive CDZ identity markers, co-localized with the PPB and the CDZ throughout mitosis. TAN as well as RanGAP1 fusion proteins were inadequately recruited to the PPB in *pok1pok2* (Walker et al., 2007; Xu et al., 2008). Moreover, TAN and RanGAP1 association with the CDZ was not maintained past metaphase, revealing the dynamic nature of the CDZ. Strikingly, *pok1pok2* phragmoplasts appeared to lack guidance (**Figure 1C**) and the cell plate fused with the parental cell wall seemingly random, wherever they encountered upon completion of cytokinesis. Since the initial recruitment of TAN and RanGAP1 to the PPB occurred independent of POKs (Xu et al., 2008; Rasmussen et al., 2011b), kinesins other than POK1 and POK2 might support this task. The C-terminus of POK1-mediated interaction with both, TAN and RanGAP1 (Muller et al., 2006; Xu et al., 2008), suggesting that POK1 itself localized to the CDZ.

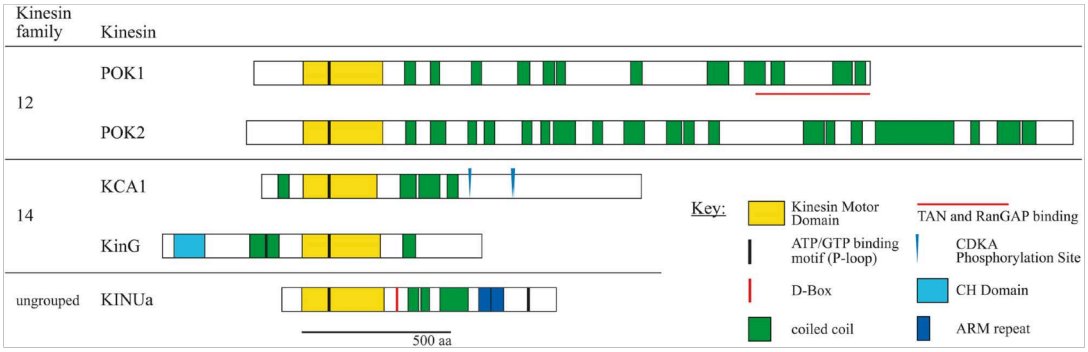

FIGURE 2 | Schematic overview of kinesin proteins implicated in cortical division site (CDS) establishment by experimental evidence. Subfamily affiliations are according to the nomenclature (Lawrence et al., 2004). Proteins were co-aligned with respect to the P-loop motifs within the motor domain. Experimentally confirmed D-BOX motifs and CDKA phosphorylation sites are indicated. Amino acid sequences were obtained from TAIR. Kinesin motor domains, P-loop motifs, armadillo (ARM) repeats, and calponin homology (CH) domains were predicted using ScanProsite tool at Expasy (http://prosite.expasy.org/scanprosite). Coiled coil domains were predicted using Parcoil2 at MIT, with a cut off value $P > 0.025$ and minimum read of 28 (http://groups.csail.mit.edu/cb/paircoil2). Proteins are drawn to scale.

CONCLUDING REMARKS

KCAs and AtKINUa are documented instances for the impact of cell cycle-dependent phospho-regulation and protein degradation on protein activity and localization. Notably, the CDK consensus motif [S/T-P-x-K/R] was detected several times in POKs, in AtKinG (KCH) and a phosphorylation site was predicted for AtKINUa (Malcos and Cyr, 2011). Furthermore, consensus D-BOX motifs [R-x_2-L-x_4-N/Q] were present in POKs (manual annotation and Vanstraelen et al., 2006a).

So far, motility was only reported for KCH kinesins. Future research assignments certainly involve *in vivo* live-cell imaging studies as well as *in vitro* assembly and imaging to investigate kinetics of kinesins taking part in CDZ selection and maintenance. However, successful analysis depends on the availability of functional fusion proteins which may be confirmed by complementation of mutants or consensus localization with specific antibodies. Furthermore, the low abundance of these kinesins poses challenges, even for sensitive imaging systems. Nevertheless, recent technical advances in imaging may contribute to tackle these objectives.

ACKNOWLEDGMENT

Work in this field of research is supported by the Deutsche Forschungsgemeinschaft (Project MU3133/1-1 to Sabine Müller).

REFERENCES

Ambrose, J. C., Shoji, T., Kotzer, A. M., Pighin, J. A., and Wasteneys, G. O. (2007). The *Arabidopsis* CLASP gene encodes a microtubule-associated protein involved in cell expansion and division. *Plant Cell* 19, 2763–2775.

Azimzadeh, J., Nacry, P., Christodoulidou, A., Drevensek, S., Camilleri, C., Amiour, N., Parcy, F., Pastuglia, M., and Bouchez, D. (2008). *Arabidopsis* TONNEAU1 proteins are essential for preprophase band formation and interact with centrin. *Plant Cell* 20, 2146–2159.

Bannigan, A., Scheible, W. R., Lukowitz, W., Fagerstrom, C., Wadsworth, P., Somerville, C., and Baskin, T. I. (2007). A conserved role for kinesin-5 in plant mitosis. *J. Cell Sci.* 120, 2819–2827.

Besson, S., and Dumais, J. (2011). Universal rule for the symmetric division of plant cells. *Proc. Natl. Acad. Sci. U.S.A.* 108, 6294–6299.

Bowser, J., and Reddy, A. S. (1997). Localization of a kinesin-like calmodulin-binding protein in dividing cells of *Arabidopsis* and tobacco. *Plant J.* 12, 1429–1437.

Buschmann, H., Chan, J., Sanchez-Pulido, L., Andrade-Navarro, M. A., Doonan, J. H., and Lloyd, C. W. (2006). Microtubule-associated AIR9 recognizes the cortical division site at preprophase and cell-plate insertion. *Curr. Biol.* 16, 1938–1943.

Buschmann, H., Green, P., Sambade, A., Doonan, J. H., and Lloyd, C. W. (2011). Cytoskeletal dynamics in interphase, mitosis and cytokinesis analysed through *Agrobacterium*-mediated transient transformation of tobacco BY-2 cells. *New Phytol.* 190, 258–267.

Camilleri, C., Azimzadeh, J., Pastuglia, M., Bellini, C., Grandjean, O., and Bouchez, D. (2002). The *Arabidopsis* TONNEAU2 gene encodes a putative novel protein phosphatase 2A regulatory subunit essential for the control of the cortical cytoskeleton. *Plant Cell* 14, 833–845.

Dhonukshe, P., and Gadella, T. W., Jr. (2003). Alteration of microtubule dynamic instability during preprophase band formation revealed by yellow fluorescent protein-CLIP170 microtubule plus-end labeling. *Plant Cell* 15, 597–611.

Frey, N., Klotz, J., and Nick, P. (2009). Dynamic bridges – a calponin-domain kinesin from rice links actin filaments and microtubules in both cycling and non-cycling cells. *Plant Cell Physiol.* 50, 1493–1506.

Frey, N., Klotz, J., and Nick, P. (2010). A kinesin with calponin-homology domain is involved in premitotic nuclear migration. *J. Exp. Bot.* 61, 3423–3437.

Goodbody, K. C., Venverloo, C. J., and Lloyd, C. W. (1991). Laser microsurgery demonstrates that cytoplasmic strands anchoring the nucleus across the vacuole of premitotic plant cells are under tension. Implications for division plane alignment. *Development* 113, 931–939.

Hoshino, H., Yoneda, A., Kumagai, F., and Hasezawa, S. (2003). Roles of actin-depleted zone and preprophase band in determining the division site of higher-plant cells, a tobacco BY-2 cell line expressing GFP-tubulin. *Protoplasma* 222, 157–165.

Kawamura, E., Himmelspach, R., Rashbrooke, M. C., Whittington, A. T., Gale, K. R., Collings, D. A., and Wasteneys, G. O. (2006). MICROTUBULE ORGANIZATION 1 regulates structure and function of microtubule arrays during mitosis and cytokinesis in the *Arabidopsis* root. *Plant Physiol.* 140, 102–114.

Kirik, A., Ehrhardt, D. W., and Kirik, V. (2012). TONNEAU2/FASS regulates the geometry of microtubule nucleation and cortical array organization in interphase *Arabidopsis* cells. *Plant Cell* 24, 1158–1170.

Klotz, J., and Nick, P. (2012). A novel actin-microtubule cross-linking kinesin, NtKCH, functions in cell expansion and division. *New Phytol.* 193, 576–589.

Lawrence, C. J., Dawe, R. K., Christie, K. R., Cleveland, D. W., Dawson, S. C., Endow, S. A., Goldstein, L. S., Goodson, H. V., Hirokawa, N., Howard, J., Malmberg, R. L., Mcintosh, J. R., Miki, H., Mitchison, T. J., Okada, Y., Reddy, A. S., Saxton, W. M., Schliwa, M., Scholey, J. M., Vale, R. D., Walczak, C. E., and Wordeman, L. (2004). A standardized kinesin nomenclature. *J. Cell Biol.* 167, 19–22.

Lee, Y. R. J., and Liu, B. (2004). Cytoskeletal motors in *Arabidopsis.* Sixty-one kinesins and seventeen myosins. *Plant Physiol.* 136, 3877–3883.

Malcos, J. L., and Cyr, R. J. (2011). An ungrouped plant kinesin accumulates at the preprophase band in a cell cycle-dependent manner. *Cytoskeleton (Hoboken)* 68, 247–258.

Marcus, A. I., Li, W., Ma, H., and Cyr, R. J. (2003). A kinesin mutant with an atypical bipolar spindle undergoes normal mitosis. *Mol. Biol. Cell* 14, 1717–1726.

Menges, M., Hennig, L., Gruissem, W., and Murray, J. A. (2003). Genome-wide gene expression in an *Arabidopsis* cell suspension. *Plant Mol. Biol.* 53, 423–442.

Muller, S. (2011). Universal rules for division plane selection in plants. *Protoplasma* 249, 239–253.

Muller, S., Han, S., and Smith, L. G. (2006). Two kinesins are involved in the spatial control of cytokinesis in *Arabidopsis thaliana. Curr. Biol.* 16, 888–894.

Murata, T., and Wada, M. (1991). Effects of centrifugation on preprophase-band formation in *Adiantum protonemata. Planta* 183, 391–398.

Panteris, E. (2008). Cortical actin filaments at the division site of mitotic plant cells: a reconsideration of the 'actin-depleted zone'. *New Phytol.* 179, 334–341.

Rasmussen, C. G., Humphries, J. A., and Smith, L. G. (2011a). Determination of symmetric and asymmetric division planes in plant cells. *Annu. Rev. Plant Biol.* 62, 387–409.

Rasmussen, C. G., Sun, B., and Smith, L. G. (2011b). Tangled localization at the cortical division site of plant cells occurs by several mechanisms. *J. Cell Sci.* 124, 270–279.

Sakai, T., Honing, H. V. D., Nishioka, M., Uehara, Y., Takahashi, M., Fujisawa, N., Saji, K., Seki, M., Shinozaki, K., Jones, M. A., Smirnoff, N., Okada, K., and Wasteneys, G. O. (2008). Armadillo repeat-containing kinesins and a NIMA-related kinase are required for epidermal-cell morphogenesis in *Arabidopsis. Plant J.* 53, 157–171.

Sano, T., Higaki, T., Oda, Y., Hayashi, T., and Hasezawa, S. (2005). Appearance of actin microfilament 'twin peaks' in mitosis and their function in cell plate formation, as visualized in tobacco BY-2 cells expressing GFP-fimbrin. *Plant J.* 44, 595–605.

Spinner, L., Pastuglia, M., Belcram, K., Pegoraro, M., Goussot, M., Bouchez, D., and Schaefer, D. G. (2010). The function of TONNEAU1 in moss reveals ancient mechanisms of division plane specification and cell elongation in land plants. *Development* 137, 2733–2742.

Suetsugu, N., Yamada, N., Kagawa, T., Yonekura, H., Uyeda, T. Q. P., Kadota, A., and Wada, M. (2010). Two kinesin-like proteins mediate actin-based chloroplast movement in *Arabidopsis thaliana. Proc. Natl. Acad. Sci. U.S.A.* 107, 8860–8865.

Vanstraelen, M., Inzé, D., and Geelen, D. (2006a). Mitosis-specific kinesins in *Arabidopsis. Trends Plant Sci.* 11, 167–175.

Vanstraelen, M., Torres Acosta, J. A., De Veylder, L., Inze, D., and Geelen, D. (2004). A plant-specific subclass of C-terminal kinesins contains a conserved a-type cyclin-dependent

kinase site implicated in folding and dimerization. *Plant Physiol.* 135, 1417–1429.

Vanstraelen, M., Van Damme, D., De Rycke, R., Mylle, E., Inze, D., and Geelen, D. (2006b). Cell cycle-dependent targeting of a kinesin at the plasma membrane demarcates the division site in plant cells. *Curr. Biol.* 16, 308–314.

Vos, J. W., Dogterom, M., and Emons, A. M. (2004). Microtubules become more dynamic but not shorter during preprophase band formation: a possible "search-and-capture" mechanism for microtubule translocation. *Cell Motil. Cytoskeleton* 57, 246–258.

Walker, K. L., Muller, S., Moss, D., Ehrhardt, D. W., and Smith, L. G. (2007). *Arabidopsis* TANGLED identifies the division plane throughout mitosis and cytokinesis. *Curr. Biol.* 17, 1827–1836.

Wright, A. J., Gallagher, K., and Smith, L. G. (2009). discordia1 and alternative discordia1 function redundantly at the cortical division site to promote preprophase band formation and orient division planes in maize. *Plant Cell* 21, 234–247.

Xu, X. M., Zhao, Q., Rodrigo-Peiris, T., Brkljacic, J., He, C. S., Muller, S., and Meier, I. (2008). RanGAP1 is a continuous marker of the *Arabidopsis* cell division plane. *Proc. Natl. Acad. Sci. U.S.A.* 105, 18637–18642.

Zhu, C., and Dixit, R. (2011). Functions of the *Arabidopsis* kinesin superfamily of microtubule-based motor proteins. *Protoplasma* doi: 10.1007/s00709-011-0343-9 [Epub ahead of print].

Conflict of Interest Statement: The authors declare that the research was conducted in the absence of any commercial or financial relationships that could be construed as a potential conflict of interest.

Received: 30 April 2012; accepted: 28 June 2012; published online: 13 July 2012.
*Citation: Lipka E and Müller S (2012) Potential roles for kinesins at the cortical division site. Front. Plant Sci. **3**:158. doi: 10.3389/fpls.2012.00158*
This article was submitted to Frontiers in Plant Cell Biology, a specialty of Frontiers in Plant Science.

7.2.2 Mechanisms of plant cell division

Lipka, E., Herrmann, A., and Mueller, S. Mechanisms of plant cell division. *Wiley interdisciplinary reviews Developmental biology* (2015).

Link: *http://wires.wiley.com/WileyCDA/WiresArticle/wisId-WDEV186.html*

Authors:
Full name and affiliation; email address if corresponding author; any conflicts of interest

First author Elisabeth Lipka, ZMBP – University of Tuebingen
Second author Arvid Herrmann, ZMBP – University of Tuebingen
Third author Sabine Mueller *, ZMBP – University of Tuebingen , sabine.mueller@zmbp.uni-tuebingen.de

The authors declare no conflict of interests.

Abstract
Plant cells are confined by a network of cellulosic walls which imposes rigid control over the selection of division plane orientations, crucial for morphogenesis and genetically regulated. While in animal cells and yeast, the actin cytoskeleton is instrumental in the execution of cytokinesis, in plant cells the microtubule cytoskeleton is taking the lead in spatially controlling and executing cytokinesis by the formation of two unique, plant specific arrays, the preprophase band and the phragmoplast. The formation of microtubule arrays in plant cells is contingent on acentrosomal microtubule nucleation. At the onset of mitosis the preprophase band defines the plane of cell division where the partitioning cell wall is later constructed by the cytokinetic phragmoplast, imposing a spatio-temporal relationship between the two processes. Current research progress in the field of plant cell division focuses on identifying and tying the links between early and late events in spatial control of cytokinesis and how microtubule array formation is regulated in plant cells.

Introduction
Cell division is a fundamentally important process, allocating cellular contents to two daughter cells. In eukaryotes, this task is in large accomplished by the highly dynamic cytoskeleton. While many cellular structures and molecular processes are conserved between eukaryotes, plant cells exhibit unique features that might be attributed to their mostly sedentary life style. Moreover, most plant cells are immobilized within the network of rigid polymeric cell walls. The microtubule cytoskeleton (Figure 1) is the main driver of cell division forming the chromosome segregating spindle which is the common mitotic feature shared by eukaryotes. However, plant cells accomplish this task by a self-organizing acentrosomal mechanism. In addition, two specialized cytoskeletal structures are instrumental in the selection and maintenance of the division plane and in the formation of the cell plate. The preprophase band (PPB) is a remarkable belt-like cortical formation of microtubules (Figure 1) and actin filaments assembling at the G2 to M transition, outlining the periphery of the future division plane. However, not all cell types (i.e. endosperm, meiocytes) utilize the PPB to determine the division site, proposing that alternative strategies exist. The other plant specific cytoskeletal array is the phragmoplast (Figure 1) that physical partitions daughter cell contents by synthesis of the cell plate. Motor and non-motor microtubule associated proteins (MAPs) reorganize microtubules by means of sliding, cross linking or severing into the characteristic functional arrays in accordance to cell cycle progression. Thus vigorous coordination of cellular signalling, cytoskeletal organization and cell cycle regulators is required for cell division. This review outlines the basic principles of plant cell division with a particular focus on recent advances on plant specific molecular mechanisms in the field of plant cell division.

DIVISION PLANE SELECTION AND ESTABLISHMENT

Regulation of division plane selection: who is to decide?

Due to the fixed position of plant cells the site of cell division is of particular significance for plant morphology. While symmetric divisions are proliferative, producing daughter cells of identical fate and equal size, formative, asymmetric divisions give rise to unequally sized daughter cells that differ in cell fate thereby steering morphogenesis. Plant developmental programs such as embryo and root development as well as lateral root and stomata formation rely on asymmetric divisions, but the knowledge about their triggers is fragmentary.

Already in the 19th century botanists formulated rules of cell division placements succinctly summarized as the "shortest wall" rule, which implicate cell geometry as the determining factor [1]. Recently the simple rule was extended by the stochastic component of several competing minimum area division planes, which best reflect the observed fluctuations in the 2D analysis of division site placement [2]. Thus, division planes approximating the "shortest wall" appear to be the geometry dependent default mechanism, likely employing the cytoskeleton as a tension sensor/generator [3, 4].

Although the geometric rule suffices to explain symmetric divisions, it fails to explain how formative divisions are controlled. However, a number of "polarizing events", such as hormone signaling, nuclear migration and polar protein distribution are implicated in division plane switching [5-9].

Recently, a 4D map of the invariant division pattern of early *Arabidopsis* embryos was constructed using high-resolution imaging and computational image analysis [10] (Figure 2A). Compellingly, the 3D analysis revealed asymmetric division planes that were not detectable in 2D analysis. *Arabidopsis* auxin response mutants abandon certain asymmetric divisions in early embryo development, but conduct symmetric divisions instead [11], suggesting that auxin triggers division plane switching in the early embryo. Suppression of transcriptional auxin response by a transgenic approach indeed provoked symmetric, minimal area divisions as seen in auxin response mutant embryos [10] (Figure 2A) and demonstrated that in embryo development, geometry based symmetric divisions are the default mechanism that is overridden by local auxin signaling (Figure 2A). Finally, a minimal set of empirically acquired geometric and volumetric rules allowed 3D computer simulations of the growing wild type embryo predicting realistic division planes and cell volumes [10]. Effectors of auxin signaling that directly link it to the asymmetric division outcome still need to be identified.

In this respect, recent progress has been made in regulation of asymmetric division in the stomatal lineage. Symmetry breaking in the self-renewing stomatal stem cell lineage is regulated by the basic helix-loop-helix transcription factor SPEECHLESS (SPCH). *BASL,* which encodes a polarly localized protein, required for asymmetric cell divisions in stomatal meristemoid cells [5] is a direct target of SPCH [12]. Moreover, the gene expression of the PPB localized kinesin ARK3/KINUa is also regulated by SPCH. Cell type specific down-regulation of ARK/KINUa by expression of *SPCHpro:amiR-ark3* caused a *basl* like phenotype directly linking SPCH to the regulation of asymmetric division in the stomatal lineage (Figure 2B). Future research should clarify how polar BASL and ARK3 interact to direct PPB positioning in asymmetric cell division.

These novel findings on the regulation of division symmetry further support the view that various "polarity cues" override the default, geometry based division plane selection mechanism. Whether a common theme of asymmetric cell division plane selection will emerge remains to be seen. In this respect the *Arabidopsis aur1aur2* double mutant which displays specific defects in formative divisions in different developmental contexts [13] might become instrumental. However, the geometry based mechanism may further be modulated without changes in cell fate. It was reported that

mechanical forces generated by growth also direct division plane selection. Mutation in the p60 subunit of the microtubule severing protein KATANIN caused PPB mis-positioning and failure to respond to mechanical forces [14] suggesting that KATANIN was required to translate cell geometry information into proper division planes.
Challenges for the future are the identification of the effectors that translate potentially variable positional cues into division planes.

Formation of the Preprophase band

PPB formation at G2/M phase involves changes in microtubule dynamics and selective microtubule stabilization resulting in the gradual clearing of microtubules in apical and basal cell regions and concomitant formation of the belt-like sub-membranous PPB (Figure 1, Figure 3) [15, 16]. Consistently, a number of microtubule associated proteins (MAPs) and components of microtubules nucleation complexes, including γ-tubulin co-localize with the PPB and aid in its organization and maintenance (reviewed in Rasmussen et al., 2013).

Microtubules structure, nucleation and dynamic behaviour

Dynamic instability is an intrinsic property of the polar microtubule. This behavior can be modulated by microtubule associated proteins (MAPs), which promote microtubule polymerization or depolymerization, regulate rescue and catastrophe rates, stabilize microtubule bundles by cross linking and sever microtubules. Microtubule nucleation *in vivo* occurs from acentrosomal nucleation complexes containing γ-tubulin and conserved GCP proteins forming a template for tube elongation by oriented addition of tubulin hetero-dimers. Additional microtubule assembly factors are GCP3-interacting proteins (GIPs) and NEDD1. All of these components play critical roles in microtubule nucleation and contribute to microtubule array patterning and mutation in either one or multiple of these genes lead to severe developmental defects in plants [17, 18]. Microtubule nucleation complexes are dispersed throughout the cell cortex and associate with existing microtubules performing angle-dependent nucleation. In addition, microtubule nucleation complexes colocalize with chromosomes. Little is known about the spatio-temporal specificity of microtubule – MAP interactions. Post-translational protein modifications are certainly involved in the regulation of MAP activity during the cell cycle. Post-translational tubulin modification such as reversible detyrosination, acetylation are suggested to provide a road map for MAPs and certain tubulin modification are predominantly associated with stable microtubules or during certain cell cycle stages. These layers of regulation add to the complexity of microtubule array organization in space and time.

These MAPs are likely targets of a protein phosphatase complex that is essential for PPB formation and consequently spatially controls cytokinesis (Figure 3, Figure 4). The heterotrimeric protein phosphatase 2 A (PP2A) consists of the regulatory B subunit FASS/TONNEAU (TON) 2 [19] and variable catalytic C and scaffolding A subunits [20]. Mutants in PP2A subunits lack PPBs and display random division planes [10, 20-22] similar to mutants lacking a pair of centrin homologous proteins, TON1a and TON1b. FASS interacts directly with TON1 and with variable TON1 RECRUITING MOTIF (TRM) proteins of a large plant specific family that targets the TTP complex (for TON1/TRM/PP2A, Figure 4 B) to the cytoskeleton [20, 23]. Mutation in several MAPs including the polymerization promoting MAP MOR1 [24] display mild PPB and cell wall positioning defects [25]. Furthermore, genetic evidence identified MOR1 and TON1 as a potential target of FASS dependent phospho-regulation [26]. Apparently, in a cell cycle dependent manner, the phosphatase complex is commissioned to spatially restrict common MAP activities allowing for the formation of the PPB.

Mutation in the CLIP170-associated protein CLASP1 causes improper placement of PPBs and subtle delays in development [27, 28]. CLASP prevents edge-induced microtubule catastrophe at sharp cell edges [29] thereby maintaining the interphase cortical MT array. The putative transmembrane protein SABRE might direct CLASP activity towards the PPB region [30]. Functional GFP-CLASP1 co-localized with misoriented PPB microtubules in *sab-5* mutants, suggesting SAB acts upstream of CLASP. In meristematic interphase cells SAB localizes to the apical and basal plasma membrane, but flanks the PPB in prophase (Figure 4). This is an intriguing finding in support of the notion that not only the cortical microtubule cytoskeleton but also the membranous region underlying the PPB becomes differentially modified in order to establish the division plane. Whether SAB localization might actually be key to restrict CLASP to the PPB zone requires further investigation.

SPINDLE FORMATION

The establishment of spindle bipolarity and spindle function as the chromosome segregating entity requires the orchestrated force balancing between antagonistically acting cytoskeletal elements. A host of cytoskeletal proteins including motor and non-motor proteins aiding in maintaining antiparallel microtubule overlap in the spindle midzone have been identified that exhibit conserved functions across biological kingdoms. Furthermore, as in all microtubule arrays microtubule nucleation by γ-tubulin ring complexes (TuRC) contribute to spindle assembly. An exhaustive review on plant spindle formation is found in Masoud et al., 2013.

In plant cells, bipolar spindles are formed by the spindle self-organizing pathway [31] also known to function in animal cells that lack centrosomes due to cell differentiation or as a consequence of genetic or laser inflicted disruptions. Here we focus on the involvement of the PPB in pro-spindle formation.

In late prophase, prospindle formation commences from the reorganization of perinuclear microtubules [32] (Figure 1, Figure 5 A). Mutants without PPBs or cells with multiple PPBs exhibit delayed bipolar prospindle formation or fail to form the prospindle [19, 33] suggesting a functional link between PPB and bipolar spindle formation. [34]. Indeed bridging microtubules are involved in the reorganization of the randomly oriented perinuclear microtubules into a bipolar prospindle oriented perpendicular to the PPB plane [34], thereby communicating positional information from the PPB to the prospindl (Figure 5A).

Kinesin-14 proteins are involved in early spindle assembly. Mutation in *Arabidopsis thaliana* kinesin (ATK) 1 or ATK5 impairs prospindle formation resulting in unfocused but fully functional spindles [35, 36]. ATK5 localization is mediated by its N-terminal tail domain that tracks microtubule plus ends, and a central motor domain, which enabled microtubule minus end directed motility in *in vitro* gliding assay [37], consistent with a role in antiparallel microtubule sliding (Figure 5B). Sliding activity is well suited to account for the alignment of perinuclear microtubules into a prospindle.

Nucleation of prospindle microtubules seems to be mediated by the conserved spindle assembly factor targeting protein for XKLP2 (TPX2) [38] (Figure 5A). In animal cells, TPX2 modulates Aurora kinase activity and regulates binding of kinesin-5 and recruitment of kinesin-14 to microtubules [32]. TPX2 inhibition by antibody injection in prophase cells delayed or arrested cell cycle progression, while later impairment had no effect, demonstrating the specific requirement of TPX2 for plant pro-spindle assembly. Plant TPX2 promotes nucleation of microtubule asters *in vitro* [38] and overexpression of TPX2 leads to the assembly of aster-like perinuclear and nuclear microtubules and a marked reduction of Ran and importin β signal in the nucleus, pointing towards Ran dependent regulation of TPX2 dependent microtubule nucleation

[39]. Furthermore, plant TPX2 co-immunoprecipitates with Aurora1 Ser/Thr kinase and with γ-tubulin in *Arabidopsis* protein extracts [40] and RNAi knock down of all three Aurora kinase homologs in *Arabidopsis* cause pleiotropic developmental defects including cell cycle arrest and ectopic re-initiation of cell division in mature tissues. These reports support a Ran GTPase dependent TPX2 mediated acentrosomal spindle assembly in plants. Whether this also includes interaction with kinesin-14s that are involved in pro-spindle formation will be interesting.

CORTICAL DIVISION SITE MAINTENANCE AND PHRAGMOPLAST GUIDANCE

Despite PPB disassembly at the end of prophase, the positional information of the preprophase band is preserved through mitosis, imposing the establishment of a molecular mechanism or structure, commonly referred to as the cortical division site (CDS) [41]. However, the identification of proteins or structures, qualifying for such a task remained challenging until genetic tagging and improved imaging systems allowed the fluorescence based detection of low abundance proteins at distinct sub-cellular localization.

Preprophase band, cortical division site and cortical division site

The preprophase band (PPB) roughly delineates the division plane at the cell cortex. The PPB also recruits a number of landmark proteins that remain in this cortical region then referred to as the cortical division zone (CDZ). Upon cytokinesis the localization of CDZ resident proteins distinctly narrows and defines the cortical division site (CDS), where cell plate attachment takes place.

The highly basic, microtubule associated protein TANGLED (TAN) was initially characterized in maize [42]. Mutations in *TAN* gave rise to stunted maize plants with narrow leave blades [43]. In *tan* mitotic leave epidermis cells, phragmoplast and cell plate positions were oblique and deviated from expected positions based on the PPB orientations, predominantly affecting longitudinal divisions [44]. These observations implicated TAN in a phragmoplast guidance mechanism. Eventually, localization of TAN-YFP in dividing *Arabidopsis* root cells established TAN as a constituent of the cortical division zone (CDZ) (Figure 4). TAN-YFP co-localized with the PPB in a microtubule dependent manner and remained at the CDZ, independent of microtubules until completion of cytokinesis (Walker et al., 2007). The expression of different TAN protein domains in tobacco BY2- and *Arabidopsis* cells revealed that two distinct regions in the N-terminal half mediate TANs localization to the CDZ at different stages of cell cycle mitosis. While one region is responsible for TAN recruitment during prophase, recruitment during cytokinesis requires a second region, which also binds the formerly identified interaction partner kinesin-12 PHRAGMOPLAST ORIENTING KINESIN (POK) 1 [45, 46]. Like TAN, POK1 localizes to the PPB and CDZ/CDS. In prophase of *Arabidopsis* root meristem cells and in BY-2 cells, YFP-POK1 showed microtubule dependent and dynamic recruitment to the PPB, as determined in fluorescence recovery after photo-bleaching (FRAP) experiments. However, YFP-POK1 association with the CDZ in metaphase cells was neither dynamic nor microtubule dependent [47] suggesting that POK1 becomes somehow tethered to the membrane in late prophase and likely act as a scaffold for CDS proteins, such as TAN. Indeed, *Arabidopsis* double mutants simultaneously mutated in *POK1* and its closest homolog *POK2* fail to retain TAN-YFP beyond metaphase [47]. In *pok1pok2* mutants, PPB and phragmoplast are misaligned due to tilting of the phragmoplast from its initial direction of expansion [47] and consistent with defects in phragmoplast guidance and/or CDZ maintenance.

The protein RanGAP1, a regulatory protein in the Ran GTPase signaling pathway shows TAN-like localization and POK1-dependency at the CDS [48] (Figure 4). However, immunolocalization experiments showed RanGAP1 at the nuclear envelope in interphase and association with kinetochores and the cell plate during mitosis. While induction of RNAi knock down of RanGAP1 and RanGAP2 results in oblique and incomplete cell plate formation [48], double knock out RanGAP1/2 confers gametophyte lethality [49]. These phenotypes might represent at least in part, misregulation of Ran and thus it is difficult to interpret how the loss of RanGAP1 at the CDZ affects cell division specifically. Currently, it is not resolved whether the *pok1pok2* phenotype merely reflects the loss of TAN and RanGAP1 at the CDZ, supporting a scaffolding function for POKs, or whether POKs actively contribute to phragmoplast guidance via interaction with phragmoplast derived microtubules, which would be in tune with molecular properties of kinesin motors.
Intriguingly, TAN, RanGAP1 and POK1, all undergo signal narrowing towards the end of cytokinesis precisely defining the cell plate insertion site (Figure 4), before they vanish upon completion of cytokinesis or shortly after. The mechanism of the narrowing is entirely unclear as well as whether it is functionally significant.

ROLE OF THE ACTIN CYTOSKELETON IN CELL DIVISION

The role of actin remains ambiguous. Mutations in actin or actin associated proteins do not inhibit plant cell division, but the treatment with actin depolymerizing drugs reliably results in misplacement of new cross walls [50]. Although a component of the PPB, F-actin is conspicuously diminished from the CDS between prometaphase and anaphase, forming the actin depleted zone (ADZ), and therefore is regarded as a negative marker of the CDZ. Remarkably the ADZ is flanked by F-actin enrichments, termed actin twin peaks [51-53], though their visualization remains challenging in many cell types. It is likely that ADZ and CDZ occupy the same membrane region although experimental evidence is not available. The ADZ is first observed in late prophase and its establishment is potentially related to the accumulation of endocytic vesicles in the PPB region [54]. Reduction of F-actin in the ADZ might result in an altered cytoplasmic composition that could limit protein dynamics. The cell cycle dependent differential protein dynamics of CDZ resident proteins TAN and POK1 certainly supports this view. Actin depolymerizing drugs might interfere with the establishment of the ADZ, which could then influence CDZ maintenance. Thus, investigation of the spatio-temporal relations between ADZ and CDZ are needed to further assess ADZ function.
The kinesin-14 KCA1 also becomes depleted from the CDZ, similar to the ADZ, but decorates the entire remaining cell cortex of BY-2 cells [55]. The depletion of KCA1 may be prevented by microtubule depolymerizing drugs, leading to cell plate misorientation. The functional significance of KCA1 depletion has not been unraveled, but it is also involved in actin dependent chloroplast movement in *Arabidopsis* [56], suggesting that KCA1 might interact with both the microtubule and actin cytoskeleton.
Recently an actin-myosin driven mechanism was implicated in phragmoplast guidance in moss. A quintuple knock out mutant of myoVIIIa-e in *Physcomitrella patens* displays mispositioned cell walls in branching protonemata cells [57]. Expression of a moss myosinVIII motor protein (Myo8A-GFP) was sufficient to partially rescue the quintuple mutant phenotype. In prometaphase, Myo8A accumulation at microtubule plus ends does not depend on actin (Figure 6). In metaphase, additional Myo8A briefly surges at spindle poles but upon anaphase Myo8A-GFP is again restricted to microtubule plus ends in the spindle midzone. Concomitantly, Myo8A-GFP signal gathers in a cortical region [57] that is most likely the equivalent of the CDZ, although these cells divide without recognizable PPB formation. The plus end association of Myo8A on dynamic

peripheral spindle microtubules that probe the space between spindle and cell cortex might actually serve as a mechanism to deliver Myo8 to the CDZ. During cytokinesis, Myo8A resides on phragmoplast microtubule plus ends of the leading edge and at the CDS. Live cell imaging revealed actin dependent centripetal mobility of microtubules with Myo8A-GFP decorated plus ends, suggesting that movement towards the phragmoplast occurred along F-actin via the Myo8 motors (Figure 6) [57]. Reportedly, F-actin does bridge the phragmoplast midzone and CDS and actin nucleating formin2 (For2) localizes to the phragmoplast midzone [57]. Thus, Myo8A at peripheral MT plus ends uses actin bridges to trail back peripheral microtubules (Figure 6), in order to preserve phragmoplast integrity. Myo8A is conserved in land plants and Myo8A-GFP in BY-2 cells localized as a ring at the cell cortex in mitosis, as well as the phragmoplast midzone [57], showing that Myo8A recognizes a predetermined site, presumably the CDZ in different plant classes, although conclusive experiments need to be performed. Also, the *Arabidopsis* myosin VIII ortholog ATM1 is highly abundant in the phragmoplast midzone and the cell plate in mitosis and along F-actin filaments in protoplasts [58, 59]. *In vitro*, ATM1 displayed rather sluggish kinetics, which suggests it might act as a tension sensor or generator rather than a transporter [59]. Taken together these observations suggest that plant myosin VIII might act in a tension sensing mechanism enabling phragmoplast expansion towards the CDS. How this actin-myosin based mechanism operates in the context of a CDZ is an interesting research questions. Intriguingly, multiple POK like kinesin-12 homologs are present in moss but their functional significance is not fully characterized [60]. Investigation of the potential interplay between POK and Myo8 dependent pathways in moss and *Arabidopsis* should also provide insight into the evolution of phragmoplast guidance in the context of increasing tissue complexity.

PHRAGMOPLAST EXPANSION AND CELL PLATE SYNTHESIS

In telophase, the phragmoplast originates from overlapping non-kinetochore microtubules that are reorganized into a barrel shaped structure containing two antiparallel sets of bundled microtubules. Microtubule plus ends extend into the opposite array, creating a region of microtubule interdigitation that is accurately positioned at the division plane [61, 62] and likely fulfils a scaffolding function (Figure 7). Golgi-derived vesicles containing cell plate components arrive in the division plane along phragmoplast microtubules and build the laterally expanding cell plate by vesicle fusion. Although several kinesins were identified at the phragmoplast direct evidence for kinesin mediated vesicle trafficking from the Golgi to the division plane is not available. Nevertheless, cell plate synthesis occurs via a succession of characteristic, ultra-structurally discernable stages of cell plate consolidation [63] and involves conserved and plant specific SNARE proteins and other components of the vesicle fusion machinery [64, 65]. The lateral progression of cell plate synthesis a is coordinated with reiteration of microtubule nucleation and polymerization at the phragmoplast leading edge on the periphery and disassembly of phragmoplast microtubules at the trailing edge in the center, driving its lateral expansion towards the CDS (Figure 7).

Mutants impaired in either vesicle fusion or microtubule-based expansion of the phragmoplast display incomplete cell walls and multi-nucleate cells. Lateral phragmoplast expansion requires the disassembly of microtubules at the trailing edge of the phragmoplast and is necessary for cell plate maturation suggesting that feedback about the state of cell plate construction is sensed by the phragmoplast. Mutation in the kinesin-7 HINKEL (HIK)/NACK1, a key driver of trailing edge microtubule disassembly causes persistence of phragmoplast microtubules and incomplete cell plates [66]. HIK controls a mitogen activated protein kinase (MAPK)

pathway by binding to the respective MAPKKK and initiates the successive phosphorylation cascade [67]. The timely initiation of the MAPK signaling pathway is controlled by transcriptional and post-translational regulation of HIK/NACK1 via cell cycle proteins [68-70]. Cyclin-dependent kinases phosphorylate both, NACK1 and NPK1 before metaphase and prevent their direct binding. Furthermore, expression of a phospho-mimic mutant of HIK/AtNACK1 did not rescue the *atnack1* mutant phenotype [71]. Thus timely cell cycle dependent phospho-regulation of NACK1 and the MAPK is crucial for progression through cytokinesis. However, a relevant phosphatase that targets NACK1 and NPK1 has not been identified to date.

MAP65 proteins are the targets of the HIK/NACK1-MAPK signaling pathway and mutations in MAP65 proteins emulate HIK/NACK phenotypes. Loss of MAP65 widened the phragmoplast midzone, and compromised microtubule interdigitation [62, 72, 73]. Indeed *Arabidopsis* AtMAP65-3 cross-link antiparallel microtubules *in vitro* [62] via its distinct C-terminal domain [74]. Kinesin-12A is completely abolished from the phragmoplast midzone, while AtPAKRP2 becomes mis-localized to the entire phragmoplast [62], indicating that MAP65 is required for proper targeting of these kinesins to the phragmoplast midzone. MAP65 microtubule cross-linking activity in cooperation with kinesin motors is a common theme to stabilize antiparallel microtubule overlaps in cell division throughout kingdoms [75].

Arabidopsis expression of a dominant-negative fragment of RUNKEL (RUK) FR5, a putative pseudo-kinase, caused mis-targeting of HIK to the entire phragmoplast and lead to incomplete cell plate formation [76] reminiscent of *ruk* mutant phenotypes [77]. In *ruk* mutants the phragmoplast midzone increases in width, linking RUK to phragmoplast organization. However, there is no evidence for kinase function, rather expression of kinase-domain mutants RUK K33W and RUK D121A fully rescued embryonic *ruk* phenotypes and partially rescued post-embryonic phenotypes [77] suggesting that RUK function is not related to phosphorylation. Although the mutant phenotype places RUK in the HIK/MAPK pathway, it is entirely unclear how exactly RUK contributes to the pathway.

While regulation and mechanisms of phragmoplast trailing edge dynamics are under investigation for quite some time, little is known about the leading edge. A recent study in BY-2 cells suggested that γ-tubulin dependent nucleation along existing stable microtubules [78]. Nucleation events occurs at 40° angles from the template microtubule and nucleation complexes visualized by γ-tubulin-GFP showed distal displacement away from the cell plate. GFP-MAP65 associated with both stable microtubule bundles as well as with dynamic microtubules, most likely cross-linking novel microtubule overlaps [78]. The authors proposed a model where new microtubules nucleate from existing microtubules at the leading edge and subsequently translocation towards the minus end of the extant microtubule and eventually become cross-linked and stabilized. This hypothesis could also explain how the phragmoplast may maintain a constant width.

Conclusion

Recently, a number of reports have started to fill some of the gaps that we face in understanding plant cell division. Regulation of division plane selection is still poorly understood on a molecular level and it is yet too early to deduce whether asymmetric divisions are regulated by common mechanisms that operate in different tissue context or whether tissue specific polarity cues trigger asymmetry. Nevertheless, the available data suggest that once the division plane is defined, the universal molecular machinery is employed to progress through mitosis. Furthermore, the use of evolutionary distant plant models and even different cell types, demonstrates that divers strategies evolved

in plant cells to achieve the accurate insertion of the new cell wall. For instance, it is yet to be determined whether actin-myosin and microtubule-kinesin based phragmoplast guidance mechanisms act entirely independently or whether they converge on the same pathway at some point. Further exciting challenges include how the acentrosomal microtubule cytoskeleton is organized into the plant specific mitotic arrays which might also bear relevant mechanistic insight for other biological kingdoms. The latest reports also show that plant cell division research is increasingly benefiting from recent advances in light microscopy and more is to be expected by application of the rapidly evolving plane illumination technology to continuously improve 3D and 4D resolution. Furthermore, computation allows taking a fresh look at longstanding hypothesis and puts them to the test.

References

1. Rasmussen CG, Wright AJ, Müller S. The role of the cytoskeleton and associated proteins in plant cell division plane determination. *The Plant Journal* 2013:n/a-n/a.
2. Besson S, Dumais J. Universal rule for the symmetric division of plant cells. *Proceedings of the National Academy of Sciences* 2011, 108:6294-6299.
3. Flanders DJ, Rawlins DJ, Shaw PJ, Lloyd CW. Nucleus-associated microtubules help determine the division plane of plant epidermal cells: avoidance of four-way junctions and the role of cell geometry. *J Cell Biol* 1990, 110:1111-1122.
4. Lloyd CW. How Does the Cytoskeleton Read the Laws of Geometry in Aligning the Division Plane of Plant-Cells. *Development* 1991:55-65.
5. Dong J, MacAlister CA, Bergmann DC. BASL Controls Asymmetric Cell Division in Arabidopsis. *Cell* 2009, 137:1320-1330.
6. Humphries JA, Vejlupkova Z, Luo A, Meeley RB, Sylvester AW, Fowler JE, Smith LG. ROP GTPases Act with the Receptor-Like Protein PAN1 to Polarize Asymmetric Cell Division in Maize. *The Plant Cell Online* 2011, 23:2273-2284.
7. Facette MR, Smith LG. Division polarity in developing stomata. *Curr Opin Plant Biol* 2012, 15:585-592.
8. Rasmussen CG, Humphries JA, Smith LG. Determination of symmetric and asymmetric division planes in plant cells. *Annu Rev Plant Biol* 2011, 62:387-409.
9. Wolters H, Anders N, Geldner N, Gavidia R, Jurgens G. Coordination of apical and basal embryo development revealed by tissue-specific GNOM functions. *Development* 2011, 138:117-126.
10. Yoshida S, Barbier de Reuille P, Lane B, Bassel GW, Prusinkiewicz P, Smith RS, Weijers D. Genetic control of plant development by overriding a geometric division rule. *Dev Cell* 2014, 29:75-87.
11. Mayer U, Ruiz RAT, Berleth T, Miseera S, Juurgens G. Mutations affecting body organization in the Arabidopsis embryo. *Nature* 1991, 353:402-407.
12. Lau OS, Davies KA, Chang J, Adrian J, Rowe MH, Ballenger CE, Bergmann DC. Direct roles of SPEECHLESS in the specification of stomatal self-renewing cells. *Science* 2014, 345:1605-1609.
13. Van Damme D, De Rybel B, Gudesblat G, Demidov D, Grunewald W, De Smet I, Houben A, Beeckman T, Russinova E. Arabidopsis α Aurora Kinases Function in Formative Cell Division Plane Orientation. *The Plant Cell Online* 2011, 23:4013-4024.

14. Uyttewaal M, Burian A, Alim K, Landrein B, Borowska-Wykret D, Dedieu A, Peaucelle A, Ludynia M, Traas J, Boudaoud A, et al. Mechanical stress acts via katanin to amplify differences in growth rate between adjacent cells in Arabidopsis. *Cell* 2012, 149:439-451.
15. Vos JW, Dogterom M, Emons AM. Microtubules become more dynamic but not shorter during preprophase band formation: a possible "search-and-capture" mechanism for microtubule translocation. *Cell Motil Cytoskeleton* 2004, 57:246-258.
16. Dhonukshe P, Gadella TW, Jr. Alteration of microtubule dynamic instability during preprophase band formation revealed by yellow fluorescent protein-CLIP170 microtubule plus-end labeling. *Plant Cell* 2003, 15:597-611.
17. Pastuglia M, Azimzadeh J, Goussot M, Camilleri C, Belcram K, Evrard J-L, Schmit A-C, Guerche P, Bouchez D. γ-Tubulin Is Essential for Microtubule Organization and Development in Arabidopsis. *The Plant Cell Online* 2006, 18:1412-1425.
18. Janski N, Masoud K, Batzenschlager M, Herzog E, Evrard JL, Houlne G, Bourge M, Chaboute ME, Schmit AC. The GCP3-interacting proteins GIP1 and GIP2 are required for gamma-tubulin complex protein localization, spindle integrity, and chromosomal stability. *Plant Cell* 2012, 24:1171-1187.
19. Camilleri C, Azimzadeh J, Pastuglia M, Bellini C, Grandjean O, Bouchez D. The *Arabidopsis TONNEAU2* gene encodes a putative novel protein phosphatase 2A regulatory subunit essential for the control of the cortical cytoskeleton. *Plant Cell* 2002, 14:833-845.
20. Spinner L, Gadeyne A, Belcram K, Goussot M, Moison M, Duroc Y, Eeckhout D, De Winne N, Schaefer E, Van De Slijke E, et al. A protein phosphatase 2A complex spatially controls plant cell division. *Nat Commun* 2013, 4:1863.
21. Torres-Ruiz RA, Jurgens G. Mutations in the FASS gene uncouple pattern formation and morphogenesis in Arabidopsis development. *Development* 1994, 120:2967-2978.
22. Traas J, Bellini C, Nacry P, Kronenberger J, Bouchez D, Caboche M. Normal differentiation patterns in plants lacking microtubular preprophase bands. *Nature* 1995, 375:676-677.
23. Drevensek S, Goussot M, Duroc Y, Christodoulidou A, Steyaert S, Schaefer E, Duvernois E, Grandjean O, Vantard M, Bouchez D, et al. The *Arabidopsis* TRM1-TON1 interaction reveals a recruitment network common to plant cortical microtubule arrays and eukaryotic centrosomes. *Plant Cell* 2012, 24:178-191.
24. Kawamura E, Wasteneys GO. MOR1, the Arabidopsis thaliana homologue of Xenopus MAP215, promotes rapid growth and shrinkage, and suppresses the pausing of microtubules in vivo. *Journal of Cell Science* 2008, 121:4114-4123.
25. Kawamura E, Himmelspach R, Rashbrooke MC, Whittington AT, Gale KR, Collings DA, Wasteneys GO. MICROTUBULE ORGANIZATION 1 regulates structure and function of microtubule arrays during mitosis and cytokinesis in the Arabidopsis root. *Plant Physiol* 2006, 140:102-114.
26. Kirik A, Ehrhardt DW, Kirik V. TONNEAU2/FASS Regulates the Geometry of Microtubule Nucleation and Cortical Array Organization in Interphase Arabidopsis Cells. *The Plant Cell Online* 2012.
27. Kirik V, Herrmann U, Parupalli C, Sedbrook JC, Ehrhardt DW, Hulskamp M. CLASP localizes in two discrete patterns on cortical microtubules and is required for cell morphogenesis and cell division in Arabidopsis. *J Cell Sci* 2007, 120:4416-4425.

28. Ambrose JC, Shoji T, Kotzer AM, Pighin JA, Wasteneys GO. The Arabidopsis CLASP Gene Encodes a Microtubule-Associated Protein Involved in Cell Expansion and Division. *The Plant Cell Online* 2007, 19:2763-2775.
29. Ambrose C, Allard JF, Cytrynbaum EN, Wasteneys GO. A CLASP-modulated cell edge barrier mechanism drives cell-wide cortical microtubule organization in *Arabidopsis. Nat. Commun.* 2011, 2:430.
30. Pietra S, Gustavsson A, Kiefer C, Kalmbach L, Hörstedt P, Ikeda Y, Stepanova AN, Alonso JM, Grebe M. Arabidopsis SABRE and CLASP interact to stabilize cell division plane orientation and planar polarity. *Nat Commun* 2013, 4.
31. Zhang H, Dawe RK. Mechanisms of plant spindle formation. *Chromosome Research* 2011, 19:335-344.
32. Masoud K, Herzog E, Chaboute ME, Schmit AC. Microtubule nucleation and establishment of the mitotic spindle in vascular plant cells. *Plant J* 2013, 75:245-257.
33. Chan J, Calder G, Fox S, Lloyd C. Localization of the microtubule end binding protein EB1 reveals alternative pathways of spindle development in *Arabidopsis* suspension cells. *Plant Cell* 2005, 17:1737-1748.
34. Ambrose JC, Cyr R. Mitotic spindle organization by the preprophase band. *Mol Plant* 2008, 1:950-960.
35. Ambrose JC, Cyr R. The kinesin ATK5 functions in early spindle assembly in Arabidopsis. *Plant Cell* 2007, 19:226-236.
36. Marcus AI, Li W, Ma H, Cyr RJ. A kinesin mutant with an atypical bipolar spindle undergoes normal mitosis. *Mol Biol Cell* 2003, 14:1717-1726.
37. Ambrose JC, Li W, Marcus A, Ma H, Cyr R. A minus-end-directed kinesin with plus-end tracking protein activity is involved in spindle morphogenesis. *Mol Biol Cell* 2005, 16:1584-1592.
38. Vos JW, Pieuchot L, Evrard J-L, Janski N, Bergdoll M, de Ronde D, Perez LH, Sardon T, Vernos I, Schmit A-C. The Plant TPX2 Protein Regulates Prospindle Assembly before Nuclear Envelope Breakdown. *The Plant Cell Online* 2008, 20:2783-2797.
39. Petrovská B, Jeřábková H, Kohoutová L, Cenklová V, Pochylová Ž, Gelová Z, Kočárová G, Váchová L, Kurejová M, Tomaštíková E, et al. Overexpressed TPX2 causes ectopic formation of microtubular arrays in the nuclei of acentrosomal plant cells. *Journal of Experimental Botany* 2013.
40. Petrovská B, Cenklová V, Pochylová Ž, Kourová H, Doskočilová A, Plíhal O, Binarová L, Binarová P. Plant Aurora kinases play a role in maintenance of primary meristems and control of endoreduplication. *New Phytologist* 2012, 193:590-604.
41. Pickett-Heaps JD, Northcote DH. Cell division in the formation of the stomatal complex of the young leaves of wheat. *J Cell Sci* 1966, 1:121-128.
42. Smith LG, Gerttula SM, Han S, Levy J. Tangled1: a microtubule binding protein required for the spatial control of cytokinesis in maize. *J Cell Biol* 2001, 152:231-236.
43. Smith LG, Hake S, Sylvester AW. The tangled-1 mutation alters cell division orientations throughout maize leaf development without altering leaf shape. *Development* 1996, 122:481-489.
44. Cleary AL, Smith LG. The *Tangled1* gene is required for spatial control of cytoskeletal arrays associated with cell division during maize leaf development. *Plant Cell* 1998, 10:1875-1888.
45. Rasmussen CG, Sun B, Smith LG. Tangled localization at the cortical division site of plant cells occurs by several mechanisms. *J Cell Sci* 2011, 124:270-279.

46. Muller S, Han S, Smith LG. Two kinesins are involved in the spatial control of cytokinesis in Arabidopsis thaliana. *Curr Biol* 2006, 16:888-894.
47. Lipka E, Gadeyne A, Stockle D, Zimmermann S, De Jaeger G, Ehrhardt DW, Kirik V, Van Damme D, Muller S. The Phragmoplast-Orienting Kinesin-12 Class Proteins Translate the Positional Information of the Preprophase Band to Establish the Cortical Division Zone in Arabidopsis thaliana. *Plant Cell* 2014, 26:2617-2632.
48. Xu XM, Zhao Q, Rodrigo-Peiris T, Brkljacic J, He CS, Muller S, Meier I. RanGAP1 is a continuous marker of the Arabidopsis cell division plane. *Proc Natl Acad Sci U S A* 2008, 105:18637-18642.
49. Rodrigo-Peiris T, Xu XM, Zhao Q, Wang H-J, Meier I. RanGAP is required for post-meiotic mitosis in female gametophyte development in Arabidopsis thaliana. *Journal of Experimental Botany* 2011, 62:2705-2714.
50. Kojo KH, Higaki T, Kutsuna N, Yoshida Y, Yasuhara H, Hasezawa S. Roles of Cortical Actin Microfilament Patterning in Division Plane Orientation in Plants. *Plant and Cell Physiology* 2013, 54:1491-1503.
51. Panteris E. Cortical actin filaments at the division site of mitotic plant cells: a reconsideration of the 'actin-depleted zone'. *New Phytol* 2008, 179:334-341.
52. Mineyuki Y, Palevitz BA. Relationship between preprophase band organization, F-actin and the division site in *Allium. J Cell Sci* 1990, 97:283-295.
53. Sano T, Higaki T, Oda Y, Hayashi T, Hasezawa S. Appearance of actin microfilament 'twin peaks' in mitosis and their function in cell plate formation, as visualized in tobacco BY-2 cells expressing GFP-fimbrin. *Plant J* 2005, 44:595-605.
54. Karahara I, Suda J, Tahara H, Yokota E, Shimmen T, Misaki K, Yonemura S, Staehelin LA, Mineyuki Y. The preprophase band is a localized center of clathrin-mediated endocytosis in late prophase cells of the onion cotyledon epidermis. *Plant J* 2009, 57:819-831.
55. Vanstraelen M, Van Damme D, De Rycke R, Mylle E, Inze D, Geelen D. Cell cycle-dependent targeting of a kinesin at the plasma membrane demarcates the division site in plant cells. *Curr Biol* 2006, 16:308-314.
56. Suetsugu N, Yamada N, Kagawa T, Yonekura H, Uyeda TQ, Kadota A, Wada M. Two kinesin-like proteins mediate actin-based chloroplast movement in Arabidopsis thaliana. *Proc Natl Acad Sci U S A* 2010, 107:8860-8865.
57. Wu S-Z, Bezanilla M. Myosin VIII associates with microtubule ends and together with actin plays a role in guiding plant cell division. *eLife* 2014, 3:e03498.
58. Reichelt S, Knight AE, Hodge TP, Baluska F, Samaj J, Volkmann D, Kendrick-Jones J. Characterization of the unconventional myosin VIII in plant cells and its localization at the post-cytokinetic cell wall. *The Plant Journal* 1999, 19:555-567.
59. Haraguchi T, Tominaga M, Matsumoto R, Sato K, Nakano A, Yamamoto K, Ito K. Molecular Characterization and Subcellular Localization of Arabidopsis Class VIII Myosin, ATM1. *Journal of Biological Chemistry* 2014, 289:12343-12355.
60. Miki T, Naito H, Nishina M, Goshima G. Endogenous localizome identifies 43 mitotic kinesins in a plant cell. *Proc Natl Acad Sci U S A* 2014, 111:E1053-1061.
61. Hiwatashi Y, Obara M, Sato Y, Fujita T, Murata T, Hasebe M. Kinesins are indispensable for interdigitation of phragmoplast microtubules in the moss *Physcomitrella patens. Plant Cell* 2008, 20:3094-3106.
62. Ho C-MK, Hotta T, Guo F, Roberson RW, Lee Y-RJ, Liu B. Interaction of antiparallel microtubules in the phragmoplast is mediated by the microtubule-associated protein MAP65-3 in *Arabidopsis. Plant Cell* 2011, 23:2909-2923.

63. Samuels AL, Giddings TH, Jr., Staehelin LA. Cytokinesis in tobacco BY-2 and root tip cells: a new model of cell plate formation in higher plants. *J Cell Biol* 1995, 130:1345-1357.
64. Jurgens G. Cytokinesis in higher plants. *Annu. Rev. Plant Biol.* 2005, 56:281-299.
65. McMichael CM, Bednarek SY. Cytoskeletal and membrane dynamics during higher plant cytokinesis. *New Phytologist* 2013, 197:1039-1057.
66. Strompen G, El Kasmi F, Richter S, Lukowitz W, Assaad FF, Jurgens G, Mayer U. The Arabidopsis HINKEL gene encodes a kinesin-related protein involved in cytokinesis and is expressed in a cell cycle-dependent manner. *Current Biology* 2002, 12:153-158.
67. Sasabe M, Machida Y. Regulation of organization and function of microtubules by the mitogen-activated protein kinase cascade during plant cytokinesis. *Cytoskeleton (Hoboken)* 2012, 69:913-918.
68. Ito M. Factors controlling cyclin B expression. *Plant Mol Biol* 2000, 43:677-690.
69. Ito M, Iwase M, Kodama H, Lavisse P, Komamine A, Nishihama R, Machida Y, Watanabe A. A novel cis-acting element in promoters of plant B-type cyclin genes activates M phase-specific transcription. *Plant Cell* 1998, 10:331-341.
70. Araki S, Ito M, Soyano T, Nishihama R, Machida Y. Mitotic cyclins stimulate the activity of c-Myb-like factors for transactivation of G2/M phase-specific genes in tobacco. *J Biol Chem* 2004, 279:32979-32988.
71. Sasabe M, Boudolf V, De Veylder L, Inzé D, Genschik P, Machida Y. Phosphorylation of a mitotic kinesin-like protein and a MAPKKK by cyclin-dependent kinases (CDKs) is involved in the transition to cytokinesis in plants. *Proceedings of the National Academy of Sciences* 2011, 108:17844-17849.
72. Muller S, Smertenko A, Wagner V, Heinrich M, Hussey PJ, Hauser MT. The plant microtubule-associated protein AtMAP65-3/PLE is essential for cytokinetic phragmoplast function. *Curr Biol* 2004, 14:412-417.
73. Kosetsu K, de Keijzer J, Janson ME, Goshima G. MICROTUBULE-ASSOCIATED PROTEIN65 Is Essential for Maintenance of Phragmoplast Bipolarity and Formation of the Cell Plate in Physcomitrella patens. *The Plant Cell Online* 2013, 25:4479-4492.
74. Ho C-MK, Lee Y-RJ, Kiyama LD, Dinesh-Kumar SP, Liu B. Arabidopsis Microtubule-Associated Protein MAP65-3 Cross-Links Antiparallel Microtubules toward Their Plus Ends in the Phragmoplast via Its Distinct C-Terminal Microtubule Binding Domain. *The Plant Cell Online* 2012, 24:2071-2085.
75. Walczak CE, Shaw SL. A MAP for Bundling Microtubules. *Cell* 2010, 142:364-367.
76. Krupnova T, Stierhof YD, Hiller U, Strompen G, Muller S. The microtubule-associated kinase-like protein RUNKEL functions in somatic and syncytial cytokinesis. *Plant J* 2013, 74:781-791.
77. Krupnova T, Sasabe M, Ghebreghiorghis L, Gruber CW, Hamada T, Dehmel V, Strompen G, Stierhof YD, Lukowitz W, Kemmerling B, et al. Microtubule-associated kinase-like protein RUNKEL needed [corrected] for cell plate expansion in Arabidopsis cytokinesis. *Curr Biol* 2009, 19:518-523.
78. Murata T, Sano T, Sasabe M, Nonaka S, Higashiyama T, Hasezawa S, Machida Y, Hasebe M. Mechanism of microtubule array expansion in the cytokinetic phragmoplast. *Nat Commun* 2013, 4.

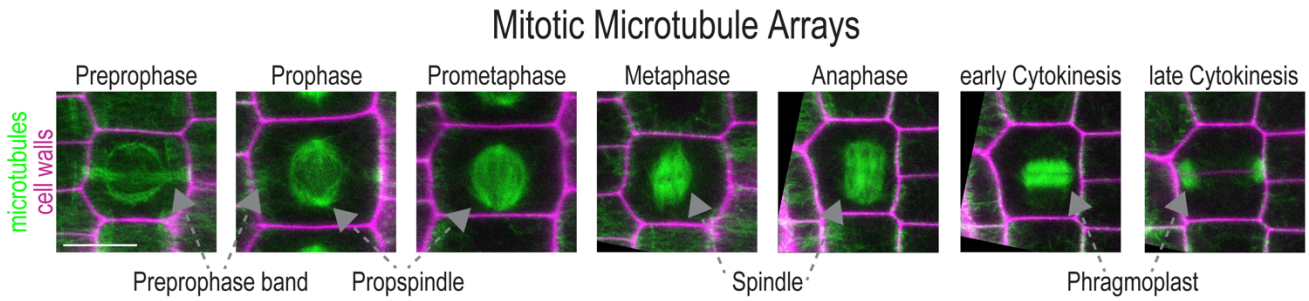

Figure 1: Micrographs of the microtubule arrays during plant cell division. Mitotic cell cycle stages are depicted in chronological order. Microtubules are visualized by GFP-MBD, depicted in green, cell walls are stained with propidium iodide (magenta). Maximum projections of GFP-MBD z-stacks are merged with a single propidium iodide image. In case were images were rotated non-imaged regions were filled with black background. Scale bar indicates 10 µm

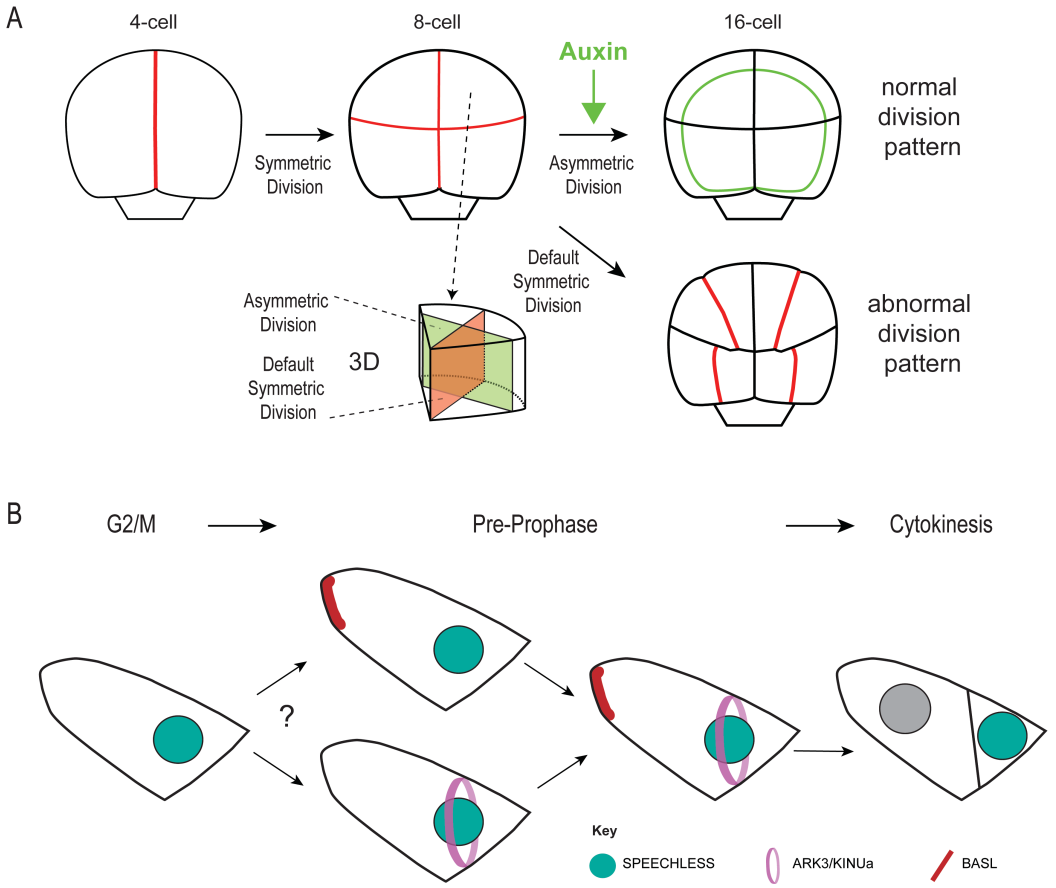

Figure 2: Regulation of division plane positioning in symmetric and asymmetric divisions. (A) Succession of divisions in the early *Arabidopsis* embryo. Chronologically invariant symmetric and asymmetric divisions contribute to normal development of globular stage embryos. Symmetric divisions give rise to the 8-cell embryo (indicated in red) obeying the geometric rule of minimal area division, while highly asymmetric divisions facilitate the separation of outer protoderm and inner cell types at the transition from 8- to 16-cell stage (indicated in green). Auxin signaling overrides default symmetric divisions, allowing asymmetric divisions. Changes in auxin response result in reversion to the geometry based symmetric default pathway. 3D reconstruction illustrates the default minimum area division plane (red) in comparison to an asymmetric division plane (green) at the transition from 8-cell to 16-cell stage. (B) Model for the transcription factor regulated control of asymmetric division in the stomatal lineage. SPEECHLESS (SPCH, green) regulates both transcription of *BASL* and kinesin *ARK3/KINUa* in a meristemoide cell. SPCH preceeds ARK3 (purple) localization at the PPB while BASL localizes at the plasma membrane opposing the imminent future division site, acting as a polarity cue. Presumably, *BASL* and *ARK3/KINUa* act in the same genetic pathway, yet the interdependency of their subcellular location needs to be clarified.

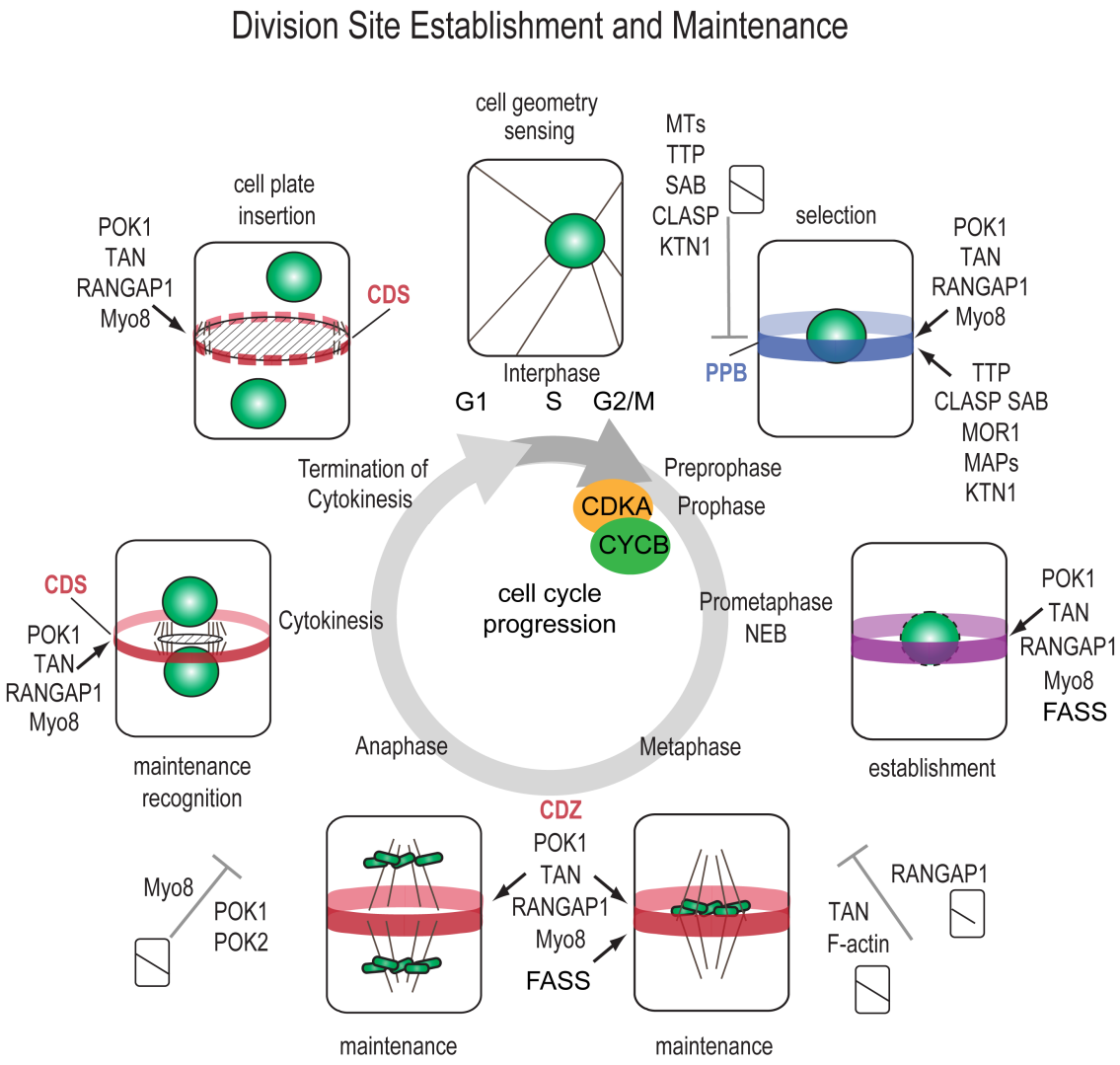

Figure 3: Overview of cortical division site establishment and maintenance. Entry into mitosis is under the control of the cell cycle. The transition from G2 phase to mitosis (M) is mediated by the CDKA;CYCB complex. The nucleus (green) gets centered as the cell enters mitosis and the preprophase band (PPB, blue) subsequently assembles depending on TTP (TON1/TRM/PP2A) protein complex and phosphatase activity. A number of microtubule associated proteins (MAP), co-localize with the PPB and direct its position (SABRE, CLASP, MOR1, KTN1, MAPs). The PPB accurately predicts the future cell plate insertion site. Mutation of proteins involved in PPB assembly leads to loss of PPB formation and in consequence mispositioned cell walls. In the presence of PPB, TANGLED (TAN), RANGAP1and POK1 are recruited to the PPB during prophase, establishing the cortical division zone (CDZ). The purple color indicates the co-localization of PPB microtubules and positive CDZ markers during prometaphase. Upon PPB disassembly the CDZ (red) preserves the positional information conveyed by the PPB. POK1 is required for the maintenance of TAN and RanGAP1 commencing in metaphase. The loss of POKs, TAN, F-actin and Myo8 leads to obliquely inserted cell walls, whereas knock down of RanGAP function causes incomplete cell walls. During cytokinesis the CDZ (including its residents) narrows to define cortical division site (CDS) as the precise cell plate insertion site. POK1 and Myo8 are required for phragmoplast (PP) guidance towards the CDS. Upon completion of cell plate insertion CDS markers disappear.

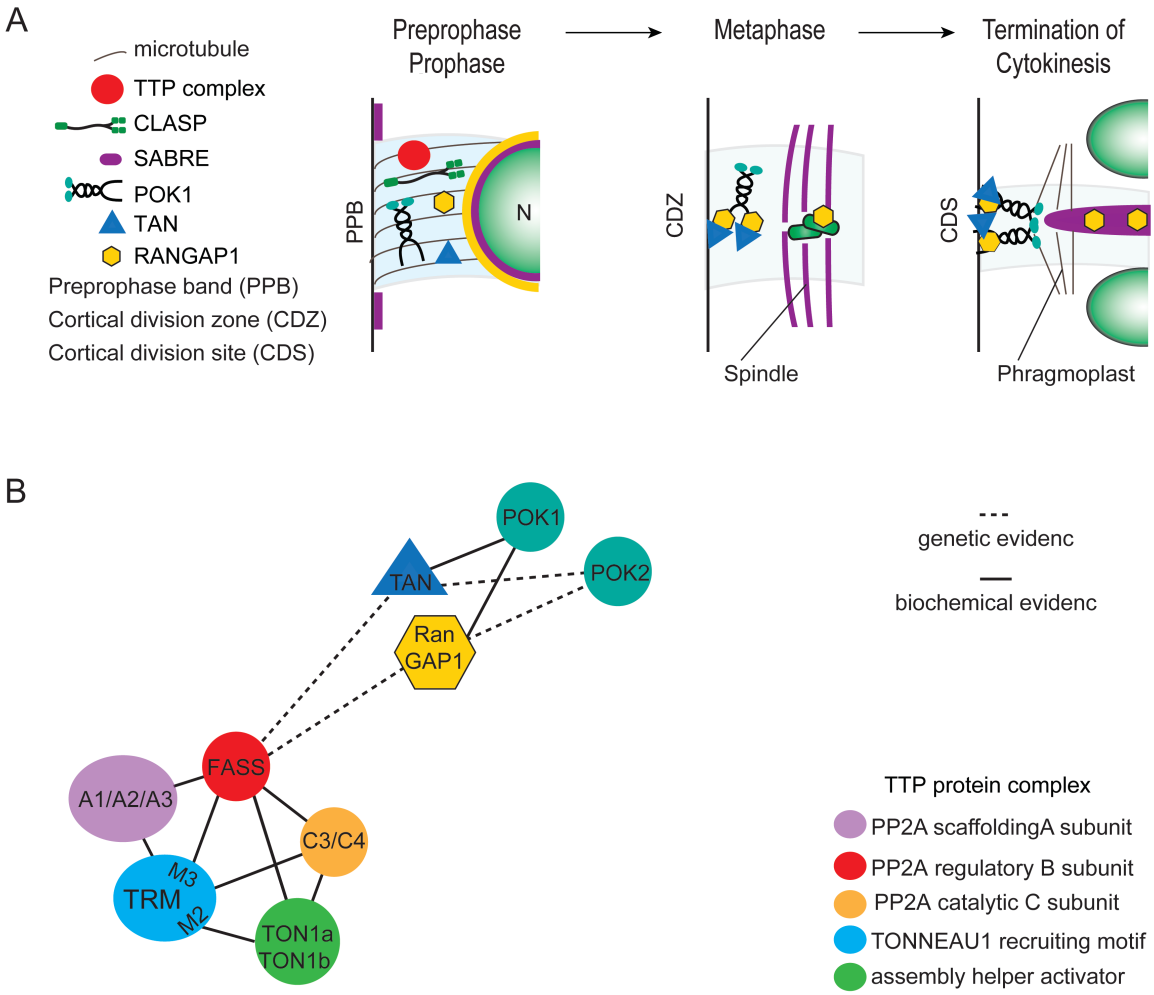

Figure 4: Protein dynamics at the cortical division site. A selection of proteins that are required for preprophase band (PPB) formation, positioning and cortical division zone (CDZ) establishment is depicted. Proteins of the TTP (TON1/TRM/PP2A, red) complex localize at the PPB and are required for its formation. CLASP (dark green) and SABRE (SAB, purple) genetically interact to position the PPB, although CLASP co-localizes with the PPB, SAB is located at its lateral boundaries. In prophase the proteins, POK1 (mint), TANGLED (TAN, blue) and RanGAP1 (yellow) are independently recruited to the PPB and remain at this cortical site beyond PPB disassembly. In metaphase POK1 is somehow tethered to the cortical division zone (CDZ) and retains TAN and RanGAP1 at this site throughout mitosis. In cytokinesis, the localization of POK1, TAN and RanGAP1 becomes narrow, most likely more accurately describing the site of cell plate fusion or cortical division site (CDS). Note that RanGAP1 also associates with the nuclear envelope in prophase and with kinetochores and the cell plate later in mitosis. (B) Interaction network of the above featured proteins at the PPB/CDZ as determined either by biochemical evidence (continuous line) or genetic evidence. The TPP complex consists of Protein Phosphatase (PP) 2A variable scaffolding A subunit, the regulatory B subunit (FASS) and the variable catalytic C subunit as well as the assembly activator TONNEAU (TON) 1a/b and variable TONNEAU1 RECRUITING MOTIF (TRM) proteins. TRM interacts with FASS via the conserved M2 motif and the interaction of TON1 with TRM M3 motif mediates cytoskeletal targeting. Localization of TAN and RanGAP1 at the PPB depends on FASS.

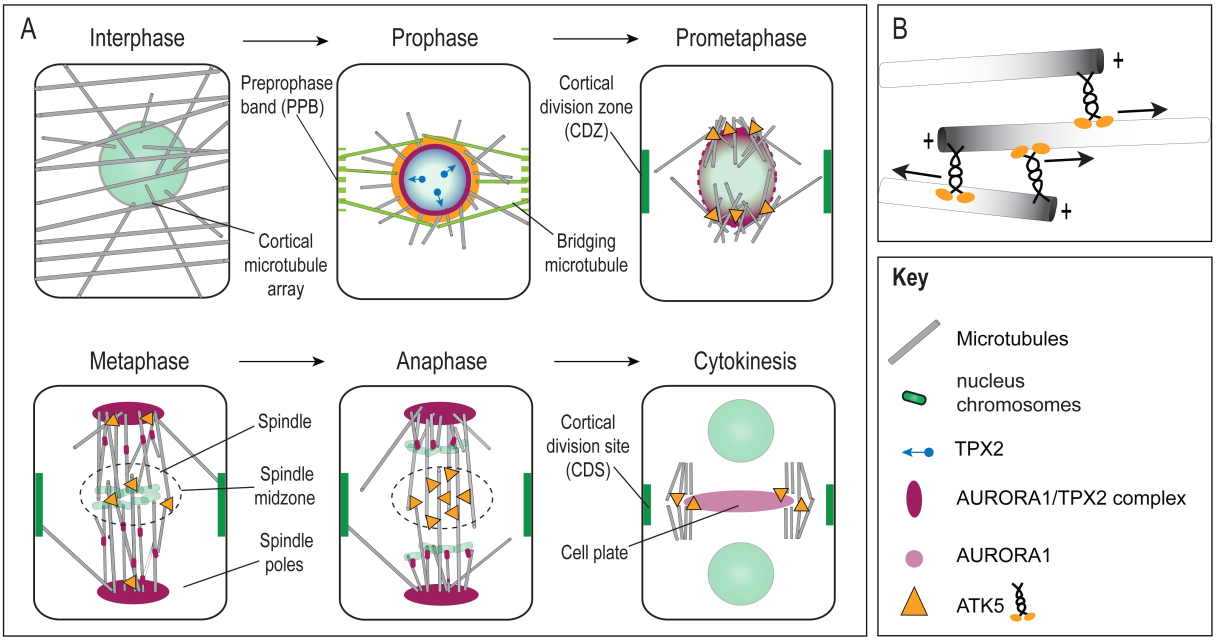

Figure 5: Schematic illustration of plant spindle formation. Cell cycle stages are illustrated as cell cross sections, while interphase is depicted as a projection. Perinuclear microtubules emanate from the nucleus and bridging microtubules (green) connect the nucleus and the preprophase band (PPB green dashed line) in late prophase. The microtubule associated protein TPX2, which accumulates in the nucleus during preprophase (blue gradient), is exported and associates with AURORA (AUR) 1 at the nuclear envelope (AUR1/TPX2 complex purple). During nuclear envelope breakdown (purple dashed line) the AUR1/TPX2 complex localizes to minus ends of perinuclear microtubules and subsequently co-localizes with spindle poles and accumulates at the spindle, presumable co-localizing with microtubule nucleation complexes. Note that the AUR1/TPX2 complex especially localizes at kinetochore microtubules during the transition from metaphase to anaphase. Whereas TPX2 rapidly disappears at the end of anaphase, AUR1 decorates the cell plate during cytokinesis (pink). Kinesin-14 ATK5 (yellow) co-localizes with perinuclear microtubules in preprophase/prophase and associates with antiparallel interpolar microtubules at the spindle midzone. During cytokinesis, ATK5 assembles at the phragmoplast midzone. (B) Microtubule plus end association of ATK5 is mediated through its C-terminal tail domain, while microtubule minus end directed mobility requires ATK5 motor domain.

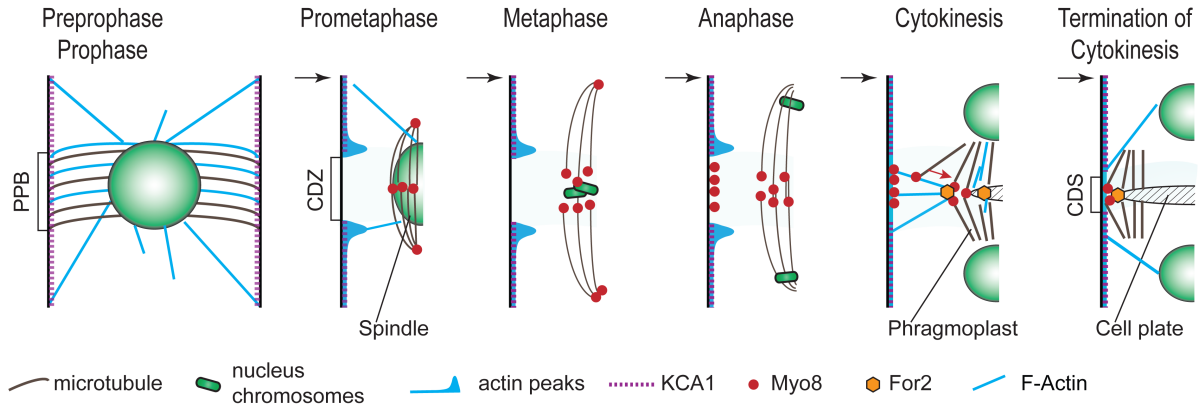

Figure 6: Illustration of the actin cytoskeleton and selected associated proteins in plant mitosis. F-actin (blue) is a component of the preprophase band (PPB) but not restricted to it. Actin-bundles span throughout the entire cell. Upon PPB disassembly in prometaphase the region of the cortical division zone remains almost devoid of F-actin, but is flanked by actin enrichments, also referred to as twin peaks. The kinesin-14 KCA1 (purple dashed line) decorates the cell cortex, but is depleted from the CDZ. Myo8 (red) associates with microtubules and localizes to the spindle poles and spindle midzone. During anaphase Myo8 locates exclusively to microtubule overlaps in the spindle midzone and also accumulates at the CDZ. During cytokinesis, Myo8 remains associated with dynamic phragmoplast microtubules at the leading edge and with peripheral microtubules that seem to contact the CDS. These

peripheral microtubules move towards the leading phragmoplast edge. It is hypothesized that Myo8 might use actin filaments spanning the distance between the phragmoplast and the CDS for the relocation of the peripheral microtubules. F-actin is indeed present between the phragmoplast and the CDS and furthermore, actin nucleating formin For2a (orange) accumulates in the phragmoplast midzone, further supporting the notion that Myo8 acts in a mechanism to maintain phragmoplast integrity.

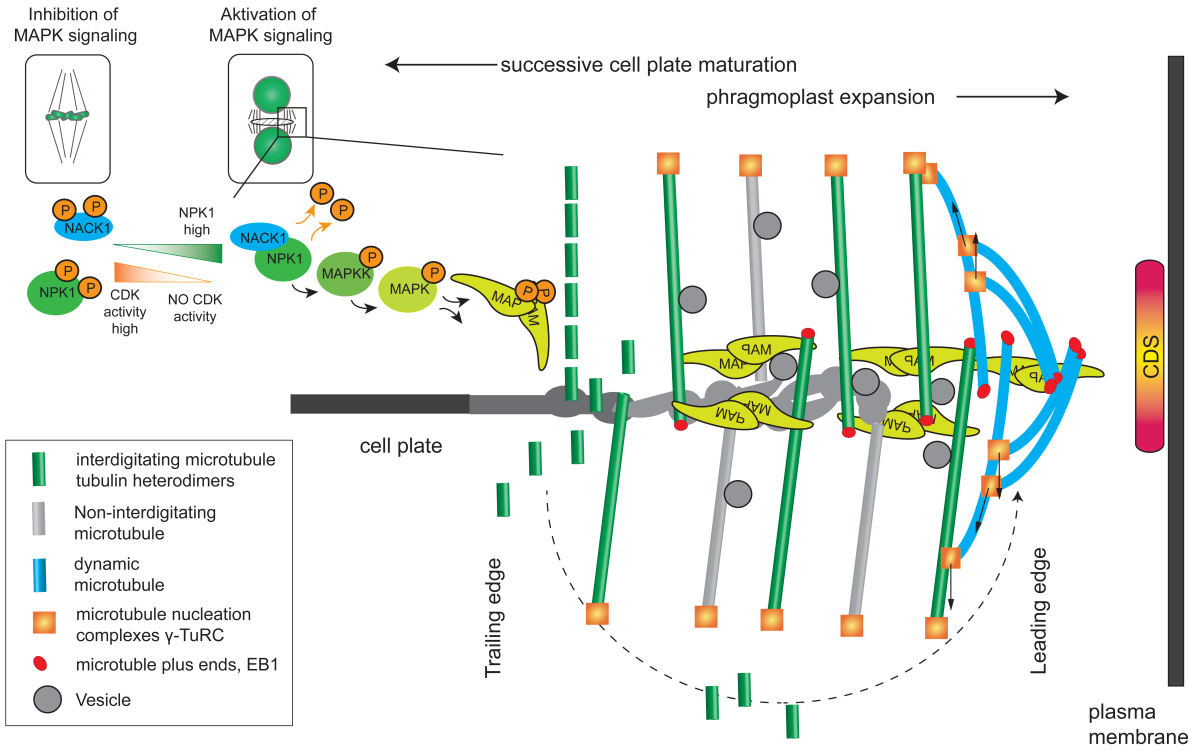

Figure 7: Regulation and mechanisms of phragmoplast expansion. HIK/NACK kinesin (blue) binding to a MAPKKK increases the kinase activity, to activate the NACK-PQR MAPK (green gradient) signaling cascade that targets MAP65 proteins. In metaphase, the NACK/HINKEL dependent mitogen activated protein kinase (MAPK) signaling cascade is inhibited by CDK dependent phosphorylation of the kinesin NACK1 and the MAPK kinase kinase NPK1 (dark green). During cell cycle progression CDK activity is switched off, allowing the accumulation of non-phosphorylated NPK1which eventually binds to non-phosphorylated NACK1 in the phragmoplast midzone regions. This complex formation triggers the kinase cascade, which targets MAP65 proteins at the trailing edge of the phragmoplast. Phosphorylation of MAP65 inhibits its cross-linking activity towards antiparallel microtubules. Consequently microtubules at the trailing edge become destabilized and disassemble, discharging tubulin heterodimers. At the leading edge of the phragmoplast, new, dynamic microtubules nucleate on existing microtubules at an angle around 40°. γ-tubulin containing nucleation sites move towards microtubule minus ends as they polymerize new microtubules. Antiparallel dynamic microtubules are bundled by MAP65. Progressively, the leading edge expands laterally allowing new vesicle fusion. At the trailing edge, where cell plate formation is completed, microtubules depolymerize.

Further Reading/Resources

http://www.els.net/WileyCDA/ElsArticle/refId-a0001686.html
http://www.els.net/WileyCDA/ElsArticle/refId-a0023760.html
http://www.els.net/WileyCDA/ElsArticle/refId-a0001685.html

Related Articles

Subtopic	Article title
Cell Biology of Plant Development	Cell division
Fertilization, Embryogenesis, and Seed Development	Patterning the embryo

7.3 Personal Contribution

Lipka, E. and Müller, S. Potential roles for kinesins at the cortical division site. Front. Plant Sci. 3:158 (2012)

For this review article I performed research, inquired data and prepared all the figures under the supervision of Sabine Müller.

Lipka, E. and Müller, S. Nitrosative stress triggers microtubule reorganization in *Arabidopsis thaliana*. J. Exp. Bot. 65:15, 4177-4189 (2014)

All data presented in this research article was collected by me under the guidance of Dr. Sabine Müller. I was responsible for the research design, experimental performance, data analysis and presentation.

Lipka, E., Gadeyne, A., Stöckle, D., Zimmermann, S., De Jaeger, G., Ehrhardt, D. W., Kirik, V., Van Damme, D. and Müller, S. The Phragmoplast-Orienting Kinesin-12 Class Proteins Translate the Positional Information of the Preprophase Band to Establish the Cortical Division Zone in *Arabidopsis thaliana*. The Plant Cell 26, 2617-2632 (2014)

Following experiments were done by me: phenotypic characterization of the new allele combination, YFP-POK1 and POK1 C-terminal fragment localization study, FRAP analysis of YFP-POK1 and microtubule dependency experiment of YFP-POK1 localization. I designed and performed the research and analyzed the data under the supervision of Dr. Sabine Müller.

Lipka, E., Herrmann, A. and Mueller, S. Mechanisms of plant cell division. Wiley Interdisciplinary Reviews: Developmental Biology (2015)

For this review article I contributed figures 1, 3, 4 and 6. I was involved in data inquiry, writing and preparation of the part “Formation of the PPB” and “Role of the actin cytoskeleton in cell division”.